Axonal tracing of fluorescently labeled varicella-zoster virus proteins after infection of rat dorsal root ganglia neurons

Dissertation

zur Erlangung des Doktorgrades

der Mathematisch-Naturwissenschaftlichen Fakultät

der Christian-Albrechts-Universität zu Kiel

vorgelegt von

Husam Taher

Kiel, 2018

Erster Gutachter:	Prof. Dr. Helmut Fickenscher
Zweiter Gutachter:	Prof. Dr. Axel Scheidig
Tag der mündlichen Prüfung:	18.04.2018

To my parents

&

Nesrin

INDEX

1 SUMMARY

Varicella-zoster virus (VZV) is a wide-spread neurotropic α-herpesvirus causing chickenpox (varicella) during primary infection and shingles (zoster) upon reactivation. During primary infection, VZV particles travel along neuronal microtubules via retrograde axonal transport from the distal axon endings to the somata of trigeminal and dorsal root ganglia DRG sensory neurons where latency is established. In contrast, upon reactivation, VZ virions migrate to the periphery by anterograde axonal transport to promote the typical symptoms of shingles. In culture, VZV replicates in a highly cell-associated manner and has a narrow host range that limits experimental animal models and restricted our approaches for studying the axonal transport of the virus particles. In this study, we used a cloned bacterial artificial chromosome (BAC) of the European wild-type isolate of VZV HJO to generate two double VZV mutants via en-passant mutagenesis in which the protein of interest and the capsid protein p23 were fused either to the enhanced green fluorescent protein or to the monomeric red fluorescent protein. The generated BACs were then transfected into permissive melanoma cells in which the cell-associated viruses were reconstituted and high-titer cell-free virus preparations were generated. Productive anterograde and retrograde infections of DRG neurons were established by the exposure to high titers of cell-free VZV of 10^4-10^5 plaque forming units/ml. Subsequently, we described the colocalization of the VZV immediate early tegument protein IE4 and the transmembrane envelope protein p65 together with p23 within axons of embryonic Wistar rat DRG neurons after anterograde and retrograde infection with VZV. The anterograde axonal transport of VZV follows most likely a “married” model. Hence, our findings provide a platform for further investigations into the axonal transport mechanisms of VZV and into the role of the relevant viral proteins as possible medicinal intervention targets in preventing or treating VZV infection and its complications.

2 ZUSAMMENFASSUNG

Varizella-Zoster-Virus (VZV) ist ein weitverbreitetes neurotropes α-Herpesvirus, das Windpocken (Varizellen) während der Erstinfektion und Gürtelrose (Zoster) nach der Reaktivierung verursacht. Während der Erstinfektion wandern die VZV-Partikel den neuronalen Mikrotubuli entlang auf dem retrograden axonalen Weg von den distalen Axon-Enden bis in die Zellkörper der sensorischen Neurone der Trigeminus- oder Spinalganglien, wo die Latenz ausgebildet wird. Im Gegensatz wandern die VZ-Virionen nach der Reaktivierung in die Peripherie über den anterograden axonalen Weg und führen zu den typischen Symptomen der Gürtelrose. In der Kultur repliziert VZV in stark zellassoziierter Weise und hat ein enges Wirtsspektrum, das experimentelle Tiermodelle limitiert und unsere Ansätze zur Untersuchung des axonalen Transports der Virus-Partikel begrenzt hat. In dieser Studie verwendeten wir ein kloniertes bakterielles artifizielles Chromosom (BAC) des europäischen Wildtyp-VZV-Isolats HJO, um zwei VZV-Doppelfusionsmutanten via en-passant-Mutagenese zu erzeugen, in denen das betreffende Protein und das Kapsid-Protein p23 entweder mit dem verstärkt grün fluoreszierenden Protein oder mit dem monomeren rot fluoreszierenden Protein fusioniert wurden. Die erzeugten BACs wurden in permissive Melanom-Zellen transfiziert, in denen zellassoziiertes Virus rekonstituiert und aus denen hochtitrige, zellfreie Viruspräparationen hergestellt wurden. Lytische anterograde und retrograde Infektionen der Spinalganglien-Neuronen wurden durch hohe Titer zellfreien Virus von 10^4-10^5 Plaque-bildenden Einheiten/ml erreicht. In der Folge beschrieben wir die Kolokalisation des sehr früh exprimierten VZV-Tegument-Proteins IE4 und des Transmembran-Hüllproteins p65 mit p23 in Axonen embryonaler Spinalganglien von Wistar-Ratten nach anterograder und retrograder VZV-Infektion. Der anterograde axonale Transport des VZV folgt höchstwahrscheinlich dem „married“-Modell. Somit liefern unsere Ergebnisse eine Plattform für weitere Untersuchungen über die axonalen Transportmechanismen des VZV und über die Rolle der betroffenen viralen Proteine als mögliche Ziele für die pharmazeutische Intervention zur Vermeidung oder Heilung der VZV-Infektion und ihrer Komplikationen.

3 INTRODUCTION

3.1 Herpesviruses

Herpesviruses are double-stranded DNA viruses with genome sizes ranging from 120 to 230-kilo base pairs and a virion diameter of approximately 150-200 nm. Herpesvirus infections are very common in humans and in a wide variety of vertebrates causing different symptoms specific for the individual herpesviruses. Despite the differences, all herpesviruses have a similar morphology and similar biological features in that they persist life-long in the host organism after the primary infection. During latency, the virus DNA is present in the cell as extrachromosomal episomes within the nucleoplasm. The production of infectious viral particles remains blocked and the cells remain viable. However, stress, immunosuppression and other poorly defined stimuli may induce reactivation of the virus leading to new symptoms. So far, the eight human herpesviruses are classified into three subfamilies, namely, α-, β-, and γ-herpesviruses. The human α-herpesviruses are characteristic for their neurotropic features and persistence in sensory neurons of the dorsal root ganglia. These viruses include the human herpesvirus 1 (herpes-simplex virus type 1, HSV-1), the human herpesvirus 2 (herpes-simplex virus type 2, HSV-2), and the human herpesvirus 3 (varicella-zoster virus, VZV) (Modrow et al., 2003).

3.2 The varicella zoster virus

3.2.1 Clinical relevance of varicella zoster virus

According to its morphology and genome structure, the human VZV is a member of the herpesvirus family and the α-herpesvirus subfamily. After primary infection, VZV causes chickenpox (varicella) primarily in children. Thereafter, the virus goes latent in sensory neurons of the dorsal root and trigeminal ganglia. Upon the reactivation of VZV from its latent persistence, herpes zoster (shingles) occurs that can induce a severe, long-lasting pain known as postherpetic neuralgia, mostly in immunodeficient persons or in elderly people. VZV exhibits a typical tropism for the skin where bullous dermal lesions are formed during chickenpox and shingles. VZV infection is initiated mainly in the mucosal epithelial cells of the upper respiratory tract by aerosol transmission or, alternatively, by direct contact with lesions of infected skin (Cohen et al., 2007; Grose, 1981).

Chickenpox is clinically well known and starts after an incubation period of about ten days to three weeks as the result of an exposure of a susceptible person to a chickenpox patient (Arvin, 2001). Varicella starts with fever, headache, fatigue, and abdominal pain. These primary symptoms last for about one to two days before itching skin lesions develop. VZV enters into the bloodstream in a cell-associated way, starting within the last few days of the

incubation period and lasting for a few days after the dermal rash emerges (Asano et al., 1990; Gershon et al., 1978; Koropchak et al., 1989, 1991; Ozaki et al., 1986). The secondary VZV disease, zoster, is induced when the latent virus is reactivated from its hiding places in sensory ganglia leading to a cutaneous rash that is generally restricted to dermatomal areas of the skin which are connected to specific sensory nerves. A severe, mostly long-lasting pain defined as postherpetic neuralgia (Annunziato et al., 2000; Hope-Simpson, 1965; Schmidt et al., 2003) additionally characterizes herpes zoster.

During chickenpox and shingles, the virus is released during lytic replication in the dermatomal epithelium or in respiratory mucous membranes (Chen et al., 2004). Since the respiratory secretions from varicella patients are highly contagious via air transmission, approximately 95% of the people in mild climates are infected with VZV up to the age of 30 years (Cohen et al., 2007; Sawyer et al., 1994), as long as no effective vaccination programs are followed. The vaccine strain Oka (v-Oka) is a live-attenuated VZV vaccine leading to dramatically decreased morbidity and mortality rates for VZV infections.

3.2.2 Structure of VZV genome

VZV has the smallest genome of the human herpesviruses, with a linear double-stranded DNA genome (125 kb) which includes two unique regions, the unique long region (UL) (105 kb) and the unique short region (US) (5.2 kb). The UL region and the US region are flanked terminally and internally by inverted repetitive sequences termed as terminal repeat long or internal repeat long (TRL/IRT) (89 bp) and terminal repeat short or internal repeat short (TRS/IRS) (7.3 kb), respectively (Davison & Scott, 1986). Two dominant isomers are found in equimolar quantities in virion DNA, since the US region exists in an equal amounts in both directions, while the UL region occurs mainly in one orientation, only (Fig. 1) (Davison, 1984).

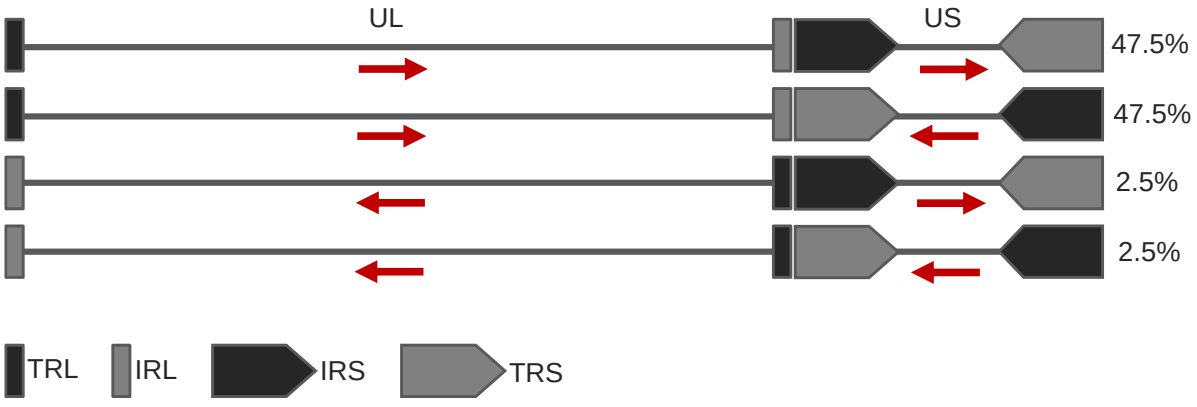

Fig. 1. Isomeric forms of the VZV genome. Isomeric variants of the linear VZV genome occurring during the replication process. Two of the four isomeric forms are found frequently (47.5%), whereas the other two forms are rare (2.5%) (Davison, 1984).

The VZV genome encodes approximately 72 open reading frames (ORFs), three of which are duplicated according to their position in the repetitive repeat short region (IRS and TRS) (ORF62/71, ORF63/70, ORF64/69) (Fig. 2). In addition, two origins of replication are located in the RS regions. Furthermore, there are five small repetitive regions (R1 to R5) distributed over the genome that vary in length according to different numbers of repeated sequence units (Davison & Scott, 1986; Hondo & Yogo, 1988). The segments R1, R2, R3, and R5 are located in the UL region, whereas R4 is placed in IRS between ORF62 and ORF63, and in TRS between ORF71 and ORF70. The R4 region is GC-rich and composed of a 27 bp unit that can be repeated several times (Casey et al., 1985). Various VZV strains have shown different numbers of repeated units (Gomi et al., 2002).The VZV genome has an unpaired G nucleotide at its left end and an unpaired C at its right end. This allows the circularization of the genome after having entered the nucleus by pairing these two single nucleotides from both ends (Davison, 1984).

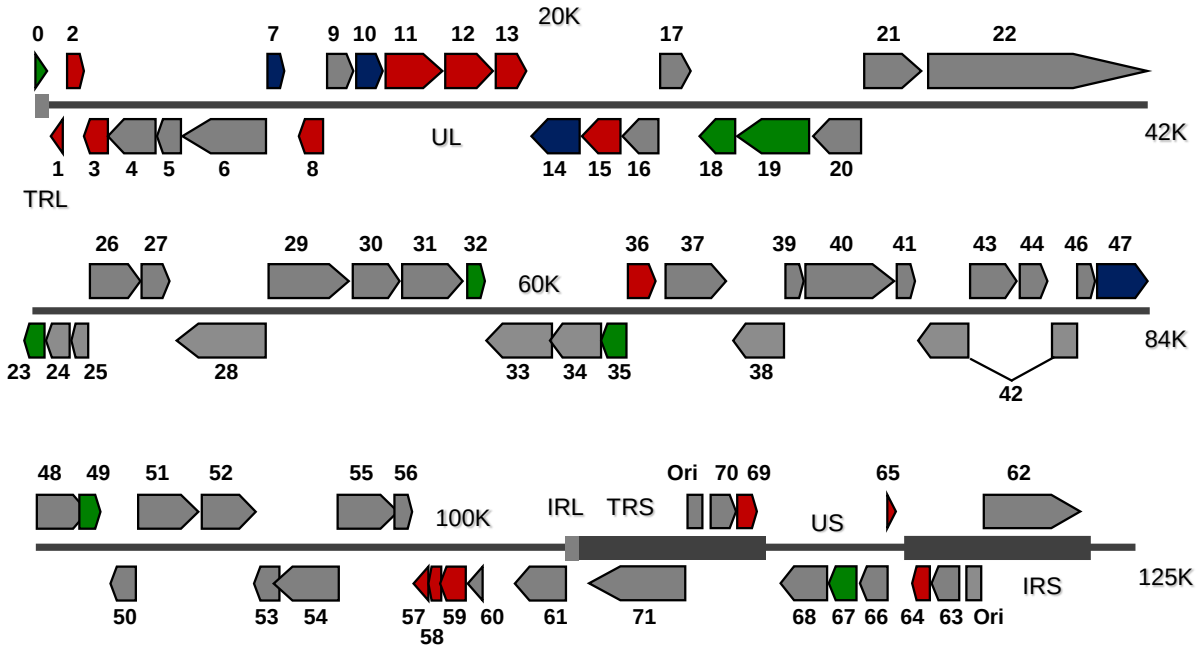

Fig. 2. Genome structure of the VZV. The red colored ORFs represent the genes that are dispensable for the viral replication in permissive melanoma cell line MeWo. The green colored ORFs represent the genes that cause a severe viral replication defect of the related ORF-deletion viral mutants in MeWo and in human fetal skin organ culture. The blue colored ORFs are skin tropic. The gray colored ORFs are essential for the viral replication. The shown scheme is adapted from Zhang et al., 2010.

3.2.3 VZV morphology and DNA replication

The VZ virion is pleomorphic and has a diameter of 180 to 200 nm (Almeida et al., 1962). The VZV capsid includes one copy of the linear double-stranded DNA (dsDNA) which is wound up on a fibrillar protein (Furlong et al., 1972; Puvion-Dutilleul et al., 1987). The virus capsid is formed by twelve pentameric (penton) and 150 hexameric (hexon) capsomers in an icosahedral shape and has a diameter of approximately 80 to 120 nm (Almeida et al., 1962). The outer envelope of the virion is composed of a binary lipid membrane, which is associated

with different VZV-specific glycoproteins. The tegument is localized between the capsid and the envelope, and is described as an amorphous protein layer which is relevant for entry and morphogenesis of herpesviruses (Kinchington et al., 1992, 1995a,b; Stevenson et al., 1994) (Fig. 3). VZV enters the cell either directly by fusion of the viral envelope with the host-cell membrane or indirectly via endocytosis (Zerboni et al., 2014). Viral envelope proteins fuse with the cell membrane through mannose-6-phosphate receptors (Chen et al., 2004; Gabel et al., 1989) or through myelin-associated glycoprotein distributed mainly in neural tissues (Suenaga et al., 2010).

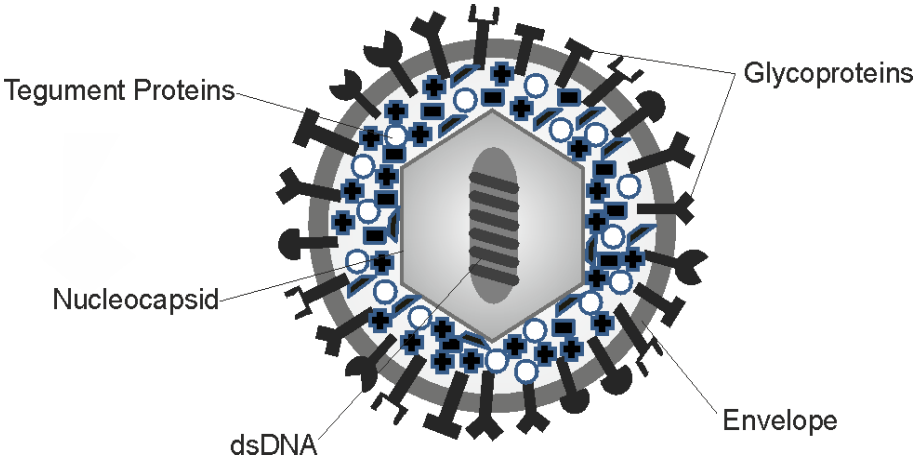

Fig. 3. Structure of the VZV virion. The shown structure is adapted from Arvin et al., 2007.

In addition, the extracellular domain of the VZV glycoprotein gE interacts with the insulin degrading enzyme (IDE) on the surface of the host-cell membrane. Blocking IDE results in a reduced infectivity and cell-to-cell spread of the virus. In non-human cells, the supplementary expression of the human IDE enhances the cellular infection with cell-free and cell-associated VZV. Accordingly, IDE is considered to act as a cellular receptor for VZV and to also promote the important role of gE (Li et al., 2006).

After entry, virions are de-enveloped, tegument proteins are released and distributed throughout the host-cell, and nucleocapsids are transported to the perinuclear space and release the viral genome into the nucleus. The initial viral gene expression is governed by the immediate-early (IE) proteins that have transactivating and transrepressing capabilities (Kinchington et al., 1995a,b). The IE proteins induce the overexpression of further IE genes and, subsequently, also of early (E) genes. Beside other E proteins, the viral DNA polymerase and the DNA-binding protein are essential for the viral DNA replication. Later on in the lytic cycle, the promoters of the late (L) genes are activated which mainly encode structure components such as capsid proteins and glycoproteins. After replication, the viral DNA is packaged into preassembled nucleocapsids. The capsids are coated and de-coated by membranes with glycoproteins as they cross the nuclear membrane towards the cytoplasm and

as they sprout into membrane vesicles from the trans-Golgi network (TGN). Approximately 9 h post infection, nascent enveloped virions are formed, and 3 h later, many of them are detectable at the cell surface of infected cells (Cohen et al., 2007; Reichelt et al., 2009; Zerboni et al., 2014). VZV spreads from cell to cell in a highly cell-associated manner upon fusion of infected and uninfected cells using the same viral entry-specific glycoproteins, forming characteristic syncytia and multinucleated polykaryocytes followed by further virus spread (Grose et al., 2010; Oliver et al., 2013).

3.2.4 Antiviral therapy and VZV vaccine

In healthy children, chickenpox is normally not treated with antiviral drugs since the development of an efficient antiviral immunity is intended. However, in immunosuppressed patients and in adults, chickenpox can induce a remarkable morbidity and mortality. Similarly, shingles show a much higher morbidity in immunodeficient individuals. Moreover, shingles can lead to long-lasting postherpetic neuralgia that can be difficult to control, especially in elderly people. The general use of antiviral nucleoside analogs has greatly improved the outcome (Arvin et al., 2007).

The most commonly used antiviral agent is aciclovir (ACV), a guanosine analog which is a selective replication inhibitor of HSV and VZV (Whitley & Gnann, 1992). ACV is monophosphorylated by the viral enzyme thymidine kinase (TK). This reaction occurs only in infected cells. Cellular kinases are responsible for the diphosphorylation and triphosphorylation steps leading to high concentrations of ACV triphosphate in VZV-infected cells. Viral DNA synthesis is suppressed by ACV triphosphate as a result of its competitive function with deoxyguanosine triphosphate as a viral DNA polymerase substrate and of the chain termination after its incorporation into the replicating virus DNA. The incorporation of ACV triphosphate into cellular DNA is unusual, since the cellular DNA polymerase has a much lower affinity to ACV triphosphate than the viral DNA polymerase (Arvin et al., 2007). However, defined mutations in the TK and/or DNA polymerase of VZV lead to therapy resistance to nucleoside analogs such as ACV (Andrei et al., 2012; Brunnemann et al., 2015). In this case, foscarnet is mostly used which blocks the pyrophosphate binding site leading to a suppression of viral DNA polymerase (Wagstaff & Bryson, 1994).

In order to prevent individuals from varicella and herpes zoster, the live-attenuated vaccine strain v-Oka is generally recommended for infants and susceptible healthy persons in many countries including Germany (Hambleton & Gershon, 2005; Krause & Klinman, 1995, 2000). The v-Oka strain was developed in Japan in the early 1970s (Takahashi et al., 1974). The varicella vaccine has been used in the United States since 1995 and has been highly effective in reducing varicella incidence, morbidity, and mortality (Vázquez et al., 2001). Moreover, a high-dose variant of the vaccine is used to reduce zoster morbidity in latently

infected elderly individuals. The shingles vaccine has shown 51.3% efficacy in decreasing herpes zoster occurrence, 66.6% efficacy in decreasing the occurrence of postherpetic neuralgia (mainly due to prohibiting herpes zoster), and 61.1% efficacy in decreasing the zoster-associated disease burden (Oxman & Levin, 2008; Oxman et al., 2005; Sperber et al., 1992). Although this vaccine is fully approved, it is not yet recommended for the general use in Germany by the permanent vaccination commission (Ständige Impfkommission, STIKO).

Recently, in October 2017, a novel adjuvanted VZV subunit vaccine (HZ/su) against herpes zoster has been approved by the food and drug administration of the United States. This vaccine consists of the recombinant VZV glycoprotein gE and a liposome-based adjuvant system (AS01B) containing 3-O-desacyl-4′-monophosphoryl lipid A (MPL) and the saponin QS-21. This vaccine has been shown to lower the risk of shingles and postherpetic neuralgia in persons 50 years of age and older and also to be more effective and less expensive than the live-attenuated herpes zoster vaccine (Chlibek et al., 2013; Cunningham et al., 2016; Lal et al., 2015; Le & Rothberg, 2018).

3.3 Axonal transport

3.3.1 Neurons and axonal transport

The main function of a neuron is to receive, conduct, and transport signals between the periphery and the central nervous system (CNS). The cell bodies of the nerve cells (somata) gather in clusters called ganglia which serve as communication centers between the periphery and the CNS. These communications are conducted through elongated extensions of the somata known as axons which transmit the signals from cell to cell at specific connection sites called synapses. When a neuron transmits sensory signals to the CNS, it is called a sensory neuron. Somata of the sensory neurons are clustered in the trigeminal and dorsal root ganglia located outside the CNS to which they transport the sensory signals (Alberts et al., 1989; Kandel et al., 2013). Cellular proteins are transported along the microtubules of neuronal axons either in the anterograde orientation toward the axonal endings or in the opposite, retrograde direction toward the somata. These proteins are categorized into two groups according to their rates of transport. Proteins, such as adenosine triphosphatase ATPase, nerve growth factor (NGF), and membranous organelles are transported at rates of 0.5-4 µm/s (fast axonal transport). Other proteins, such as actin, tubulin, and proteins of the cytoplasmic matrix are transported at rates of 0.01-0.05 µm/s (slow axonal transport; Lasek et al., 1984). These cellular proteins are transported along the microtubules of neural axons via two major motor proteins known as kinesins and dyneins. While kinesins are responsible for the anterograde axonal transport, dyneins govern mainly the retrograde axonal transport (Goldstein & Yang, 2000).

3.3.2 Axonal transport of α-herpesviruses

For the α-herpesviruses HSV-1 and the porcine pseudorabies virus (PrV), there is the plausible consensus that the viral capsid travel in retrograde direction without envelope using specific dynein-associated viral tegument proteins. In contrast, the anterograde axonal transport mechanisms seem to be more controversial leading to the different so-called “married” and “unmarried” (separate) axonal transport models. This results in the open question if the viral capsid of a herpesvirus travels with or without envelope in the axon (Diefenbach et al., 2008). Nevertheless, it was suggested that PrV capsids migrate according to the “married” model with envelope in anterograde axonal direction. Generally, a similar anterograde axonal transport model seems to be probable for HSV-1, assuming that both α-herpesviruses share the same axonal transport mechanisms (Diefenbach et al., 2008; Kratchmarov et al., 2012).

3.3.3 Axonal transport of VZV and relevant proteins

Unlike its close relatives HSV-1 and PrV whose axonal transport mechanisms have been extensively studied, the axonal transport of VZV is still poorly investigated due to the highly cell-associated spread of the infection in culture and the lack of an appropriate animal model (Steain et al., 2010). However, kinetic analysis of VZV expressing the capsid protein p23 (encoded by ORF23) in fusion with the enhanced green fluorescent protein (eGFP) showed that the movement of viral capsids/virions within axons of retrogradely VZV-infected sensory neuron-like cells is discontinuous and bidirectional with a net retrograde motion (Grigorian et al., 2012). These data, which were generated with in-vitro neuron-like cells differentiated human embryonal stem cells, suggest consistency with the axonal dynamics of capsids/ virions of HSV-1 and PrV according to the homology of ORF23 to VP26 of HSV-1 and to UL35 of PrV (Antinone & Smith, 2010; Smith et al., 2001).

VZV ORF65 encodes the envelope transmembrane protein type II p65 that is known to be neither essential for the virus replication in vitro, nor for the infection of human skin and T-cells in vivo (Cohen et al., 2001; Niizuma et al., 2003). This protein shares the topology and the cellular localization in infected cells of its homologous US9 proteins of HSV-1 and PrV. The so called “axonal guidance” US9 proteins, in turn, play an essential role in anterograde transport and virus assembly in neuronal cells suggesting that VZV p65 would play the same role (DuRaine et al., 2017; Lyman et al., 2008, 2009; Miranda-Saksena et al., 2016).

The immediate early protein IE4 of VZV, encoded by ORF4, is a tegument phosphoprotein conserved among all α-herpesviruses. It transactivates genes of all three phases of the virus replication cycle and was shown to be essential for the viral replication in vitro (Sato et al., 2003). IE4 has also been marked as a potential alternative antiviral target as a nucleocytoplasmic shuttling protein for mRNA export (Ote et al., 2010). Furthermore, cotton rats inocu-

lated with ORF4-null VZV revealed the critical role of IE4 in the establishment of latency in DRG (Cohen et al., 2005).

Understanding the axonal transport patterns of IE4 as a component of the tegument and of p65 as an envelope protein would help to understand the type of axonal transport of VZV particles in anterograde and retrograde infections of DRG neurons.

3.4 Mutagenesis of herpesvirus genomes

Herpesviruses have large linear double-stranded DNA genomes, the smallest of which belongs to VZV with a 125 kb genome encoding approximately 72 genes (Davison & Scott, 1986; McGeoch et al., 2006). This size of the genome hampered the development of efficient strategies for the manipulation of the viral genome. However, several genetic methods have been developed that enable the manipulation of most genes of interest.

The method of the cosmid complementation (van Zijl et al., 1988) formed the basic step. In this technique, several overlapping cosmids are used, each of which harbors one part of the entire viral genome that can be mutated in *Escherichia (E.) coli* cells. At the end, all cosmid-cloned segments of the viral genome with overlapping sequences are co-transfected into permissive eukaryotic cells. Due to the recombination between the overlapping homologous regions, the whole genome is reassembled enabling virus reconstitution with the desired mutations. Nevertheless, during the recombination process undesired mutations may occur, which are difficult to be excluded (van Zijl et al., 1988).

Later on, the use of bacterial artificial chromosomes (BAC) made it greatly easier to study and manipulate the viral genes (Shizuya et al., 1992). The BAC vectors are able to carry foreign DNA segments up to 300 kb which permits to clone any herpesvirus genome at once. The vector part includes a resistance gene, an origin of replication, and all required genes from the bacterial F-plasmid (mini-F) that allows the BAC-DNA to be maintained in just one to two copies in bacterial cells. In general, the vector (mini-F) is transfected into eukaryotic cells, either infected with the virus, or alternatively, together with appropriately mutated viral cosmid clones. Through homologous recombination between the vector segment and the viral genome, the vector is inserted into a non-coding position of the viral DNA. Since the DNA is circularized during the replication process, the constructed BAC can then be extracted from the eukaryotic cells and transfected into bacterial cells (Brune et al., 2000; Messerle et al., 1997; Wagner et al., 2002). BACs can be specifically manipulated in bacteria by homologous recombination. Based on these principles, an infectious BAC-clone was prepared from the wild-type isolate HJO of VZV (Schmidt, 2005; Wussow et al., 2009).

The ET cloning method enables the specific and efficient mutagenesis of the BAC-cloned viral genome. Specific mutations are introduced into the viral genome via homologous re-

combination of 50 bp sequences by the RecET proteins. In addition, a selection gene (antibiotic resistance gene) is required in order to allow the selection for the clones, in which the recombination took place. Such selection genes have often been flanked by loxP sequences. These marker genes can then be eliminated through inducible Cre-recombinase activity (Muyrers et al., 1999; Zhang et al., 1998).

In 2006, Tischer et al. developed another novel method, which enables the insertion of small or large sequences into the viral genome, or point mutations, or the deletion of entire genes without leaving behind any unwanted external operational sequences. This technique was termed “en-passant mutagenesis” and is based on two consequent, Red-protein mediated homologous recombination steps.

In the case of a fusion of an ORF with a fluorescent protein, a polymerase-chain reaction (PCR) product is first amplified which includes a selective marker (kanamycin resistance, kan^R), the specific recognition sequence (18 bp) for the endonuclease I-SceI, and fluorescent protein sequences with a homologous 50 bp-duplicated region. These segments are flanked by duplicated 50 bp sequences flanking the ORF fusion site. The PCR product is then electroporated into bacteria, namely the *E. coli* strain GS1783. The genome of this bacterial strain encodes the Red proteins exo, beta, and gam, the selection enzyme, and also the inducible endonuclease I-SceI.

During the first Red recombination step, the PCR product is fused to the ORF of interest as a result of the homologous recombination of the homologous 50 bp sequences of the fusion site. The recombinant clone is then selected on agar plates containing kanamycin as selective drug. During the second Red recombination step, the endonuclease I-SceI is induced. Consecutively, the kanamycin resistance cassette can be removed from the selected recombinant after homologous recombination of the homologous 50 bp sequences of the fluorescent protein, resulting in the viral mutant BAC with the targeted fusion without any further changes (Fig. 4) (Tischer et al., 2006).

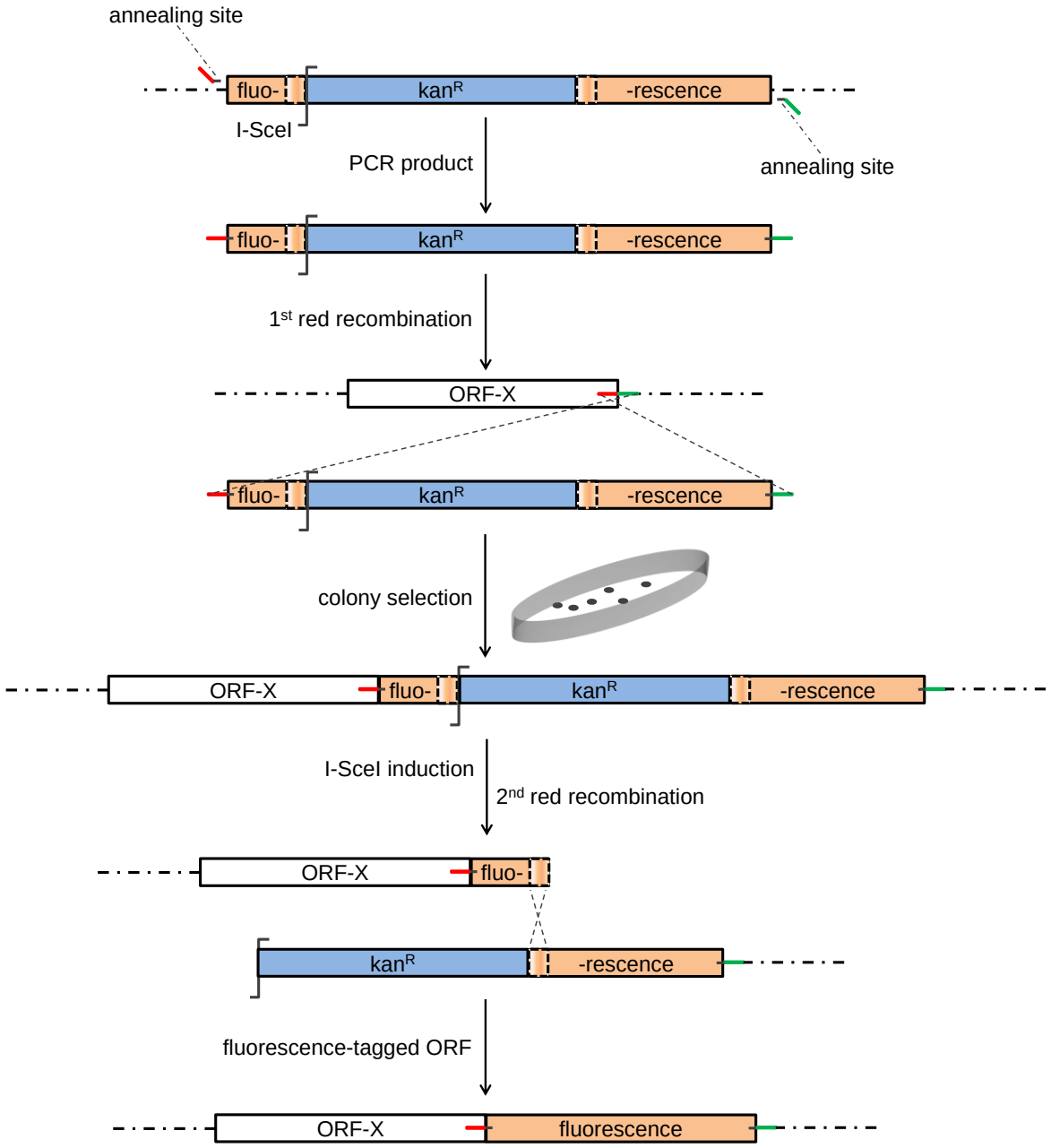

Fig. 4. En-passant mutagenesis. Generation of a gene fusion between a viral ORF and a fluorescent protein. First, a PCR product is amplified containing fluorescent protein sequences with a homologous 50 bp duplicated region (dash-framed regions), a positive selection marker (kan^R), and an I-SceI recognition site with primers of two 50 bp homologous extensions of the corresponding ORF fusion site (red and green bars). After the first recombination, the ORF of interest is fused to the PCR product and then positive clones are selected out on agar plate with kanamycin. Finally, upon I-SceI induction via arabinose, a double strand break occurs at the I-SceI site causing the elimination of the kan^R and a subsequent fusion of the fluorescent protein to the ORF of interest due to homologous recombination of the homologous regions (dash-framed highlighted boxes). The generated BAC carries the targeted fusion, however, without any additional changes. The scheme is adapted from Tischer et al., 2006.

3.5 Aims of the study

Varicella-zoster virus (VZV) has evolved mechanisms for its infection of sensory neurons and subsequent transport along microtubules of neuronal axons of the dorsal root ganglia (DRG). Understanding these poorly studied mechanisms is highly relevant to identify and target the

key viral genes and proteins in order to prevent the virus from going latent in DRG or to block its reactivation from latency. In the present study, embryonic Wistar rat DRG neurons shall be efficiently and productively infected with fluorescence-labeled double mutant models of VZV using compartmentalized cultivation systems, in order to trace the axonal colocalization of VZV proteins. For this purpose, a cloned BAC of the European wild-type genome HJO of VZV shall be used to generate two double mutants via en-passant mutagenesis. In these two double mutants, the protein of interest (IE4 or p65) and the capsid protein p23 of VZV shall be fused either to the enhanced green fluorescent protein (eGFP) or to the monomeric red fluorescent protein (mRFP). Productive anterograde and retrograde infections of DRG neurons shall be achieved by the exposure to high titers of cell-free VZV of 10^4-10^5 plaque forming units PFU/ml. Consecutively, the axonal colocalization of IE4 and p65 together with the capsid protein p23 shall be observed and, accordingly, the axonal transport models of VZV have to be analyzed and discussed. With this regard, this study aims to open the way for further investigations into the axonal transport mechanisms of VZV and into the role of the relevant viral proteins as possible medicinal intervention targets in preventing or treating VZV infection and its complications.

4 RESULTS

4.1 Generation of double-color viral mutant BACs

Double fluorescence-labeled VZV was used as a model to study the colocalization patterns of viral proteins within axons of embryonic Wistar rat DRG neurons after anterograde and retrograde infections with VZV. In this study, the colocalization patterns were investigated concerning the tegument protein IE4 and the envelope transmembrane protein p65 of VZV together with the capsid protein p23 that served as an axonal reference protein, in order to understand more the axonal transport models of the VZV particles. For this purpose, two double fluorescence-tagged viral mutant BACs were at first generated in which ORF4 or ORF65 and ORF23 were fused either to eGFP or to mRFP moiety.

4.1.1 BAC mutant pHJOpac-eGFP4-mRFP23

Using the cloned European wild-type VZV BAC of HJO isolate (pHJOpac) (Wussow et al., 2009), the viral BAC construct pHJOpac-eGFP4 was initially cloned in a previous project (Fig. 5, Spieckermann, Dissertation, 2013). In this construct, eGFP was fused to the N-terminus of ORF4 via en-passant mutagenesis (Tischer et al., 2006).

In the present study, pHJOpac-eGFP4 was manipulated via en-passant mutagenesis, in order to generate the double fluorescently labeled BAC pHJOpac-eGFP4-mRFP23 (Fig. 6). For this purpose, the transfer-vector pEP-mRFP1-in (Tischer et al., 2006) was used as a template for the amplification of a PCR product composed of the mRFP sequences, the positive selection marker (kanamycin resistance, Kan^R), and the I-SceI recognition site with specific primers (Tab. 15). These primers bind to the homologous extensions of the fusion site at the N-terminal end of ORF23 (Fig. 6, green and blue bars). The amplified PCR product (1762 bp) was then purified and electroporated into *E. coli* GS1783 harboring the BAC-cloned genome of pHJOpac-eGFP4 (Fig. 6). After the first Red-recombination step, bacterial colonies from agar plates with kanamycin selection were tested by colony PCR for signals indicating the correct recombination products. This PCR was performed with two primers, one of which binds within the kan^R gene and the other one downstream of the insertion position. DNA fragments of 604 bp were visualized by gel electrophoresis and indicated colonies that carried the presumably correct recombination product (data not shown).

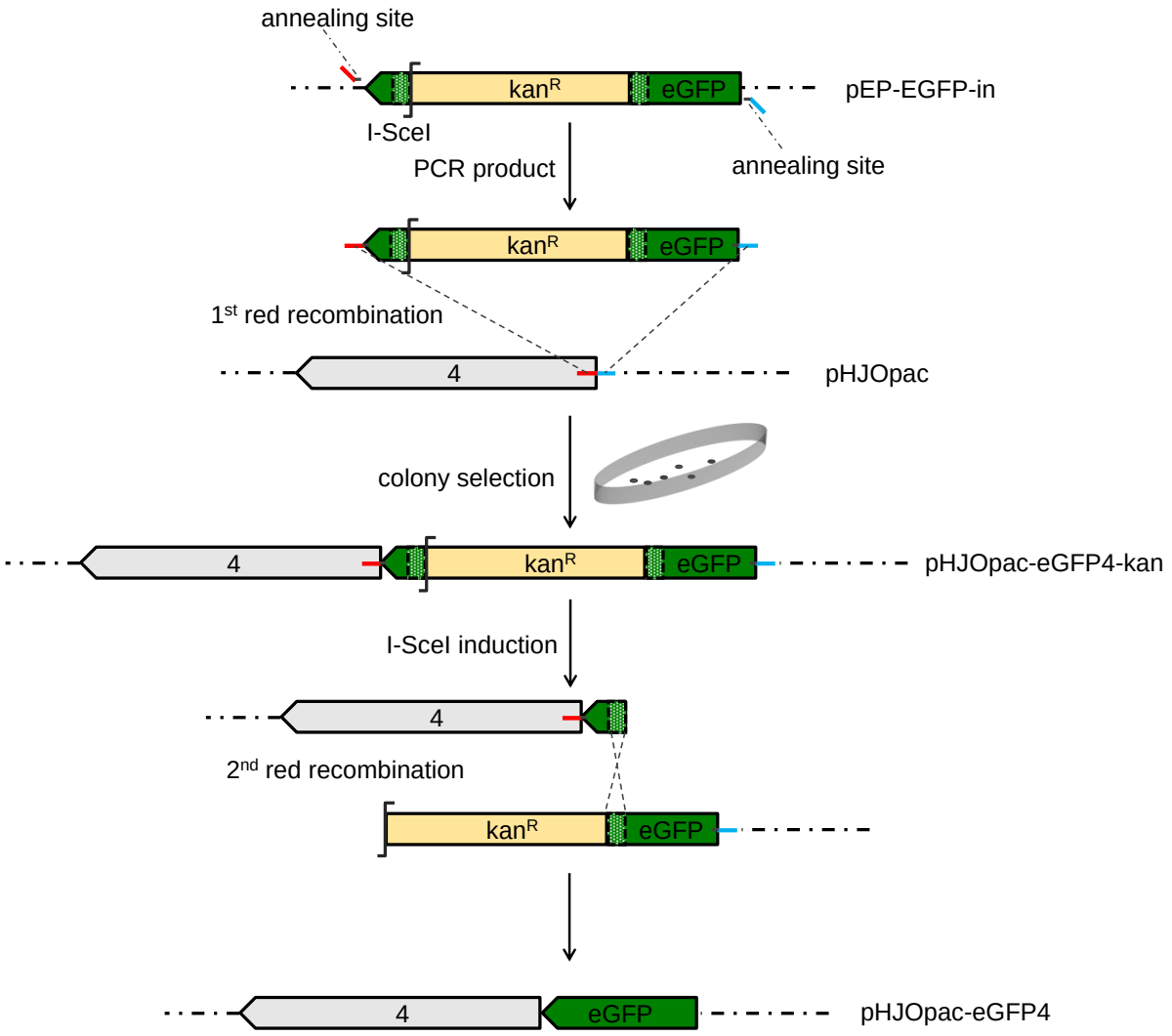

Fig. 5. Generation of pHJOpac-eGFP4 by en-passant mutagenesis. Using the vector pEP-EGFP-in, a PCR product was amplified containing eGFP sequences with a homologous 50 bp duplicated region (dash-framed regions), a positive selection marker (kan^R), and an I-SceI recognition site with primers of two 50 bp homologous extensions of the fusion site at ORF4 (red and blue bars). The resulted PCR product was then electroporated into *E. coli* harboring pHJOpac. After the first recombination, ORF4 was fused to the PCR product and then positive clones were selected out on agar plate with kanamycin. Finally, upon I-SceI induction via arabinose, a double strand break occurs at the I-SceI site causing the elimination of the kan^R and a subsequent fusion of eGFP to the N-terminus of ORF4 due to homologous recombination of the homologous sequences (dash-framed regions), however, without leaving any additional changes in the genome.

In order to confirm that the presumably positive colonies contain intact genomes except the insertion of the fusion sequences, the BAC-cloned genome of pHJOpac-eGFP4 (pG4) and the resulting BAC genome pHJOpac-eGFP4-mRFP23-kan (pG4R23-kan) were tested via restriction fragment length polymorphism (RFLP) analysis by digestion with the restriction enzymes HindIII and XhoI (Fig. 7).

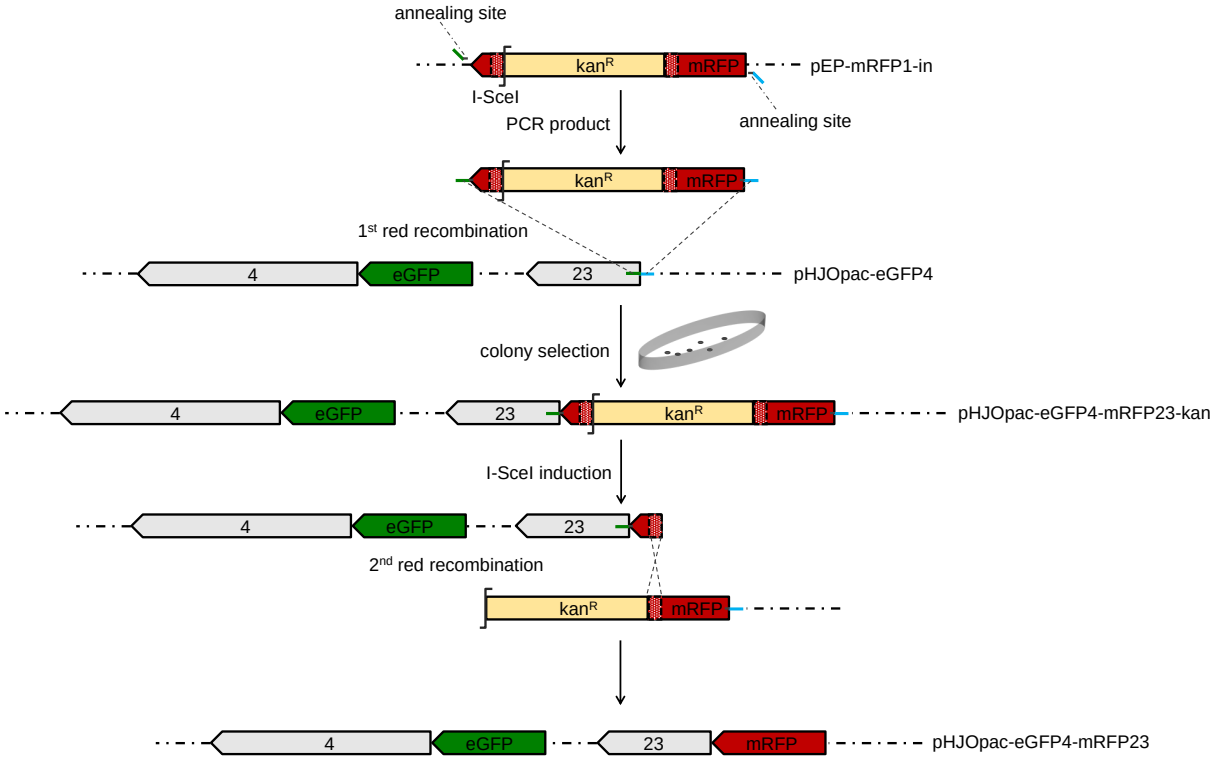

Fig. 6. Generation of pHJOpac-eGFP4-mRFP23 by en-passant mutagenesis. Using the vector pEP-mRFP1-in, a PCR product was amplified containing mRFP sequences with a homologous 50 bp duplicated region (dash-framed regions), a positive selection marker (kan^R), and an I-SceI recognition site with primers of two 50 bp homologous extensions of the fusion site at ORF23 (green and blue bars). The resulted PCR product was then electroporated into *E. coli* harboring pHJOpac-eGFP4. After the first recombination, ORF23 was fused to the PCR product and then positive clones were selected out on agar plate with kanamycin. Finally, upon I-SceI induction via arabinose, a double strand break occurs at the I-SceI site causing the elimination of the kan^R and a subsequent fusion of mRFP to the N-terminus of ORF23 due to homologous recombination of the homologous sequences (dash-framed regions), however, without leaving any additional changes in the genome.

The previously confirmed positive colony (Fig. 7, pG4R23-kan) was used for the second step of Red-recombination. Similarly, the colonies that were grown on agar plates with arabinose (in order to induce I-SceI expression) and without kanamycin were tested by colony PCR with two primers, one of which binds within the mRFP gene and the other one downstream of the fusion position (Tab. 15). DNA fragments of 978 bp were observed by gel electrophoresis referring to putatively positive colonies (data not shown).

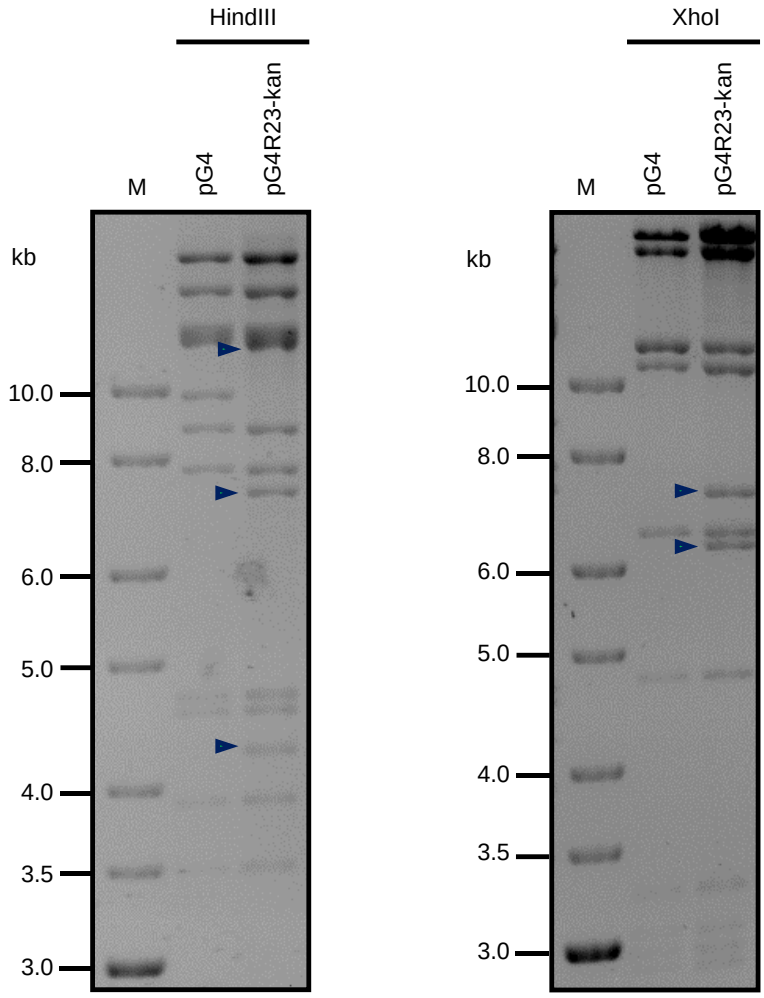

Fig. 7. RFLP analysis of pHJOpac-eGFP4-mRFP23-kan. RFLP analysis of HindIII- and XhoI-digested DNA of pHJOpac-eGFP4-mRFP23-kan (pG4R23-kan) in comparison to pHJOpac-eGFP4 (pG4) as control. The arrows indicate the DNA fragments confirming the colony harboring the expected BAC-cloned genome. Marker (M). Kilobase pairs (kb).

For the confirmation of the positive colonies, RFLP analysis was performed based on restriction enzyme digestion of the BAC-cloned pG4R23-kan and the resulting BAC-clones, presumably of pHJOpac-eGFP4-mRFP23 (pG4R23), with HindIII and XhoI restriction enzymes (Fig. 8). Finally, the region was PCR-amplified flanking the OFR23 fusion site in the newly generated mutant BAC pHJOpac-eGFP4-mRFP23. The sequence analysis did not show mutations at the fusion site and in its flanking region (data not shown). This indicated that this construct was appropriate for the further experiments.

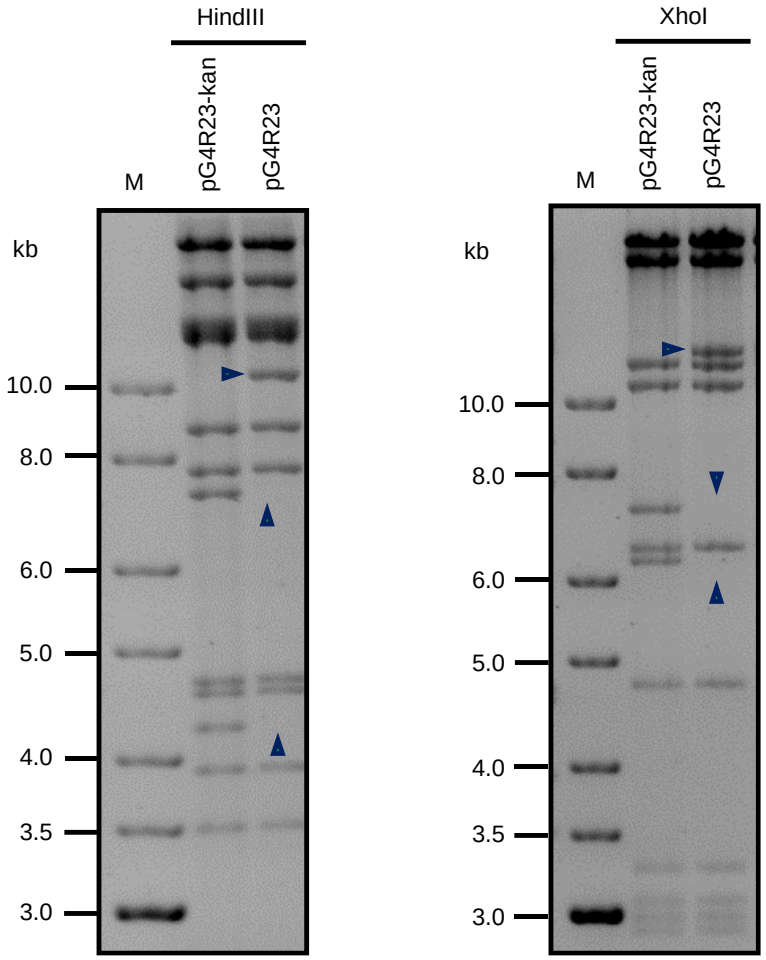

Fig. 8. RFLP analysis of pHJOpac-eGFP4-mRFP23. RFLP analysis of HindIII- and XhoI-digested DNA of pHJOpac-eGFP4-mRFP23 (pG4R23) in comparison to pHJOpac-eGFP4-mRFP23-kan (pG4R23-kan) as control. The arrows indicate the presence or absence of DNA fragments confirming the colony harboring the expected BAC-cloned genome.

4.1.2 BAC mutant pHJOpac-eGFP23-mRFP4

The second construct also carried two different fused reading frames, the first one between eGFP and ORF23 and the second one between mRFP and ORF4. Starting again with the cloned BAC of the wild-type HJO of VZV (pHJOpac), the viral BAC construct pHJOpac-eGFP23 was initially cloned via en-passant mutagenesis, in which eGFP was fused to the N-terminus of ORF23 (Fig. 9, Spieckermann, Dissertation, 2013).

Here, pHJOpac-eGFP23 was manipulated via en-passant mutagenesis, in order to generate the double fluorescently labeled BAC pHJOpac-eGFP23-mRFP4 (Fig. 10). For this purpose, the transfer-vector pEP-mRFP1-in was used as a template for the amplification of a PCR product composed of the mRFP sequences, the positive selection marker (kanamycin resistance, Kan^R), and the I-SceI recognition site with specific primers (Tab. 15). These primers bind to the homologous extensions of the fusion site at the N-terminal end of ORF4 (Fig. 10, green and blue bars).

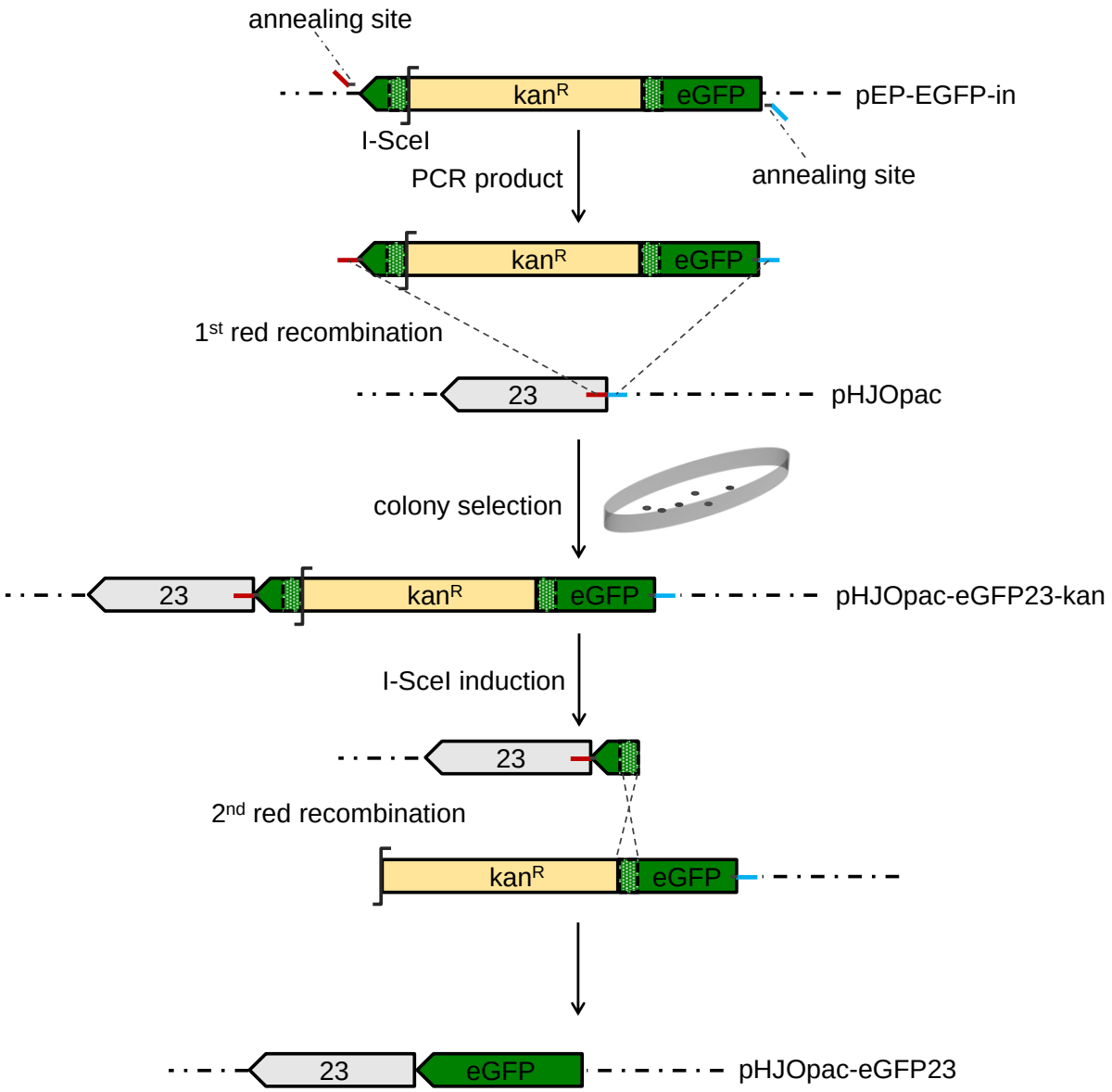

Fig. 9. Generation of pHJOpac-eGFP23 by en-passant mutagenesis. Using the vector pEP-EGFP-in, a PCR product was amplified containing eGFP sequences with a homologous 50 bp duplicated region (dash-framed regions), a positive selection marker (kan^R), and an I-SceI recognition site with primers of two 50 bp homologous extensions of the fusion site at ORF23 (red and blue bars). The resulted PCR product was then electroporated into *E. coli* harboring pHJOpac. After the first recombination, ORF23 was fused to the PCR product and then positive clones were selected out on agar plate with kanamycin. Finally, upon I-SceI induction via arabinose, a double strand break occurs at the I-SceI site causing the elimination of the kan^R and a subsequent fusion of eGFP to the N-terminus of ORF23 due to homologous recombination of the homologous sequences (dash-framed regions), however, without leaving any additional changes in the genome.

The amplified PCR product (1821 bp) was then purified and electroporated into *E. coli* GS1783 harboring the BAC-cloned genome of pHJOpac-eGFP4 (Fig. 10). After the first Red-recombination step, bacterial colonies from agar plates with kanamycin selection were tested by colony PCR for signals indicating the correct recombination products. This PCR was performed with two primers, one of which binds within the kan^R gene and the other one downstream of the insertion position. DNA fragments of 662 bp were visualized by gel elec-

trophoresis and indicated colonies that carried the presumably correct recombination product (data not shown).

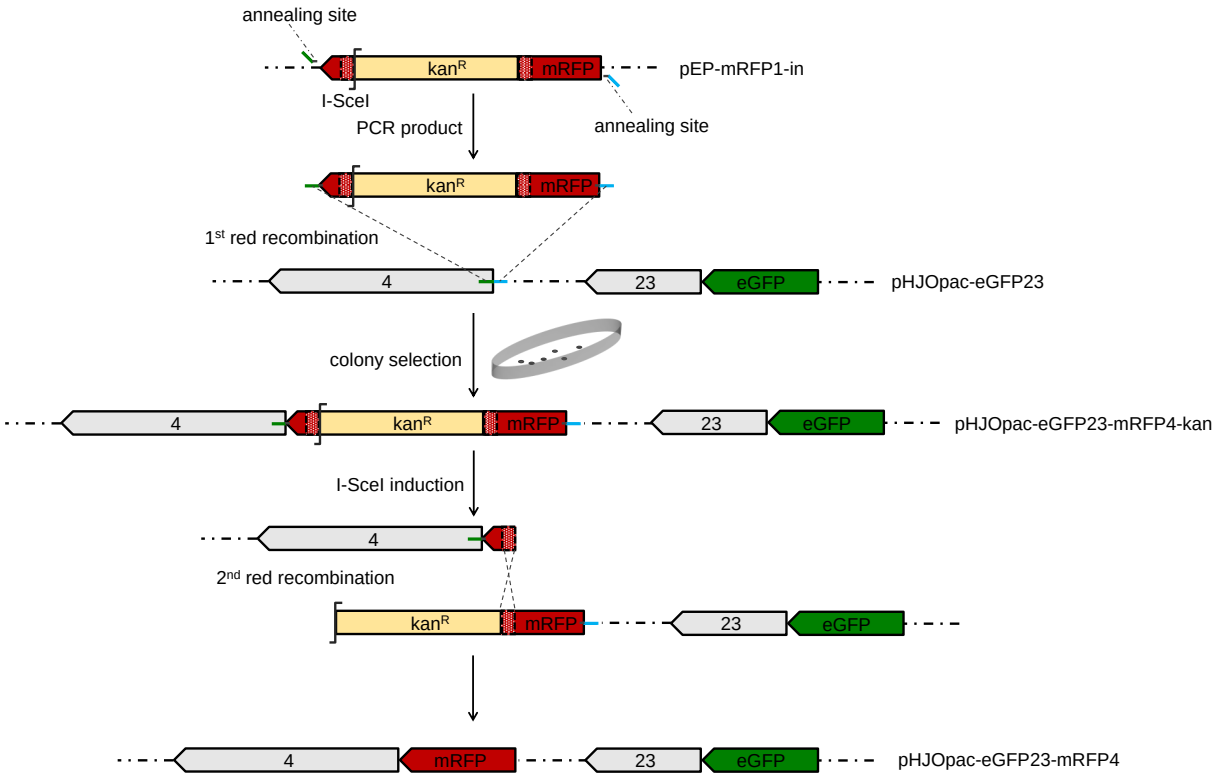

Fig. 10. Generation of pHJOpac-eGFP23-mRFP4 by en-passant mutagenesis. Using the vector pEP-mRFP1-in, a PCR product was amplified containing mRFP sequences with a homologous 50 bp duplicated region (dash-framed regions), a positive selection marker (kan^R), and an I-SceI recognition site with primers of two 50 bp homologous extensions of the fusion site at ORF4 (green and blue bars). The resulted PCR product was then electroporated into *E. coli* harboring pHJOpac-eGFP23. After the first recombination, ORF4 was fused to the PCR product and then positive clones were selected out on agar plate with kanamycin. Finally, upon I-SceI induction via arabinose, a double strand break occurs at the I-SceI site causing the elimination of the kan^R and a subsequent fusion of mRFP to the N-terminus of ORF4 due to homologous recombination of the homologous sequences (dash-framed regions), however, without leaving any additional changes in the genome.

In order to confirm that the presumably positive colonies contain intact genomes except the insertion of the fusion sequences, the BAC-cloned genome of pHJOpac-eGFP23 (pG23) and the resulting BAC genome pHJOpac-eGFP23-mRFP4-kan (pG23R4-kan) were tested via RFLP analysis by digestion with the restriction enzymes BglII and XhoI (Fig. 11).

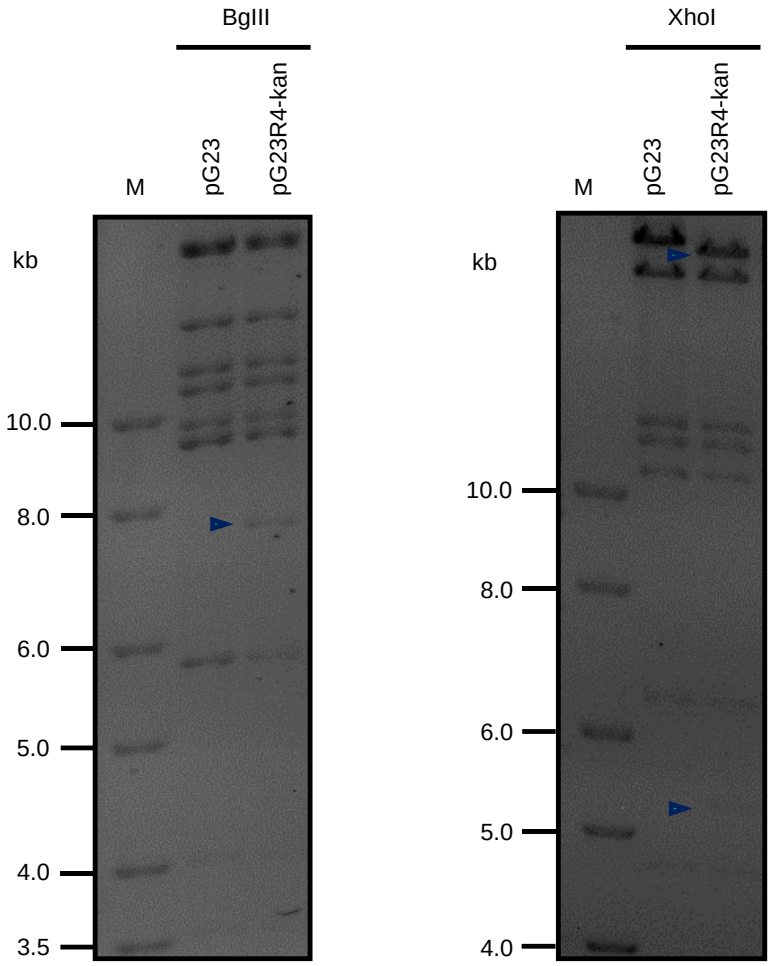

Fig. 11. RFLP analysis of pHJOpac-eGFP23-mRFP4-kan. RFLP analysis of BglII- and XhoI-digested DNA of pHJOpac-eGFP23-mRFP4-kan (pG23R4-kan) in comparison to pHJOpac-eGFP23 (pG23) as control. The arrows indicate the DNA fragments confirming the colony harboring the expected BAC-cloned genome.

The previously confirmed positive colony (Fig. 11) was used for the second step of Red-recombination. Similarly, the colonies that were grown on agar plates with arabinose (in order to induce I-SceI expression) and without kanamycin were tested by colony PCR with two primers, one of which binds within the mRFP gene and the other one downstream of the fusion position (Tab. 15). DNA fragments of 878 bp were observed by gel electrophoresis referring to putatively positive colonies (data not shown). For the confirmation of the positive colonies, RFLP analysis was performed based on restriction enzyme digestion of the BAC-cloned pG23R4-kan and the resuling BAC-clones, presumably of pHJOpac-eGFP23-mRFP4 (pG23R4), with BglIII and XhoI restriction enzymes (Fig. 12). Finally, the region was PCR amplified flanking the OFR4 fusion site in the newly generated viral mutant BAC pHJOpac-eGFP23-mRFP4. The sequence analysis showed no mutations at the fusion site and in its flanking region (data not shown). This indicated that this construct was appropriate for the further experiments.

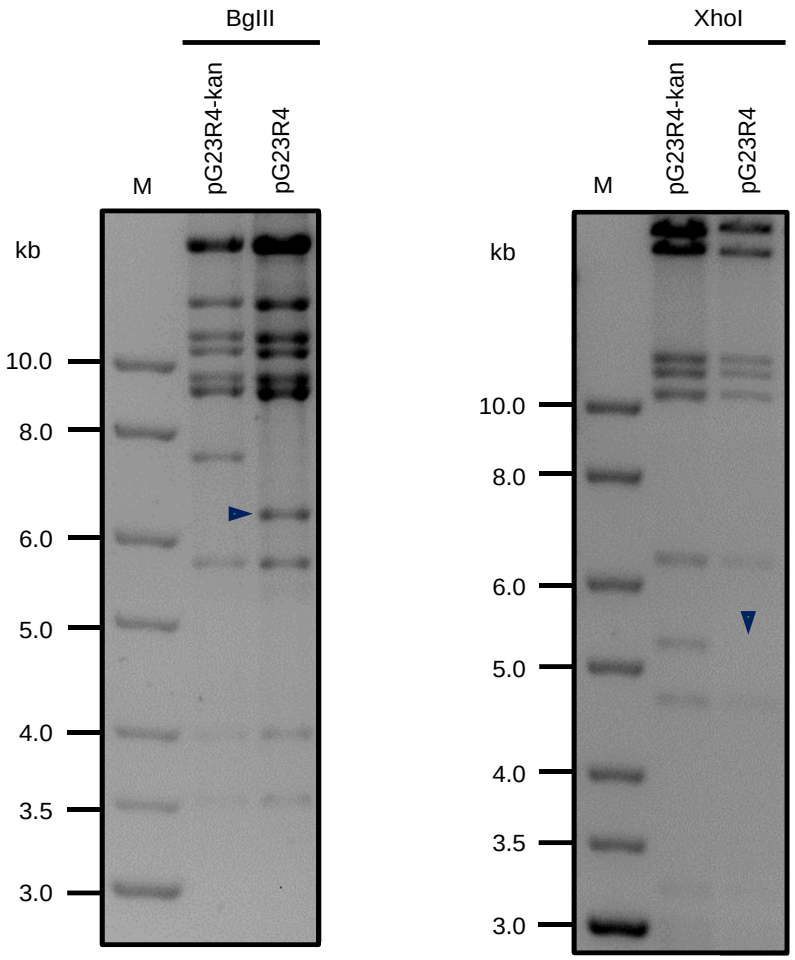

Fig. 12. RFLP analysis of pHJOpac-eGFP23-mRFP4. RFLP analysis of BglII- and XhoI-digested DNA of pHJOpac-eGFP23-mRFP4 (pG23R4) in comparison to pHJOpac-eGFP23-mRFP4-kan (pG23R4-kan) as control. The arrows indicate the presence or absence of DNA fragments confirming the colony harboring the expected BAC-cloned genome.

4.1.3 BAC mutant pHJOpac-eGFP23-4mRFP

As described above for the previously generated BAC pHJOpac-eGFP23-mRFP23 (Fig. 10), the next double-labeled BAC was cloned from pHJOpac-eGFP23 via en-passant mutagenesis, however, in which mRFP was fused to the C-terminal end of ORF4 to generate the double fluorescence-tagged BAC pHJOpac-eGFP23-4mRFP (Fig. 13). In order to clone this construct, pEP-mRFP1-in transfer-vector was used as a template for the amplification of a PCR product composed of the mRFP sequences, the positive selection marker (kanamycin resistance, Kan^R), and the I-SceI recognition site with specific primers (Tab. 15). These primers bind to the homologous extensions of the fusion site at the C-terminus of ORF4 (Fig. 13, green and blue bars).

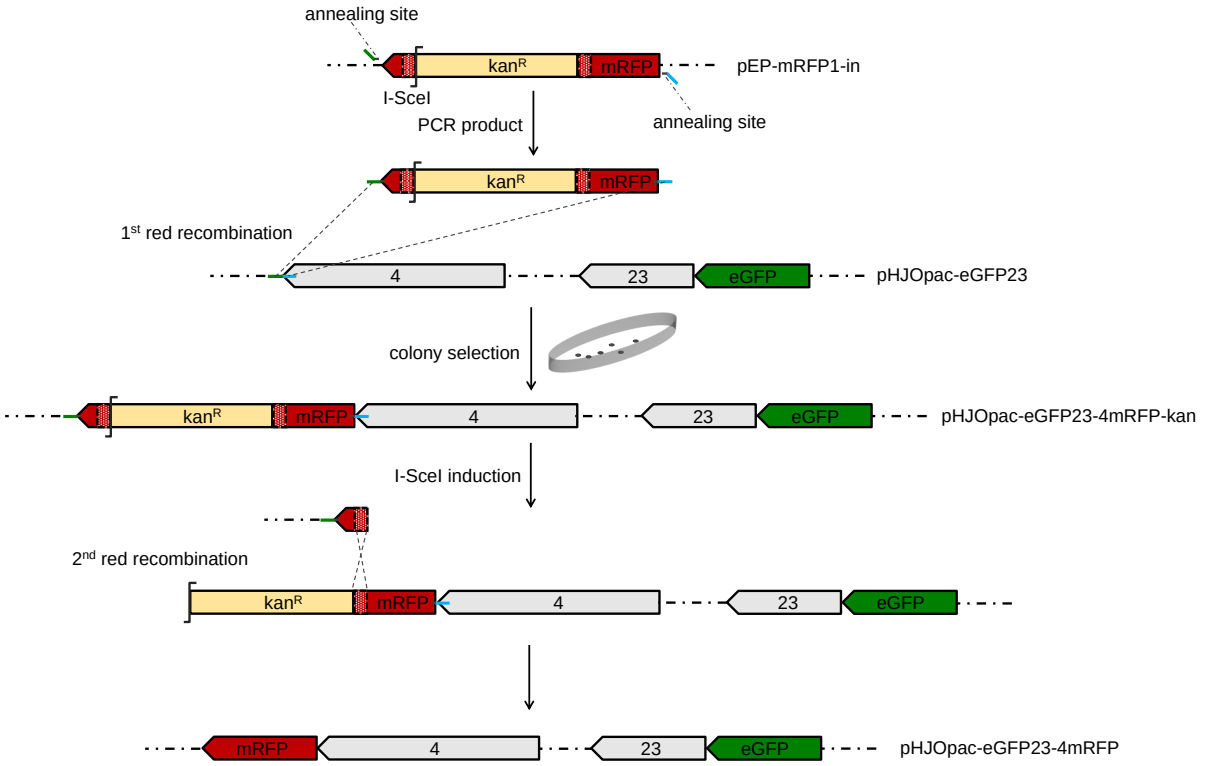

Fig. 13. Generation of pHJOpac-eGFP23-4mRFP by en-passant mutagenesis. Using the vector pEP-mRFP1-in, a PCR product was amplified containing mRFP sequences with a homologous 50 bp duplicated region (dash-framed regions), a positive selection marker (kan^R), and an I-SceI recognition site with primers of two 50 bp homologous extensions of the fusion site at ORF4 (green and blue bars). The resulted PCR product was then electroporated into *E. coli* harboring pHJOpac-eGFP23. After the first recombination, ORF4 was fused to the PCR product and then positive clones were selected out on agar plate with kanamycin. Finally, upon I-SceI induction via arabinose, a double strand break occurs at the I-SceI site causing the elimination of the kan^R and a subsequent fusion of mRFP to the C-terminal end of ORF4 due to homologous recombination of the homologous sequences (dash-framed regions), however, without leaving any additional changes in the genome.

The amplified PCR product (1821 bp) was then purified and electroporated into *E. coli* GS1783 harboring the BAC-cloned genome of pHJOpac-eGFP4 (Fig. 13). After the first Red-recombination step, bacterial colonies from kanamycin selection agar plates were tested by colony PCR for signals indicating the correct recombination products. This PCR was performed with two primers, one of which binds within the kan^R gene and the other one upstream of the insertion position. DNA fragments of 684 bp were visualized by gel electrophoresis and indicated colonies that carried the presumably correct recombination product (data not shown).

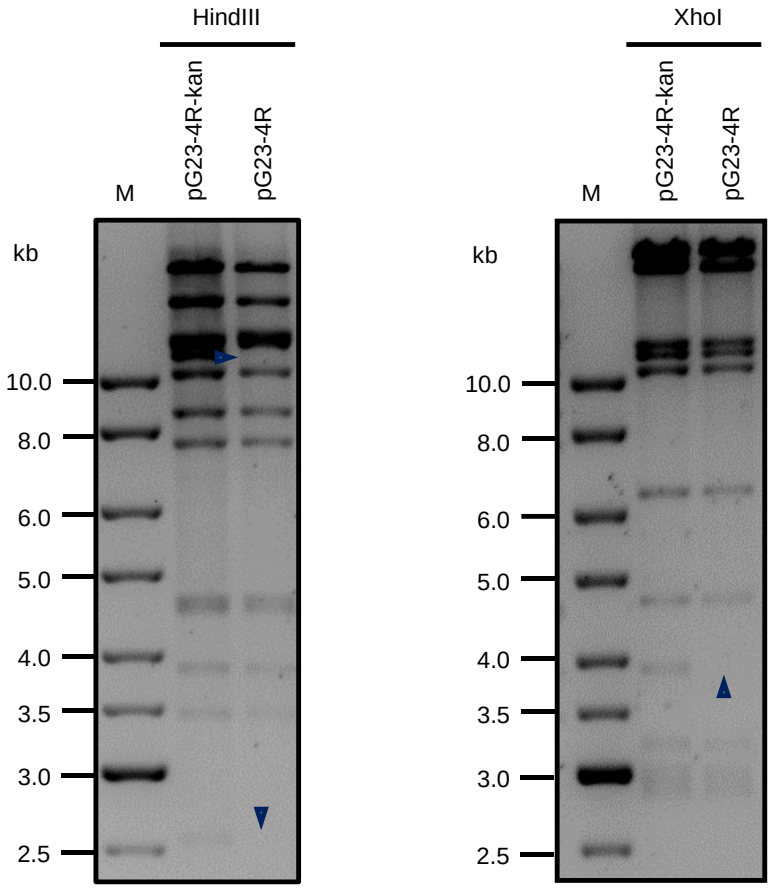

Fig. 14. RFLP analysis of pHJOpac-eGFP23-mRFP4. RFLP analysis of HindIII- and XhoI-digested DNA of pHJOpac-eGFP23-4mRFP (pG23-4R) in comparison to pHJOpac-eGFP23-4mRFP-kan (pG23-4R-kan) as control. The arrows indicate the absence of DNA fragments confirming the colony harboring the expected BAC-cloned genome.

In order to confirm that the presumably positive colonies contain intact genomes except the insertion of the fusion sequences, the BAC-cloned genome of pHJOpac-eGFP23 and the resulting BAC genome pHJOpac-eGFP23-4mRFP-kan were tested via RFLP analysis by digestion with the restriction enzymes HidIII and XhoI. Confirmed positive colonies were then used for the second step of Red-recombination. Similarly, the colonies that were grown on agar plates with arabinose (in order to induce I-SceI expression) and without kanamycin were tested by colony PCR with two primers, one of which binds within the mRFP gene and the other one upstream of the fusion position (Tab. 15). DNA fragments of 1454 bp were observed by gel electrophoresis referring to putatively positive colonies (data not shown). For the confirmation of a correct mutagenesis of the generated mutants, RFLP analysis was performed based on restriction enzyme digestion of the BAC-cloned pHJOpac-eGFP23-4mRFP-kan (pG23-4R-kan) and the resuling BAC-clones, presumably of pHJOpac-eGFP23-4mRFP (pG23-4R), with HindIII and XhoI restriction enzymes (Fig. 14). For additional confirmation of a correct mutagenesis of the final double fluorescence-labeled pG23-4R, RFLP analysis was performed based on restriction enzyme digestion of the BAC-cloned

pHJOpac (pHJO), pG23, pG23-4R-kan, and pG23-4R with HindIII and XhoI restriction enzymes (Fig. 15).

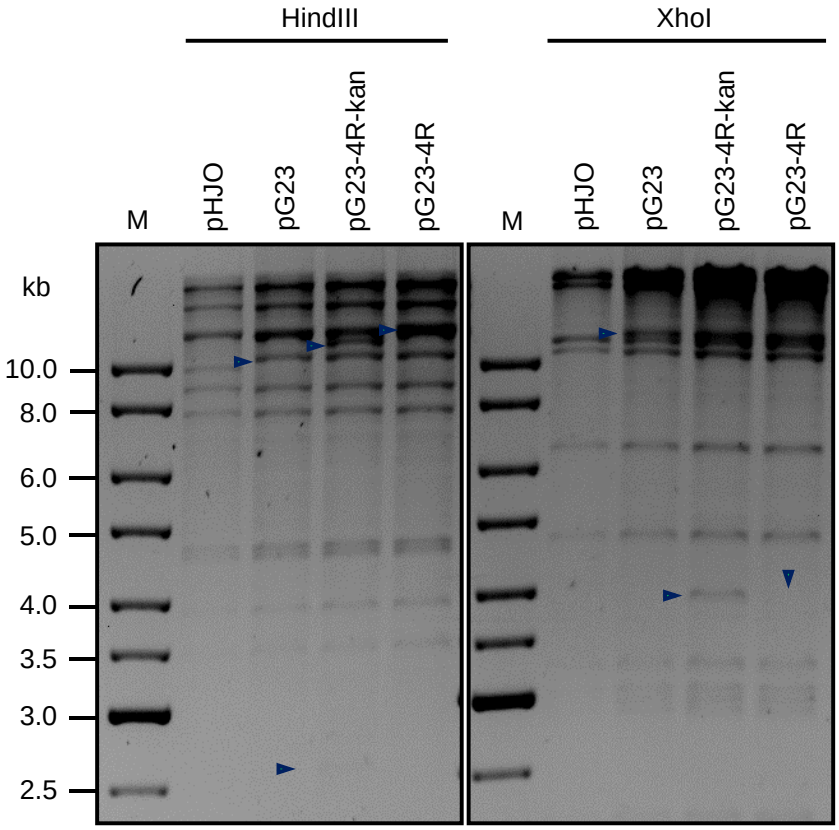

Fig. 15. En-passant mutagenesis confirmation via RFLP analysis. RFLP analysis of HindIII- and XhoI-digested DNA of pG23, pG23-4R-kan, and pG23-4R in comparison to the wild-type pHJOpac (pHJO) as control. The arrows indicate the presence or absence of DNA fragments confirming the correct mutagenesis of the expected BAC-cloned genomes.

Finally, the region was PCR amplified flanking the OFR4 fusion site in the newly generated viral mutant BAC pHJOpac-eGFP23-4mRFP. The sequence analysis showed no mutations at the fusion site and in its flanking region (data not shown). This indicated that this construct was appropriate for the further experiments.

4.1.4 BAC mutant pHJOpac-eGFP65-mRFP23

This construct was completely generated by our group in a previous project (Spieckermann, Dissertation, 2013) and used in this study for further experiments. In brief, similar recombineering techniques were used to generate the double color mutant BAC pHJOpac-eGFP65-mRFP23 (Fig. 16, 17).

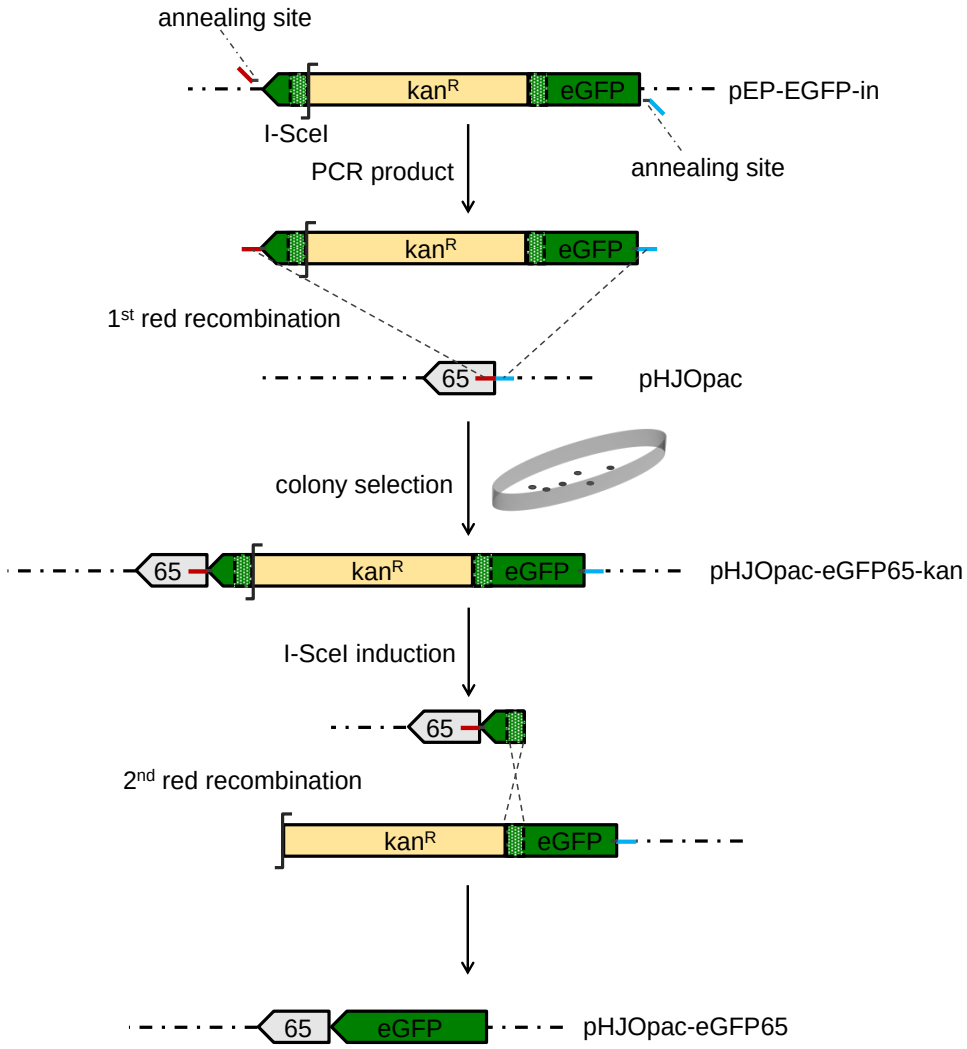

Fig. 16. Generation of pHJOpac-eGFP65 by en-passant mutagenesis. Using the vector pEP-EGFP-in, a PCR product was amplified containing eGFP sequences with a homologous 50 bp duplicated region (dash-framed regions), a positive selection marker (kan^R), and an I-SceI recognition site with primers of two 50 bp homologous extensions of the fusion site at ORF65 (red and blue bars). The resulted PCR product was then electroporated into *E. coli* harboring pHJOpac. After the first recombination, ORF65 was fused to the PCR product and then positive clones were selected out on agar plate with kanamycin. Finally, upon I-SceI induction via arabinose, a double strand break occurs at the I-SceI site causing the elimination of the kan^R and a subsequent fusion of eGFP to the N-terminus of ORF65 due to homologous recombination of the homologous sequences (dash-framed regions), however, without leaving any additional changes in the genome.

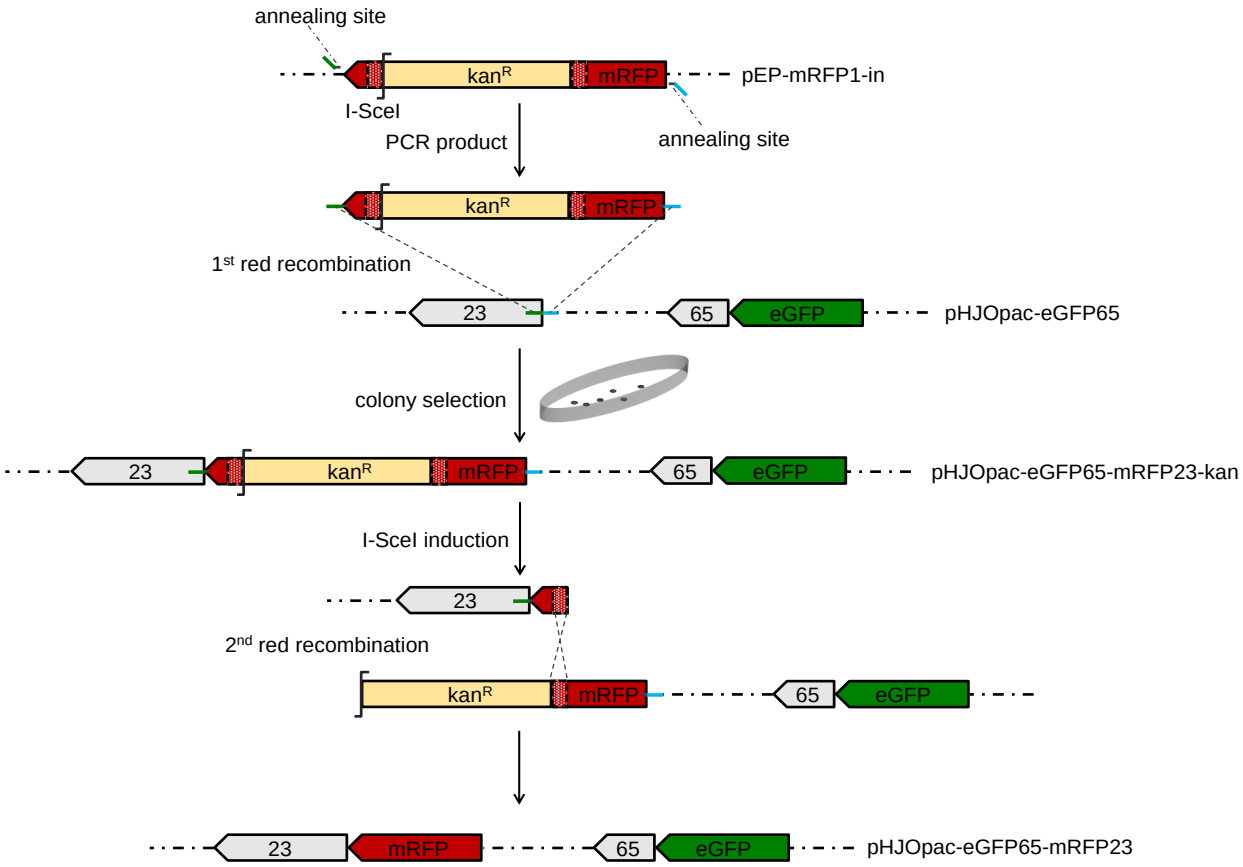

Fig. 17. Generation of pHJOpac-eGFP65-mRFP23 by en-passant mutagenesis. Using the vector pEP-mRFP1-in, a PCR product was amplified containing mRFP sequences with a homologous 50 bp duplicated region (dash-framed regions), a positive selection marker (kan^R), and an I-SceI recognition site with primers of two 50 bp homologous extensions of the fusion site at ORF23 (green and blue bars). The resulted PCR product was then electroporated into *E. coli* harboring pHJOpac-eGFP65. After the first recombination, ORF23 was fused to the PCR product and then positive clones were selected out on agar plate with kanamycin. Finally, upon I-SceI induction via arabinose, a double strand break occurs at the I-SceI site causing the elimination of the kan^R and a subsequent fusion of mRFP to the N-terminal end of ORF23 due to homologous recombination of the homologous sequences (dash-framed regions), however, without leaving any additional changes in the genome.

4.2 Virus reconstitution from cloned VZV-BACs

4.2.1 Lipofection of cloned VZV-BACs into permissive melanoma cells

All BAC-cloned VZV genomes were extracted from *E. coli* by alkaline lysis and then lipofected using Lipofectamine 2000 into permissive human MeWo melanoma cells. The reconstitution and the replication of the viral variants in the permissive MeWo cells were established upon formation of viral cytopathogenic effects (CPEs) under the tissue culture microscope. After detection of first CPEs (approximately 5-10 d post-transfection, dpt), the transfected MeWo cells were passaged several times. Since VZV is a cell-associated virus, the infected MeWo cells harboring the infectious viral mutants were later on harvested, portioned into samples, and finally stored frozen at -80°C for further analysis. The first two double fluorescence-tagged VZV mutant BACs pHJOpac-eGFP4-mRFP23 and pHJOpac-eGFP23-mRFP4 did not show any CPEs after lipofection into permissive melanoma cells and even after several passaging. In order to assure that these BACs are not reconstitutable, the nuc-

leofection technique was additionally applied. After yielding the same results, these cloned BACs were confirmed to be replication-incompetent. In contrast, the cloned wild-type BAC pHJOpac and the two generated double fluorescently labeled VZV mutant BACs pHJOpac-eGFP23-4mRFP and pHJOpac-eGFP65-mRFP23 were confirmed to be replication-competent upon observing CPEs at 5-10 dpt using the lipofection technique. These three viral recombinants were termed HJO, G23-4R, and G65R23, respectively, and then used for further analysis and experiments.

4.2.2 Replication kinetics of the replication-competent virus variants

In order to study the replication kinetics of all described reconstitutable viral variants, the preserved infected MeWo cells were used at first for the quantification of the virus load. After the number of plaque forming units (PFU) of each viral variant from the preserved samples had been quantified, replication kinetics of all recombinant viruses were performed and analyzed in comparison to those of the wild-type HJO. The total result of three independent experiments did not show relevant differences and this was even more obvious after normalization of all initial PFU/ml values to 100 (Fig. 18). These independent experiments were conducted by using three separate samples of each viral variants. In each experiment, the virus titers were performed in four separate cultures for each viral variant. The infected MeWo cells were then harvested daily until d5 post-infection (pi). Thereafter, the PFU of the harvested infected MeWo cells from each day (d1 through d5) were counted using the fluorescence microscope. In parallel, cultured uninfected MeWo cells were infected with 100 PFU/ml of each viral variant on the first day of the experiment to determine the virus titers at 0 dpi. Finally, the resulting PFU values of each viral variant were analyzed (Tab. 1-5, Fig. 18).

Tab. 1. Plaque forming units (PFU)/ml of wild-type HJO for five days after infection of MeWo cells

HJO			**d0**	**d1**	**d2**	**d3**	**d4**	**d5**
sample	1	1	120	300	3,000	1,000	4,000	7,000
		2	110	200	4,000	4,000	2,000	8,000
		3	90	250	4,000	4,000	6,000	9,000
		4	120	300	2,000	3,000	1,000	8,000
sample	2	1	70	100	1,500	10,000	20,000	7,000
		2	60	100	1,200	8,000	20,000	12,000
		3	40	80	1,500	14,000	20,000	4,000
		4	10	30	1,100	7,000	20,000	9,000
sample	3	1	50	80	1,200	4,000	5,000	6,000
		2	70	80	1,600	3,000	8,000	4,000
		3	50	90	1,200	6,000	8,000	8,000
		4	50	80	1,600	5,000	10,000	6,000

Tab. 2. Plaque forming units (PFU)/ml of G23 for five days after infection of MeWo cells

G23			d0	d1	d2	d3	d4	d5
sample	1	1	110	300	400	4,000	4,000	2,000
		2	80	200	1,000	7,000	10,000	3,000
		3	140	100	500	3,000	5,000	2,000
		4	70	100	400	6,000	10,000	3,000
sample	2	1	50	100	800	2,000	10,000	7,000
		2	80	100	700	5,000	16,000	6,000
		3	130	280	300	5,000	7,000	4,000
		4	90	120	300	1,000	13,000	6,000
sample	3	1	110	40	1,100	4,000	10,000	7,000
		2	60	70	900	2,000	12,000	6,000
		3	120	30	500	2,000	9,000	8,000
		4	120	40	700	5,000	5,000	9,000

Tab. 3. Plaque forming units (PFU)/ml of G23-4R for five days after infection of MeWo cells

G23-4R			d0	d1	d2	d3	d4	d5
sample	1	1	140	200	800	1,000	5,000	2,000
		2	120	300	700	2,000	6,000	4,000
		3	90	300	500	4,000	13,000	5,000
		4	60	100	600	6,000	7,000	3,000
sample	2	1	110	200	200	1,700	6,000	2,500
		2	110	200	500	2,000	5,000	2,500
		3	90	100	300	2,000	2,700	2,500
		4	50	70	500	2,000	3,300	2,500
sample	3	1	60	50	300	10,000	2,400	3,000
		2	40	50	200	9,000	2,200	2,300
		3	60	100	400	8,000	5,000	2,400
		4	50	40	500	14,000	2,200	2,200

Tab. 4. Plaque forming units (PFU)/ml of G65 for five days after infection of MeWo cells

G65			d0	d1	d2	d3	d4	d5
sample	1	1	80	200	700	2,000	3,000	4,000
		2	90	400	1,300	5,000	5,000	4,000
		3	30	100	1,200	5,000	6,000	5,000
		4	60	200	1,000	4,000	7,000	4,000
sample	2	1	80	150	500	4,000	7,000	1,000
		2	50	300	700	2,000	2,000	1,900
		3	40	100	200	2,000	6,000	1,000
		4	70	200	1,100	3,000	7,000	1,200
sample	3	1	40	50	900	4,000	6,000	8,000
		2	30	120	1,000	2,400	1,000	6,000
		3	50	130	1,200	2,000	4,000	7,000
		4	60	90	1,400	3,000	2,000	4,000

Tab. 5. Plaque forming units (PFU)/ml of G65R23 for five days after infection of MeWo cells

G65R23			d0	d1	d2	d3	d4	d5
sample	1	1	50	50	400	2,000	5,000	4,000
		2	70	100	400	4,000	3,000	2,000
		3	50	100	400	2,000	2,000	2,000
		4	60	50	500	1,000	3,000	1,500
sample	2	1	40	200	800	1,400	6,000	900
		2	50	80	700	1,500	6,000	1,000
		3	50	100	300	2,000	3,000	2,000
		4	30	200	300	1,200	3,000	600
sample	3	1	30	70	100	200	600	600
		2	10	70	100	400	1,000	700
		3	40	80	300	400	500	1,000
		4	10	90	100	600	1,000	600

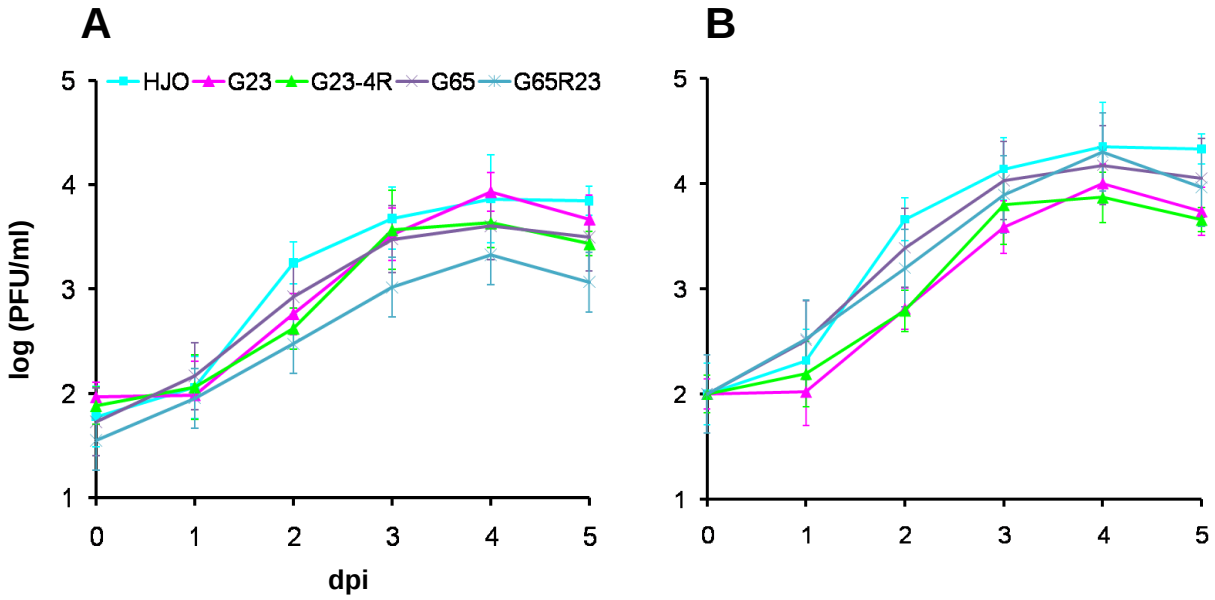

Fig. 18. Replication kinetics of recombinant viruses derived from HJO, G23, G23-4R, G65, and G65R23. (A) The replication curves of the generated VZV recombinants compared to those of the wild-type HJO do not show relevant differences. At d0, permissive MeWo cells were infected with 100 PFU/ml of each variant in 6-well dishes in triplicates at separate intervals. The infected MeWo cells were then harvested daily until 5 dpi. The harvested MeWo cells were then used to infect 50% confluent permissive MeWo cells seeded in 24-well dishes for the titer quantification. The PFU titers of each day were measured each time from four parallel cell cultures in each case. The PFUs were counted under the fluorescence microscope and the values from the triplicate results were averaged. The replication curves were generated after plotting the logarithmic values of the averages against the day post infection values. Error bars represent standard deviation for three replicates. (B) The replication curves after normalizing the previous results to the value of 100 PFU/ml at 0 dpi. This result did not show again relevant differences of the replication kinetics of all viral variants.

4.2.3 Confirmation of the correct fusion sites from total DNA of permissive cells

In order to confirm that the generated double fluorescently tagged viruses carry the expected fusions, isolated DNA from infected melanoma cells MeWo was analyzed by PCR. Since VZV is highly cell-associated, infected MeWo cells with each viral mutant were harvested and the total DNA was isolated. Afterwards, PCR fragments from each isolate were amplified with primers flanking the protein-protein fusion sites of G23, 4R, G65, and R23 (Tab. 15).

After analysis of the viral DNA fragment sizes of the protein-protein fusions, all fused protein-coding genes were confirmed to be fully valid (Fig. 19).

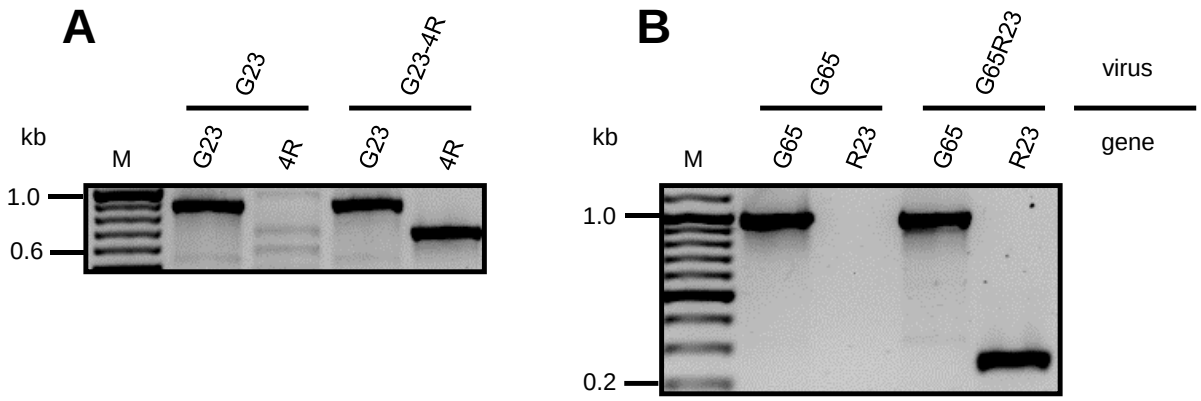

Fig. 19. PCR analysis of recombinant viruses. PCR analysis of G23-4R and G65R23 genomes in comparison to their intermediate products G23 and G65, respectively (upper line of the labeling on top). The amplified PCR products (lower line of the labeling on top) of the total DNA isolated from infected MeWo cells using primers flanking the fusion sites confirm the validity of the final virus recombinants G23-4R and G65R23. (A) PCR analysis of G23 with primers flanking the fusion sites G23 and 4R yielded one DNA fragment of 871 bp referring to the fusion site of G23 (first two lanes after the marker M). PCR analysis of G23-4R with primers flanking the same fusion sites yielded two DNA fragments 871 bp and 681 bp referring to the fusion sites of G23 and 4R, respectively, confirming the validity of the first double fluorescent mutant G23-4R (second two lanes). (B) PCR analysis of G65 with primers flanking the fusion sites G65 and R23 yielded one DNA fragment of 973 bp referring to the fusion site of G65 (first two lanes after the marker M). PCR analysis of G65-R23 with primers flanking the same fusion sites yielded two DNA fragments 973 bp and 254 bp referring to the fusion sites of G65 and R23, respectively, confirming the validity of the second double fluorescent mutant G65-R23 (second two lanes).

4.2.4 Fusion gene transcription from permissive melanoma cells

Total RNA was isolated from infected MeWo melanoma cells for the control of the viral gene expression in the double mutant viruses G23-4R and G65R23.

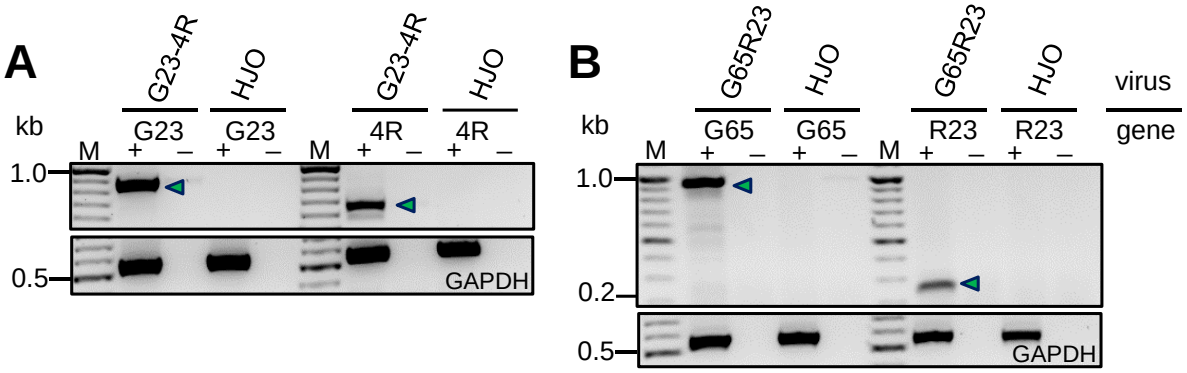

Fig. 20. RT-PCR analysis of recombinant viruses. RT-PCR analysis of G23-4R and G65R23 transcripts in comparison to that of the recombinant wild-type HJO (upper line of the labeling on top). The amplified RT-PCR products (lower line of the labeling on top) of the total RNA isolated from infected MeWo cells using primers flanking the fusion sites confirm the validity of the generated G23-4R and G65R23 virus recombinants. GAPDH (540 bp) served as a cellular control and the analysis was performed in the presence (+) or absence (-) of reverse transcriptase. (A) RT-PCR analysis of G23-4R with primers flanking the fusion sites G23 and 4R yielded DNA fragments of 871 bp and 681 bp, respectively (arrows). (B) RT-PCR analysis of G65-R23 with primers flanking the fusion sites G65 and R23 yielded DNA fragments of 973 bp and 254 bp, respectively (arrows).

After isolation, RNA samples were treated with deoxyribonuclease I (DNAse I), in order to degrade the residual chromosomal and viral DNA prior to complementary cDNA synthesis. Finally, reverse transcriptase (RT) PCR analysis of cDNA was performed in parallel with control samples without RT treatment showing relevant bands of all viral fusion gene expression in G23-4R and G65R23. However, as expected, bands were not detected for the viral fusion gene expression in the wild-type HJO. Furthermore, glyceraldehyde 3-phosphate dehydrogenase (GAPDH) transcripts were detected as a positive cellular reference in all samples confirming the correct cDNA synthesis (Fig. 20).

4.2.5 Viral fusion protein expression via immunoblot analysis

For the detection of the viral proteins in infected permissive cells, protein lysates of G23-4R- and G65R23-infected MeWo melanoma cells were subjected to sodium dodecyl sulfate (SDS) polyacrylamide gel electrophoresis and detected with anti-GFP and anti-RFP antibodies (Fig. 21).

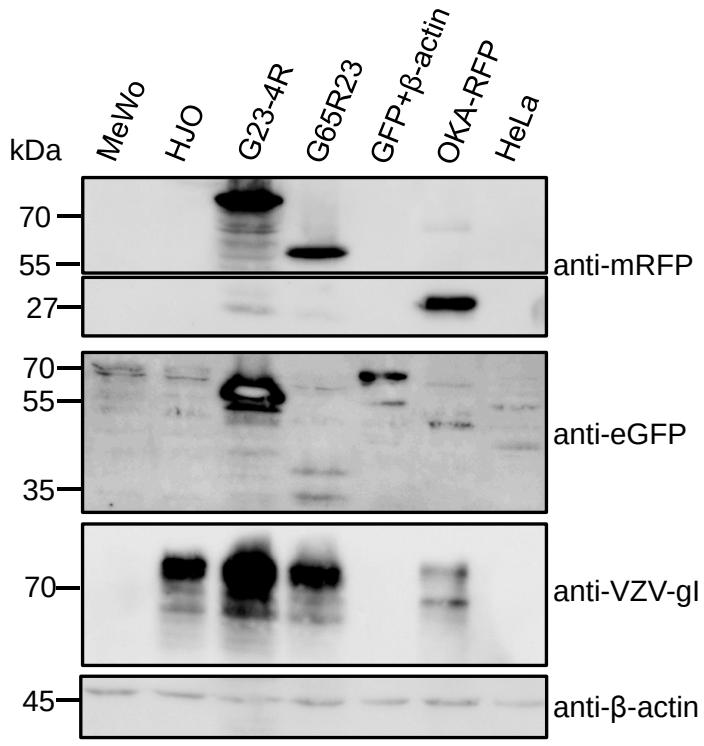

Fig. 21. Immunoblot analysis of recombinant viruses. Immunoblot of protein lysates from infected versus uninfected MeWo cells with antibodies to mRFP (27 kDa), eGFP (27 kDa), VZV-gI (53-100 kDa) as a viral control, or β-actin (45 kDa) as a cellular control show valid expression bands of all fusion proteins G23/R23 (52-60 kDa), 4R (78 kDa), and G65 (33-40 kDa). Lysates from MeWo cells infected with an mRFP-expressing VZV Oka strain and from HeLa cells transfected with an expression vector of eGFP-β-actin (72 kDa) fusion protein were used to control the expression of the mRFP and eGFP moiety, respectively (lanes 5, 6). Uninfected MeWo and HeLa cells did not show relevant proteins bands (lanes 1, 7).

As expected, the G23 fusion protein was detected at approximately 52-60 kDa, referring to the non-phosphorylated and the phosphorylated forms of p23 fused to 27 kDa of eGFP (Fig. 21, lane 3) and a similar size was observed for the R23 fusion protein (Fig. 21, lane 4). For

the fluorescence-labeled immediate-early fusion protein 4R, the immunoblot yielded a 78 kDa band of mRFP fused to 51 kDa of IE4 and an additional weak signal at approximately 27 kDa probably related to non-fused mRFP (Fig. 21, lane 3). For the fusion protein G65, the immunoblot showed two bands which are likely to result from differential phosphorylation (Fig. 21, lane 4). As viral and cellular controls, anti-VZV-gI and anti-β-actin antibodies were applied in addition to mRFP and eGFP controls (Fig. 21, lanes 5, 6). However, lysates from non-infected cells did not show relevant protein expression (Fig. 21, lanes 1, 7).

4.3 Cellular localization of viral fusion proteins

4.3.1 Intracellular localization of IE4, p65, and p23 in non-neuronal cells

Permissive MeWo melanoma and HFF fibroblast cells were propagated on coverslips and inoculated with G23-4R, G65R23, or G65 to demonstrate the localization patterns of the fusion proteins. Accordingly, infected cells were fixed at 2 dpi and stained with Hoechst 33342, then monitored by confocal imaging (Fig. 22).

The capsid protein p23 is expected to localize in the nucleus of infected cells, since it was suggested to play a role in the nuclear transport of viral proteins during virus replication and also to be situated within the nuclear promyelocytic leukemia PML cages (Chaudhuri et al., 2008; Reichelt et al., 2011). Consistently, the G23 and R23 proteins were detected within the nucleus with a strong expression and only weak punctuated signals were found in the cytoplasm of infected MeWo melanoma and HFF fibroblast cells (Fig. 22).

The fusion protein 4R was distributed more often in the cytoplasm than in the nucleus of infected MeWo and fibroblast cells at 2 dpi (Fig. 22). This result is consistent with the assumption that during the early state of infection IE4 is located in the nucleus, then during ongoing infection it is distributed to the cytoplasm (Cohen et al., 2005; Lungu et al., 1998; Ote et al., 2010), which concludes that at 2 dpi more cells have switched to the late state of infection.

In the case of the transmembrane protein p65, the fusion protein G65 of the double mutant G65R23 was detected on the surface of the infected cells and also in perinuclear structures as expected for such type II membrane protein which had been described also in the trans-Golgi network (TGN) (Lyman et al., 2009) (Fig. 22). In order to confirm the TNG localization, G65-infected MeWo and fibroblast cells were fixed at 2 dpi, then stained with the anti golgin-97 antibody as TGN marker before nuclear staining with Hoechst 33342. The TGN localization of G65 was confirmed upon observing accumulation signals of G65 expression at the distribution sites of the golgin-97 TGN marker (Fig. 23). However, viral signals were not detected in non-infected MeWo and fibroblast cells (Fig. 22, 23).

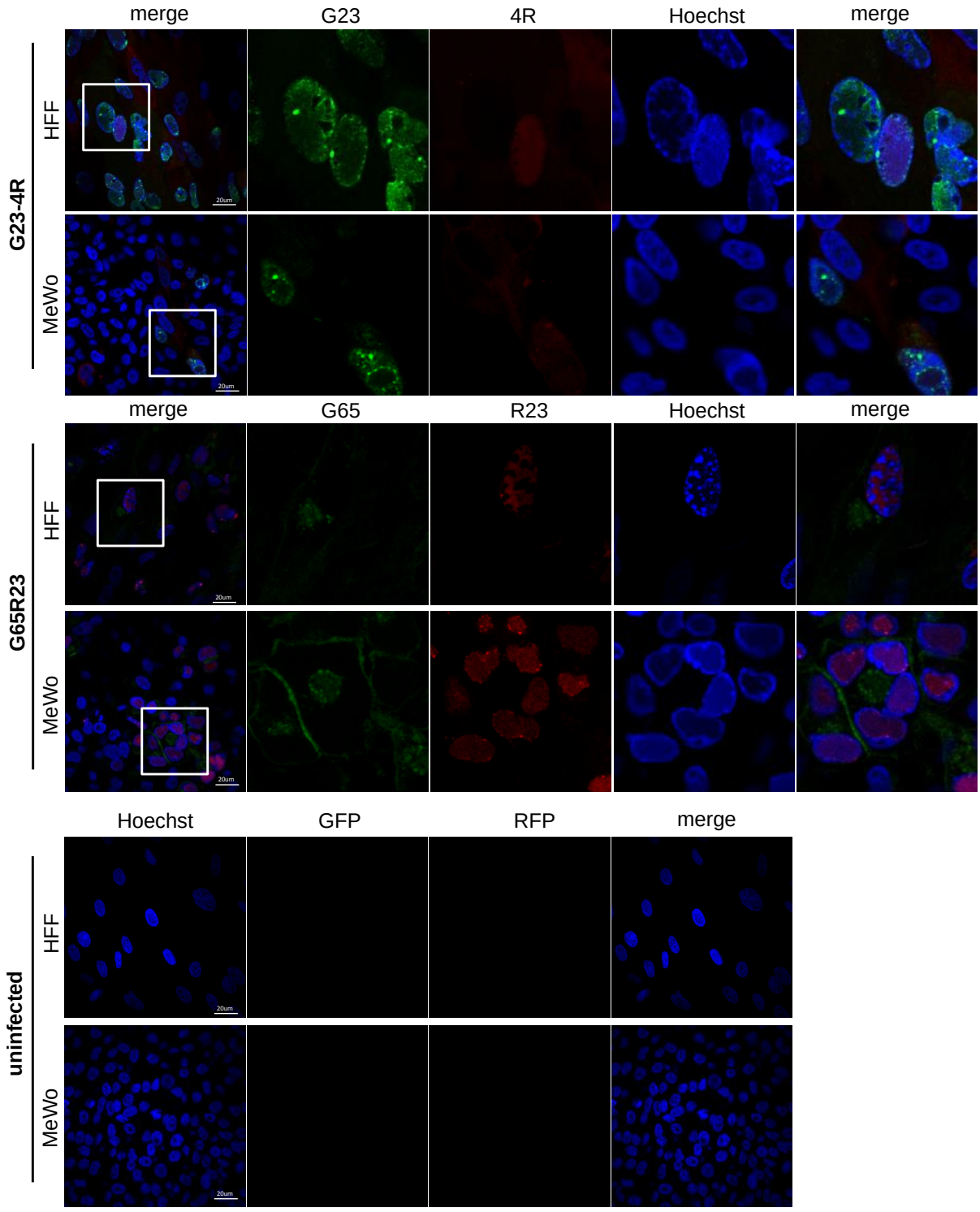

Fig. 22. Intracellular localization of IE4, p65, and p23 in permissive non-neuronal cells. Fibroblasts and MeWo cells were infected with the virus recombinants G23-4R or G65R23, then fixed, stained with Hoechst 33342, and visualized by Olympus fluorescence confocal microscopy at 2 dpi. The first four images on the left side show the merged images of the same viral recombinants with the nuclear Hoechst stain. The following images on the right side show unmerged and merged magnifications of the white-framed area. The lower two panels show the results of mock-infected cells. Scale bar of the original images, 20 µm.

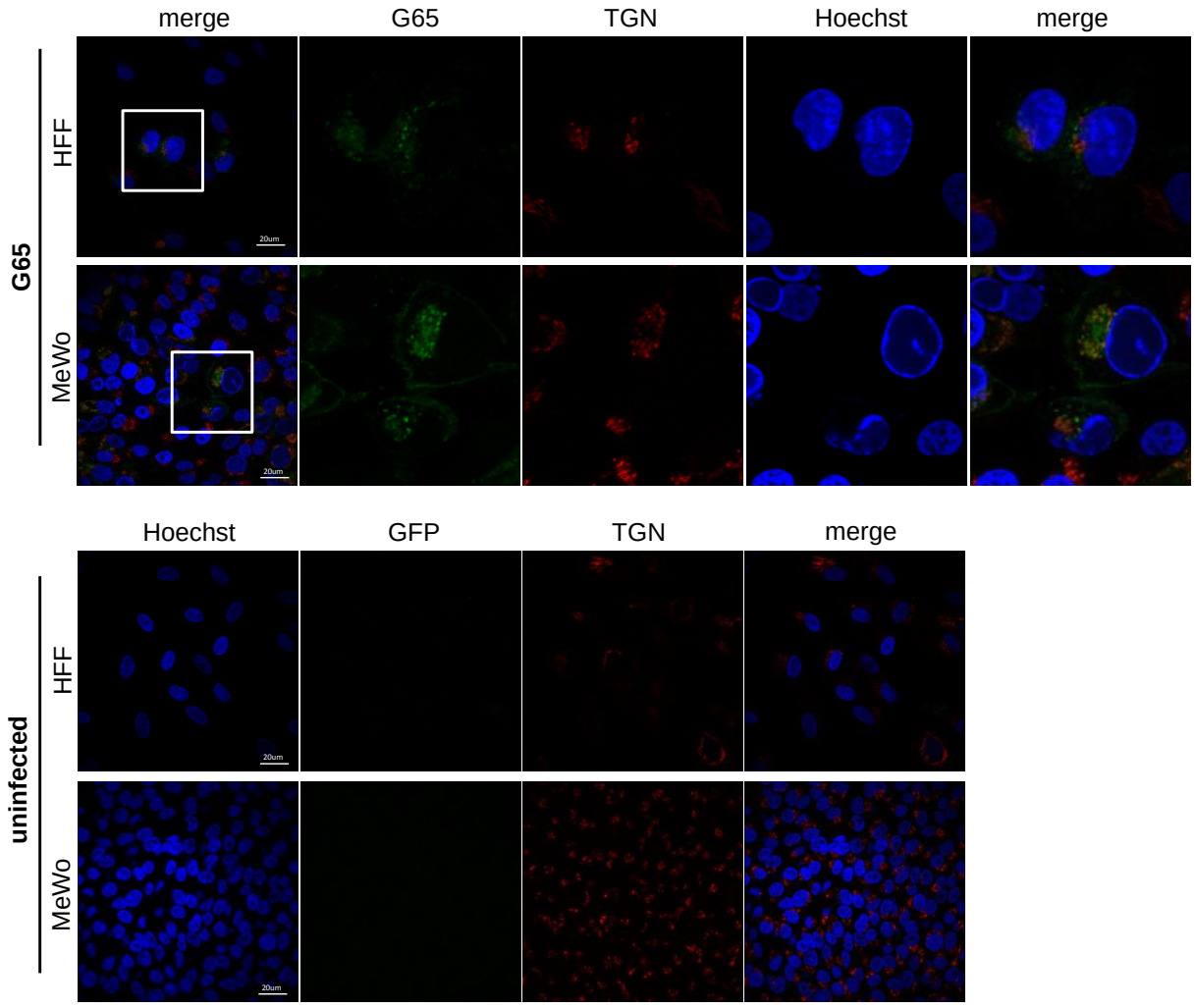

Fig. 23: p65 distribution in permissive non-neuronal cells. Fibroblasts and MeWo melanoma cells were infected with G65 recombinant virus, then fixed, permeabilized, stained with anti golgin-97 and Hoechst 33342, and visualized by Olympus fluorescence confocal microscopy at 2 dpi. The first two images on the left side show the merged images of G65 with TGN stain and the nuclear stain Hoechst 33342. The following images on the right side show unmerged and merged magnifications of the white-framed area. The lower two panels show the results of uninfected cells. Scale bar of the original images, 20 µm.

4.3.2 Localization of IE4, p65, and p23 in neurons

DRG-derived sensory neurons from d18 rat embryos (E18) were co-cultivated with G23-4R or G65R23 infected fibroblasts within channels of ibidi µ-slides $6^{0.4}$. At 2 dpi, cells were fixed and stained for the immunofluorescence analysis. The G23 and R23 fusion proteins were localized predominantly in the nucleus of infected sensory neurons with only weak punctuated expression in the cytoplasm, consistent with the previous observation for p23 in infected neurons at 3-7 dpi (Markus et al., 2011). In contrast, the G65 fusion protein was only detectable in the cytoplasm of infected sensory neurons (Fig. 24).

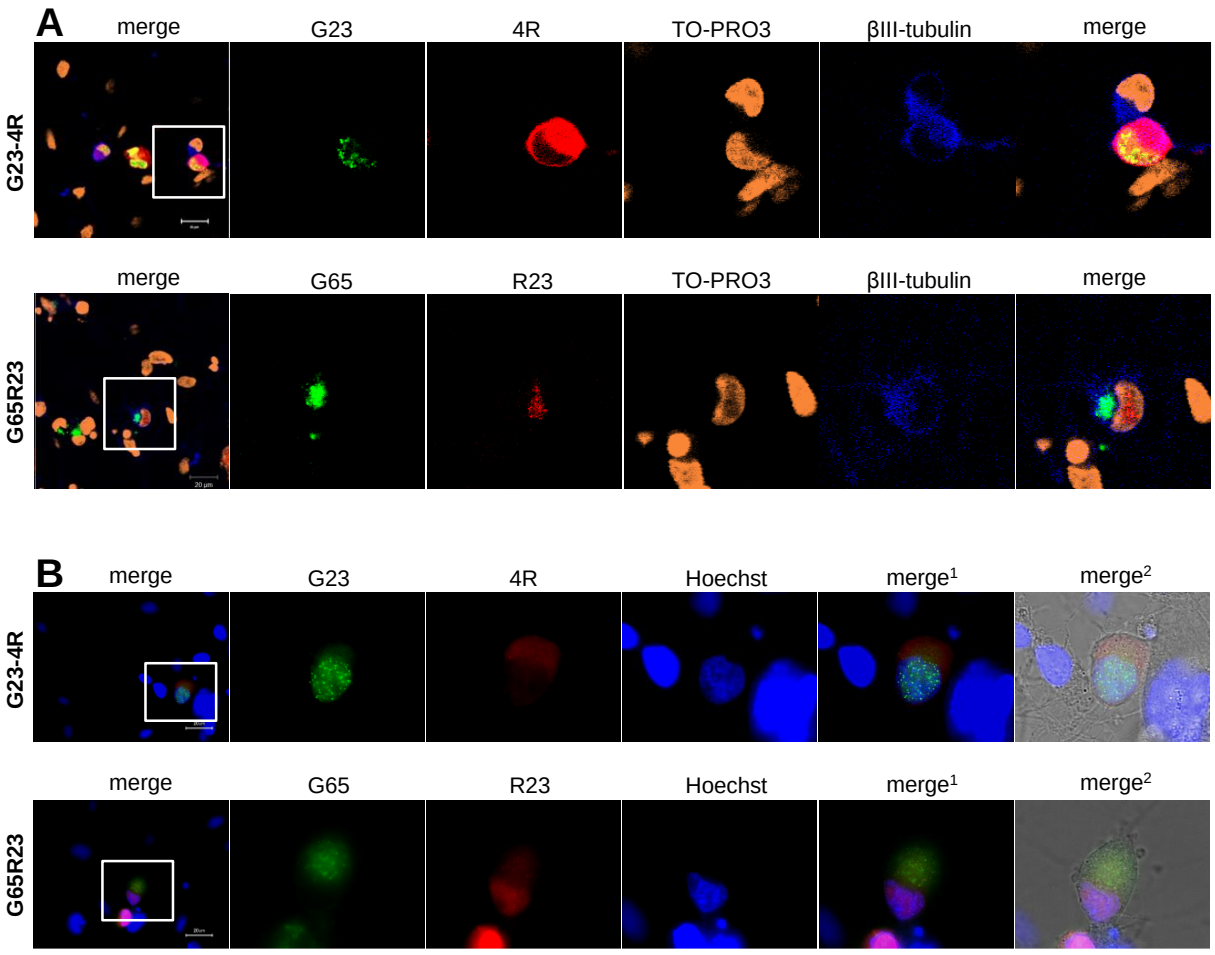

Fig. 24: Localization of IE4, p65, and p23 in neuronal cells. (A) Sensory neurons were co-cultured with G23-4R- and G65R23-infected fibroblasts, then fixed, permeabilized, stained with TO-PRO-3 and anti βIII-tubulin, and visualized by Zeiss fluorescence confocal microscopy at 2 dpi. The first two images on the left side show the merged images of the viral recombinants with the nuclear stain TO-PRO3 and the neuron-specific stain anti βIII-tubulin. The following images on the right side show unmerged and merged magnifications of the white-framed area. (B) Similarly, co-infected sensory neurons were fixed, stained with Hoechst 33342, and visualized by Keyence fluorescence microscopy at 2 dpi. Scale bar of the original images, 20 µm.

In latently infected neurons, IE4 had been suggested to localize only to the cytoplasm, whereas its expression was distributed almost alike between the nucleus and cytoplasm upon reactivation (Gershon et al., 2008; Lungu et al., 1998). However, in productively infected sensory neurons of E18, 4R expression was predominantly but not exclusively in the cytoplasm (Fig. 24), which is largely consistent with the spreading pattern of 4R expression in non-neuronal cells explained above. In this respect, we consider the infection state of E18 sensory neurons to be rather lytic than latent, due to the observed neuronal death at later times after infection, the spreading pattern of the infection, and the expression of the late capsid protein p23 which is typical for the lytic replication and does not belong to the latently expressed VZV proteins (Cohrs et al., 1996, 2003; Kennedy et al., 1999; Meier et al., 1993).

4.4 Axonal colocalization of viral fusion proteins

4.4.1 Axonal co-transport of IE4, p65, and p23 after anterograde infection of DRG neurons with VZV

The compartmentalized DRG cell cultivation system with two chambers separated by a 17 mm long channel filled with agarose had been efficiently used before to study the axonal transport of rabies virus (Bauer et al., 2014). This system allowed us to monitor the colocalization of IE4 and p65 with the small capsid protein p23 within axons of E18 rat embryos DRG neurons. Freshly prepared DRG cells were seeded into the somal chamber (proximal) and the axons were allowed to grow through the agarose-filled channel for approximately 4 weeks until they reached the distal axonal chamber supported by a 10-fold NGF concentration in the distal compartment (Fig. 5A).

For the anterograde infection, DRG cells were inoculated in the proximal chamber with high titers of cell-free G23-4R or G65R23 for 2-3 h and then further cultivated in virus-free medium. Subsequently, the live axons in the middle of the channel were monitored for fluorescent signals of VZV proteins and potential protein-protein colocalizations by BZ-9000 Keyence fluorescence microscope. Apparently, fluorescent signals were too weak to be detectable by our microscope at 0-1 dpi. However, several axons in the middle of the channel were detectable with respective fluorescence signals from 2 dpi, and at 3 dpi most axons were filled with fluorescent particles (Fig. 5B, C). Based on daily observations, infected axons collapsed at approximately 10 dpi (data not shown) confirming the productive infection type and the axonal spread of the virus. At 3 dpi, almost all green spots of G23 expression were noticed to coincide with the red 4R signals within axons of anterogradely infected DRG cells (Fig. 5B). Similar colocalization patterns were also observed for G65 and R23 (Fig. 5C), together suggesting a simultaneous transport of IE4 and p65 with the VZV capsid during anterograde infection in DRG cells.

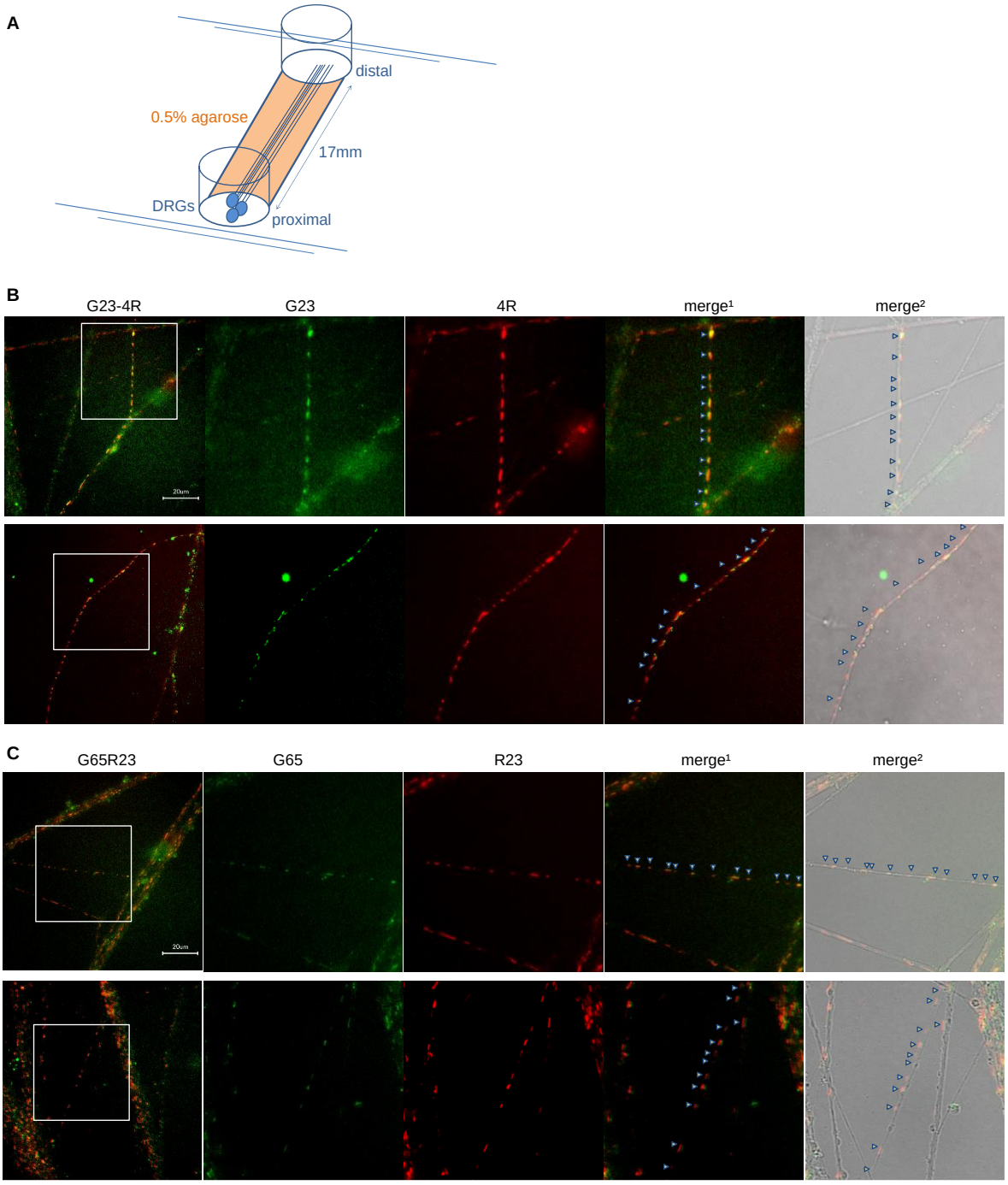

Fig. 25. Axonal colocalization of IE4, p65, and p23 after anterograde infection of DRG neurons. (A) Embryonic rat DRG cells were seeded into the proximal chamber (somal site) and axons were allowed to grow through a 0.5% agarose-filled channel toward the distal chamber for 3-4 weeks. Anterograde and retrograde infections of DRG cells at the proximal or the distal chamber, respectively, allowed tracing of the axonal colocalization of the fluorescence-tagged VZV proteins. Axons in the middle of the channel were daily live-monitored and protein-protein colocalizations were imaged by Keyence fluorescence microscope at 3 dpi. (B) The first two images on the left side show the merged images of axons of G23-4R-infected DRG neurons followed by unmerged and merged magnification of the white-framed area from two independent observations. Arrowheads highlight a number of p23 (green) colocalization signals with IE4 (red). Colocalization was confirmed after observation of closely neighboring G23 and 4R identical signals upon slight shifting of the images before merging (lower panel). (C) Analogous observations for axons of G65-R23-infected DRG neurons. Scale bar of the original image, 20 µm.

4.4.2 Axonal colocalization of IE4, p65, and p23 after retrograde infection of DRG neurons with VZV

Similar to the anterograde infection, 3-4 week grown DRG neurons were cultivated in the distal chamber with high titers of cell-free G23-4R or G65R23 for 2-3 h and then further cultivated in virus-free medium. Thereafter, the live axons in the middle of the channel were monitored for fluorescent signals of VZV proteins and potential protein-protein colocalizations and noted at 3 dpi by BZ-9000 Keyence fluorescence microscope (Fig. 26). At 3 dpi, almost all green signals of G23 expression were observed coinciding with the red 4R signals within axons of retrogradely infected DRG cells (Fig. 26A). Similar colocalization patterns were also observed for G65 and R23 (Fig. 26B).

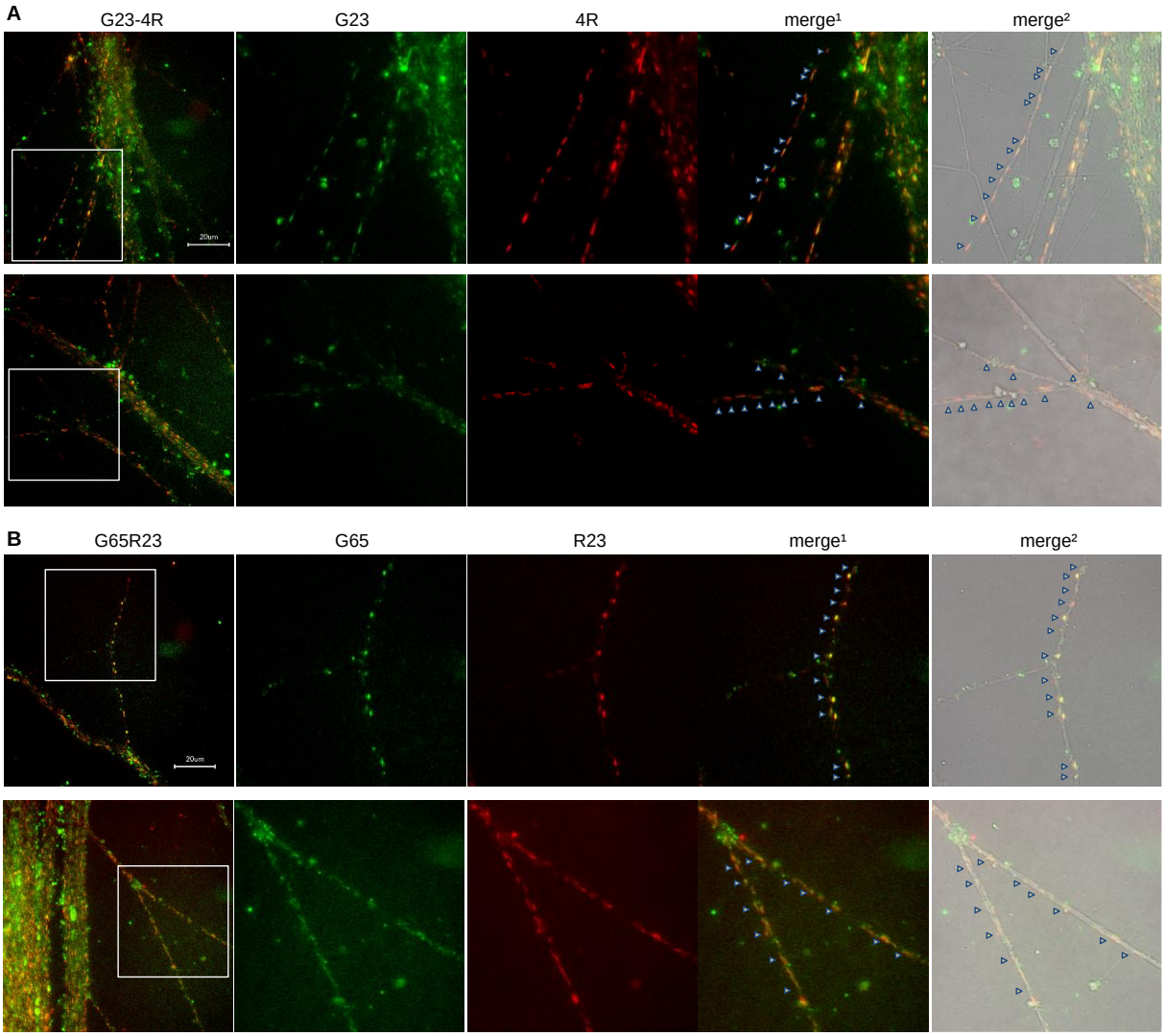

Fig. 26. Axonal colocalization of IE4, p65, and p23 after retrograde infection of DRG neurons. Axons of retrogradely infected DRG neurons in the middle of the channel were similarly (Fig. 25) live-monitored and protein-protein colocalizations were imaged by Keyence fluorescence microscope at 3 dpi (A) The first two images on the left side show the merged images of axons of G23-4R-infected DRG neurons followed by unmerged and merged magnification of the white-framed area from two independent observations. Arrowheads highlight a number of p23 (green) colocalization signals with IE4 (red). (B) Same axonal observation for axons of retrogradely G65-R23-infected DRG cells. Scale bar of the original image, 20 µm.

Although the colocalization patterns during anterograde and retrograde infections seemed to be absolutely identical, in the case of the retrograde infection we could not observe any fluorescent signals until the infection had spread into the somal site and was detectable at approximately 2 dpi. At the same time, live tracking of the fluorescently tagged proteins in both directions did not detect movement at the times of observation, probably due to the late detection of fluorescent viral particles. As a result, we could neither confirm nor deny the assumption of a “married” or an “unmarried” model for the retrograde axonal transport of VZV in DRG cells. Nevertheless, it led us to the conclusion that the “married” model of VZV anterograde axonal transport is most likely during the course of infection in sensory neurons.

4.4.3 Development of a novel adaptive compartmentalized neurons cultivation system

Since we seeded the whole ganglion during VZV infection to study the axonal transport, we asked if the individual sensory neurons would give the same results. For this purpose, we developed a novel compartmentalized cultivation system based on that applied above. Using ibidi chemotaxis µ-slides 3D, dissociated sensory neurons were seeded into the proximal chamber and axons were allowed to grow through the agarose-filled channel for 1-2 weeks prior to the anterograde infection with cell-free G23-4R in the proximal chamber (Fig. 27A). After 2-3 h, medium was replaced with a virus-free medium and the infection was then observed under the Keyence fluorescence microscope as described for the first method. Similar colocalization signals of G23 and 4R within the infected sensory neurons axons in addition to infected somata were detected from 1-2 dpi and imaged at 3 dpi (Fig. 27B) showing results comparable to those of the ibidi µ-slides $6^{0.4}$ (Fig. 25B). However, the new method was much faster and more efficient. Both the former and the later method were reliable and reproducible according to the similar results from several independent experiments, further supporting our observations of “married” mode of axonal transport.

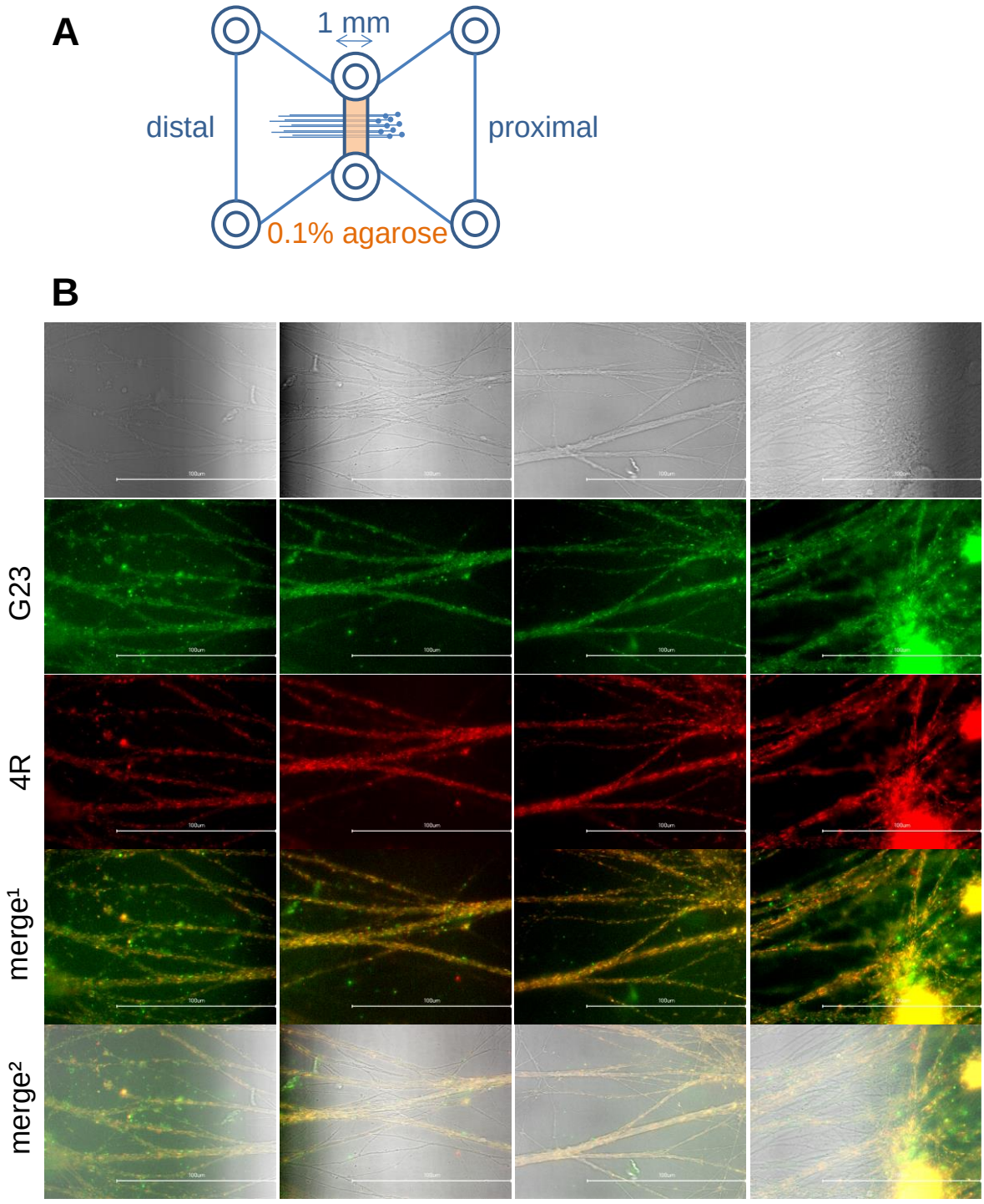

Fig. 27: A novel compartmentalized cultivation system for the observation of axonal transport. (A) Dissociated sensory neurons were seeded into the proximal chamber and axons were allowed to grow through a 0.1% agarose-filled channel toward the distal chamber for 1-2 weeks. Anterograde and retrograde infections at the proximal or the distal chamber, respectively, allowed tracing of the axonal colocalization of the fluorescence-tagged VZV proteins. Infected neurons were live-monitored and protein-protein colocalizations were imaged by Keyence fluorescence microscope at 3 dpi. (B) The upper panel show the images of growing sensory neurons from the somata in the proximal chamber (far right) through the agarose-filled channel (two images in the middle) toward the distal chamber (far left). The lower panels represent G23, 4R, and merged images of the anterogradely G23-4R-infected sensory neurons showing the spread of infection to the somata and a similar colocalization pattern of IE4 and p23 as observed above (Fig. 25B). Scale bars, 100 µm.

5 DISCUSSION

5.1 Efficient en-passant mutagenesis of herpesvirus genomes in *E. coli*

The development of the en-passant mutagenesis method by Tischer et al. in 2006 provided a highly efficient technique for the manipulation of bacterial artificial chromosome (BAC) constructs harboring infectious herpesvirus genomes. The VZV genome used in this study is maintained by a low-copy mini-F vector in the *E. coli* GS1783 strain. The mini-F cassette is located at the genomic terminal junction and released upon virus reconstitution and after three to four passages in permissive MeWo cells, resulting in an infectious virus without any foreign sequences. This system was developed by our research group by applying duplicated viral sequences from both ends of the mini-F integration site that allowed the constant maintenance of the cloned herpesvirus genomes in the Red recombination-competent *E. coli* GS1783 strain. Therefore, these herpesvirus BACs can be repeatedly modified by the en-passant mutagenesis method based on Red recombination (Fig. 28; Wussow et al., 2009).

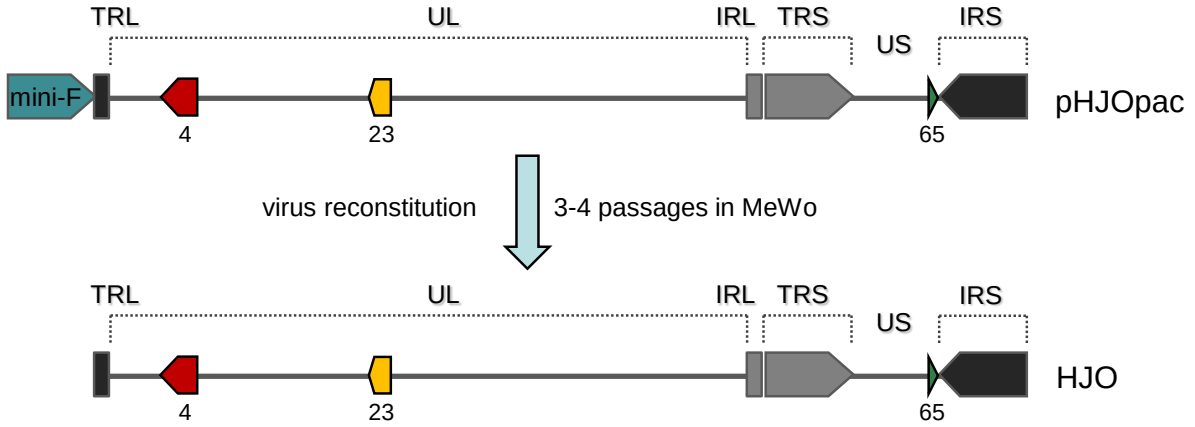

Fig. 28. Elimination strategy of the mini-F moiety. The mini-F cassette locates at the genomic terminal junction of a cloned-BAC genome of the wild-type isolate HJO of VZV (pHJOpac). Sequences of the mini-F plasmid are released upon reconstitution of pHJOpac in permissive MeWo cells and after three to four consecutive passages of the reconstituted virus (HJO).

The en-passant mutagenesis was used for the generation of double fluorescently labeled VZV mutants with ORF-fluorescence fusions providing novel functions for VZV. In view of the retrograde axonal transport of the VZV small capsid protein p23 in comparison to its homologs of HSV-1 and PrV (Antinone & Smith, 2010; Grigorian et al., 2012; Smith et al., 2001), we used a fluorescently labeled p23 in two viral double mutants as a VZV capsid control, in order to observe colocalizations with the tegument protein IE4 and also with the transmembrane envelope protein p65 within axons of VZV-infected embryonic Wistar rat DRG cells, in order to better understand the axonal trafficking models of the VZV virions/particles in DRG neurons.

5.2 Recombinant viruses

5.2.1 Replication-competence of recombinant viruses

The open reading frame (708 bp) ORF23-encoded protein p23 is the smallest capsid protein of VZV according to its homology to the VP26/UL35 of HSV-1 that is known to be produced during the late phase of the virus replication cycle (Booy et al., 1994; McNabb & Courtney, 1992). Besides p23, the products of ORFs 20, 33, 33.5, 40, and 41 form the VZV capsid. Based on the conserved functions among herpesviruses, the capsid proteins p20, p23, p40, and p41 form the outer layer of VZV capsid (Cohen et al., 1980; del Rio et al., 2005; Gibson & Roizman, 1972; Kut & Raschaert, 2004). Although the N-terminus of ORF23 conserves most of the amino acids of its herpesvirus homologs, its C-terminus has unique amino acid residues that characterize its nuclear localization capacity. Moreover, co-expression with ORF23 resulted in nuclear import of the major capsid protein of ORF40. Thus, an mRFP fusion to the C-terminus of ORF23 resulted in a replication-incompetent virus in permissive melanoma cells suggesting incompatibility with capsid formation when mRFP is fused directly before the stop codon of ORF23 (Chaudhuri et al., 2008). Accordingly, only N-terminal fluorescent fusions of ORF23 were established by our group, which resulted in a replication-competent virus upon reconstitution in permissive melanoma cells.

VZV ORF4 (1359 bp) encodes an immediate early tegument protein (IE4) of VZV that is homologous to ICP27 (infected cell protein 27) of HSV-1. While the amino acids of both homologs show approximately 45% conserved sequences of which the C-terminal sequences are almost identical, IE4 could not functionally compensate for the loss of its homolog in an ICE27-null mutant of HSV-1. IE4 has transcriptional and posttranscriptional functions during all phases of the virus replication cycle and is known to be essential for the viral replication in vitro (Defechereux et al., 1993, 1997; Moriuchi et al., 1994; Perera et al., 1994; Sato et al., 2003). These transactivating properties are obtained during protein dimerization for which the central domain and the C-terminal cysteine-rich domain of ORF4 are important. These dimerization-important regions in addition to the arginine-rich domains Rb and Rc of the N-terminal region of ORF4 were also proved to be essential for the gene transactivation (Baudoux et al., 2000). Furthermore, IE4 has been found to function as a nucleocytoplasmic shuttling protein for the nuclear export of the viral mRNA. These shuttling properties are established by a nuclear localization signal identified within the Rb domain of the N-terminal region of ORF4 and a nuclear export mechanism partially depending on chromosome region maintenance 1 (CRM1). For the posttranscriptional function of ORF4, the nuclear localization signal was shown also to be indispensable (Baudoux et al., 2000; Huang et al., 2014; Ote et al., 2010). By our group, both C-terminal and N-terminal fusions of ORF4 and a fluorescent protein were conducted and yielded replication-competent viruses. However, in the case of a double fluorescence-tagged VZV genome, the cloned-BACs pG4R23 and pG23R4 were not

reconstitutable, whereas pG23-4R produced a replication-competent recombinant virus G23-4R upon transfection into permissive melanoma MeMo cells. According to these results, it seems that a fluorescence fusion at the N-terminus of ORF4 or ORF23 was incompatible with the viral replication in a double fluorescence-labeled VZV. This could be a result of conformational changes in structures of both fluorescence-tagged viral proteins that interfered with transfection, reconstitution or replication in permissive MeWo cells. In the case of an established transfection, these structural changes could also block the viral genome entry or the virus egress from the cellular nucleus during the replication cycle, and could alternatively interfere with the previously described functional properties of the N-terminal regions of both viral proteins, which resulted in interference with the virus replication. On the other hand, an mRFP fusion to the C-terminus of ORF4 in a double fluorescence-tagged VZV genome retained the functional properties of both fluorescently tagged viral proteins IE4 and p23 in culture.

The US region of the VZV genome encodes four ORFs. ORF65 (309 bp) is the smallest that encodes the transmembrane protein type II p65, which is known to be non-essential for the virus replication in vitro and for the infection of human skin and T-cells in vivo (Cohen et al., 2001; Niizuma et al., 2003; Zhang et al., 2010). This protein is highly conserved among other α-herpesviruses such as the US9 proteins of the VZV close relatives HSV-1 and PrV (Cohen et al., 2001; Frame et al, 1986). In the VZV genome, the ORF65 gene differs from its US9 homologs of HSV-1 and PrV in that it is dispensable for virus replication and it cannot replace the function of its homolog in a US9-null mutant of PrV (Cohen et al., 2001; Longnecker & Roizman, 1986; Mettenleiter et al, 1988). This protein has a hydrophobic C-terminus and 20% serine and threonine residues in the N-terminal region and is phosphorylated by casein kinase II resulting in an apparent protein size of 16 kDa. According to the sequence of p65, the first 78 amino acids region is located in the cytoplasm, followed by an 18 amino acid region located in the membrane, and a 6 amino acid region forming the extracellular domain (Cohen et al., 2001; Davison & Scott, 1986). Since p65 is non-essential for virus replication, fluorescent protein fusions at the N-terminus and C-terminus of ORF65 were established by our group generating a replication-competent virus with a fluorescently expressed p65. For the double fluorescence-labeled viral recombinant G65R23, eGFP was fused to the intracellular N-terminus of ORF65 expecting the eGFP moiety to be directed toward the cytosolic side upon virus reconstitution in permissive cells. Our results showed that both recombinant double color viruses G23-4R and G65R23 have replication kinetics similar to those of the wild-type HJO (Fig. 18). Moreover, a PCR analysis of the isolated viral DNA of G23-4R and G65R23 from infected melanoma cells in comparison to their intermediates G23 and G65 confirmed the correct fusion sites (Fig. 19). Together, these results indicate the validity of the generated double fluorescence-labeled recombinant viruses for further analysis.

5.2.2 Verification of viral fusion gene expression

First, the transcription of the fusion genes from the recombinant viruses G23-4R and G65R23 was monitored by detecting the viral mRNA from infected permissive MeWo cells via RT-PCR analysis. The results showed that all fusion transcripts were detectable and that the fusion sites were correct in comparison to the transcripts of the corresponding non-fusion genes from wild-type HJO-infected MeWo cells (Fig. 20).

Second, the fusion proteins from lysates of G23-4R- and G65R23-infected MeWo cells were monitored by observing the related bands by immunoblot analysis using anti-GFP and anti-RFP antibodies (Fig. 21). In previous studies, the capsid protein p23 showed a band of approximately 30-35 kDa, which is slightly higher than the calculated molecular size (24.4 kDa). This was suggested as a result of the phosphorylation of p23 at its 13 (six serine und seven threonine) possible phosphorylation sites (Chaudhuri et al., 2008; Lenac et al., 2013; Markus et al., 2011). In the present study, the G23 fusion protein was detected as expected at approximately 52-60 kDa, referring to the non-phosphorylated (24.4 kDa) and the phosphorylated (30-35 kDa) forms of p23 fused to 27 kDa of eGFP (Fig. 21, lane 3). A similar size was seen for the R23 fusion protein expression in addition to a very weak band at 27 kDa which may be related to a non-fused mRFP moiety (Fig. 21, lane 4).

For the fluorescence-labeled immediate early fusion protein 4R, expression yielded a 78 kDa band due to a fusion of 27 kDa of mRFP to 51 kDa of IE4, in agreement with the calculated molecular weight of IE4 and also to previous observations (Davison & Scott, 1986; Lenac et al., 2013; Ng et al., 1994). In addition, our immunoblot of 4R showed another very weak signal at 27 kDa that might refer to an unfused mRFP moiey (Fig. 21, lane 3).

Although the calculated molecular weight of the transmembrane protein p65 is 11 kDa (Davison & Scott, 1986), previous immunoblot analyses of p65 had exhibited a higher band at 16 kDa of the predicted p65-phosphorylated form (Cohen et al., 2001; Lenac et al., 2013; Niizuma et al., 2003). This phosphorylation was shown to be due to phosphorylation by casein kinase II at the serine and threonine residues sites located in the N-terminal half of p65 (Cohen et al., 2001). Our Western blot analysis of the fusion protein G65 showed a band at 38-40 kDa that is likely to relate to the 11 kDa of the p65-unphosphorylated form fused to 27 kDa of eGFP (Fig. 21).

As viral and cellular controls, anti-VZV-gI and anti-β-actin antibodies were applied illustrating expected bands at (53-100 kDa relating to the heterodimer gE/gI, Oliver et al., 2011) and 45 kDa of β-actin (Fig. 21). In addition, MeWo cells infected with mRFP-expressing VZV and HeLa cells transfected with an expression vector of eGFP-β-actin fusion protein (72 kDa), were used to control the expression and the 27 kDa molecular weight of eGFP (Fig. 21, lane 5) and mRFP (Fig. 21, lane 6). Lysates from uninfected cells did not show relevant viral or

fluorescent protein expression. Together, all fusion proteins were detectable at the expected molecular size via Western blot analysis.

5.3 Cellular localization of viral proteins

5.3.1 Intracellular localization in non-neuronal cells

The intracellular distribution of p23, IE4, and p65 was examined at first in VZV-infected permissive MeWo melanoma and HFF fibroblast cells by confocal imaging at 2 dpi (Fig. 22, 23).

The capsid protein p23 is known to be expressed during the late phase of VZV replication cycle after infection. Since the viral capsid is assembled in the nucleus of infected cells, p23 is predicted to localize mainly in the nucleus. Moreover, this protein was suggested to play a role in the nuclear transport of viral proteins during virus replication and also to be localized within the nuclear promyelocytic leukemia PML cages (Chaudhuri et al., 2008; Reichelt et al., 2011). Consistently, our results showed that G23 and R23 proteins were detected within the nucleus with a strong expression and only weak punctuated signals were found in the cytoplasm of infected MeWo melanoma and HFF fibroblast cells (Fig. 22).

As a transcriptional regulator protein, the VZV tegument IE4 is known to be expressed during the immediate-early or early phase of VZV replication cycle upon infection. While IE4 was suggested to localize in the nucleus during the early state of infection, it was predicted to translocate to the cytoplasm during ongoing infection (Cohen et al., 2005; Lungu et al., 1998; Ote et al., 2010). At 2 dpi, our results showed that the fusion protein 4R was distributed more often in the cytoplasm than in the nucleus of infected MeWo and fibroblast cells, which concludes that at 2 dpi more cells have switched to the late state of infection (Fig. 22).

As a late VZV transmembrane type II protein, p65 was suggested to localize to the membrane and also to be distributed to TGN of infected permissive cells (Lyman et al., 2009). In the present study, the fusion protein G65 was detected on the surface of the infected cells and also in perinuclear structures of infected MeWo and HFF cells at 2 dpi, which turned to be at the distribution sites of the TGN marker golgin-97 (Fig. 22, 23). Together, these results were in agreement with previous data describing the distribution manners of the relevant viral proteins in VZV-infected non-neuronal cells (summarized in Tab. 6).

5.3.2 Localization in neuronal cells

The cellular distribution of p23, IE4, and p65 was also monitored in VZV-infected DRG-derived sensory neurons from E18 rat embryos by confocal and fluorescent imaging at 2 dpi (Fig. 24).

Similar to the distribution manners of the capsid protein p23 in non-neuronal cells, this protein was suggested to localize predominantly in the nucleus of infected neurons at 3-7 dpi

(Markus et al., 2011). Our results showed also that the G23 and R23 fusion proteins were localized mainly in the nucleus of infected sensory neurons with only weak punctuated signals in the cytoplasm. In contrast, the G65 fusion protein was only detectable in the cytoplasm of infected sensory neurons (Fig. 24).

In the case of IE4, previous studies suggested that IE4 is present only in the cytoplasm in latently infected neurons, whereas its expression was distributed almost alike between the nucleus and cytoplasm upon reactivation (Gershon et al., 2008; Lungu et al., 1998). However, our results demonstrated that IE4 is predominantly but not exclusively in the cytoplasm of productively infected sensory neurons of E18 (Fig. 24), which is greatly consistent with its spreading patterns in non-neuronal cells discussed above. Together, these results were consistent with previous data defining the localization of the relevant viral proteins in VZV-infected neuronal cells (summarized in Tab. 6).

Tab. 6. Intracellular localization of IE4, p65, and p23

Protein	Localization in non-neuronal cells*	Localization in neuronal cells**
IE4	cytoplasm > nucleus	cytoplasm >> nucleus
p23	nucleus >>> cytoplasm	nucleus >>> cytoplasm
p65	TGN and membranes	cytoplasm***

*described also in previous studies (Chaudhuri et al., 2008; Cohen et al., 2001, 2005; Lungu et al., 1998; Lyman et al., 2009; Ote et al., 2010; Reichelt et al., 2009, 2011). **described also in previous studies (Gershon et al., 2008; Markus et al., 2011; Lungu et al., 1998). ***novel in this study.

5.4 Axonal transport of VZV

To investigate the axonal transport models of VZV, DRG neurons were infected with high titers of cell-free VZV using compartmentalized cultivation systems similar to those used earlier to study the axonal transport of rabies virus (Bauer et al., 2014). Although it was shown that infecting the neuronal cells with cell-free VZV induced a latent (non-productive) infection (Gershon et al., 2008), a later study suggested that productive or non-productive infections of neuronal cells in culture are dependent upon the titers of the infectious cell-free preparations. While infection of neuronal cells with low titers of cell-free VZV resulted in a latent infection, high titers of infectious cell-free VZV induced a productive infection (Sluotskin et al., 2013). Based on that, productive infections of E18 sensory neurons were established by using high titers of infectious cell-free VZV of approximately 10^4-10^5 PFU/ml.

5.4.1 Retrograde axonal transport of VZV

During primary infection, α-herpesviruses are considered to reach the nuclei of DRG neurons by two mechanisms, either by the infected immune cells circulating in the blood vessels surrounding the DRG sites or by fusion to the axonal membrane at the peripheral endings of the growth cones that innervate the infected peripheral tissues. Thus, the virus loses its envelop and most of the tegument proteins and the capsid is connected via the remaining tegument

proteins to the retrograde motor protein dynein (Diefenbach et al., 2008; Goldstein & Yang, 2000; Ouwendijk et al. 2012; Smith, 2012). Dynein can also move anterogradely in a less effective way and can affect the overall transport velocity (Gross et al., 2000; Ross et al., 2006; Smith, 2012). A kinetic analysis of the GFP-tagged VZV capsid protein p23 within axons of retrogradely VZV-infected neuronal cells showed that the movement of the viral capsid was detectable at 1 h post infection and turned to be discontinuous and bidirectional with a net retrograde motion which was at 6-10 h post infection significantly slower. At the late stage of infection, a high proportion of the observed viral capsids seemed to show a slower movement or to become stationary. This could be a result of the bidirectional transport of dynein, the limited quantity of dynein available, and/or the decreased concentrations of adenosine triphosphate needed for axonal transport (Grigorian et al., 2012). Accordingly, we presume that the elongated forms of viral fluorescence signals detected from 2 dpi represent rather static clusters of several viral virions/particles remaining at the same position in the axons. Our results further showed that in axons of retrogradely infected DRG neurons, the capsid was almost exclusively colocalized with the tegument protein IE4 and with the transmembrane envelope protein p65. Separate punctuated red and green signals were rarely observed (Fig. 25, 26). However, shortly after infection and probably due to the limited resolution of our non-confocal fluorescence microscope, axonal protein signals could not be detected as previously described (Grigorian et al., 2012). Later on (from 2 dpi), the signals had spread into the somata indicating that the detected signals might result rather from anterograde than of retrograde axonal transport (Fig. 26). In addition, axonal kinetics of the observed viral proteins could not be observed which made it difficult to determine precisely the retrograde axonal transport type of VZV virions/particles. Therefore, the retrograde axonal transport model of VZV still needs further studies preferably by detecting the colocalization of the viral proteins immediately after infection with a much more sensitive microscopy technique.

5.4.2 Anterograde axonal transport of VZV

For the α-herpesviruses HSV-1 and PrV, there is the plausible consensus that the viral capsid travels in retrograde direction without envelope using specific dynein-associated viral tegument proteins. In contrast, the anterograde axonal transport mechanisms seem to be more controversial leading to theories of two different axonal transport models called “married” and “unmarried” (separate) models. This results in the open question if the viral capsid travels with or without envelope in the axon (Diefenbach et al., 2008). Nevertheless, it was suggested that PrV capsids migrate according to the “married” model with envelope in anterograde axonal direction. Generally, a similar anterograde axonal transport model seems to be probable for HSV-1, assuming that both α-herpesviruses share the same axonal transport mechanisms (Diefenbach et al., 2008; Kratchmarov et al., 2012). In the present study, VZV p23

appeared to colocalize with 4R and p65 within axons of anterogradely infected DRG neurons (Fig. 25B, C) suggesting a simultaneous transport of IE4 and p65 with the VZV capsid. Consequently, we strongly suggest that VZV capsids do not travel naked along axons of DRG neurons after reactivation of VZV, since IE4 is known to be part of the tegument and p65 is a transmembrane envelope protein of VZV (Cohen et al., 2001; Sato et al., 2003). As such, we prefer the “married” model of VZV anterograde axonal transport in DRG neurons, resembling that suggested for HSV-1 and PrV45.

In anterograde infection of HSV-1 and PrV, the heterodimer transmembrane type I glycoprotein gE/gI and the transmembrane type I protein US9 are supposed to promote the anterograde transport of the virus particles from the neuronal cytoplasm into axons (Howard et al., 2014; Johnson & Baines, 2011; Lyman et al., 2008; Miranda-Saksena et al., 2016). A significant assembly defect of “married” virions in addition to the missorting of enveloped and non-enveloped virus particles in the cytoplasm of infected neurons with gE-null and/or US9-null viral mutants resulted in a reduced anterograde transport of the virus particles. These defects suggest that gE/gI and US9 initiate assembly of enveloped particles in the cytoplasm and transport them into axons (DuRaine et al., 2017). So far, previous studies on the VZV gE/gI showed a role of the protein complex in the axonal spread of virus and viral proteins in DRG neurons (Christensen et al., 2011; Zerboni et al., 2007, 2011). Furthermore, our results showed that the US9 homolog of VZV p65 is a component of the trafficking virus particles along axons of DRG neurons after anterograde infection with VZV. However, it remains interesting to examine whether p65 together with the VZV heterodimer gE/gI plays the same role in the anterograde axonal transport as that of the homologous proteins of the VZV close relatives HSV-1 and PrV.

Based on these data, we approach another possible model for the anterograde axonal transport of VZV in addition to the previously suggested “married model” (Fig. 29). By a “married model”, the VZV particles travel along the microtubules of the sensory neurons axons as completely assembled virions in anterograde direction (Fig. 29A). By an “alternative model”, capsids of incompletely assembled VZV virions migrate together with a portion of the tegument involving IE4 and a portion of the envelope involving the “axonal guidance” p65 and the heterodimer gE/gI (Fig. 29B).

In culture, VZV replicates in a highly cell-associated manner and shows a narrow host range that limits the use of animal experiments. However, rats have been valuable as a behavioral model for VZV-induced allodynia and hyperalgesia (Fleetwood-Walker et al., 1999; Kress & Fickenscher, 2001). Sensory neurons from rat DRGs can be infected in cell culture with VZV showing signs of productive virus replication. Moreover, wild-type virus infected rat sensory neurons became sensitive to the pain-associated neurotransmitter noradrenalin, whereas this effect was almost absent when the cells were infected with the attenuated vaccine strain

Oka (Kress & Fickenscher, 2001; Schmidt et al., 2003). In the present study, we could also present embryonic Wistar rat DRG cells as valuable targets for the study of the axonal transport of VZV.

Taken together, the presented data establish that embryonic E18 rat DRG neurons are permissive to VZV and the applied compartmentalized cultivation systems are suited to further explore axonal transport mechanisms of VZV. Moreover, we emphasize the importance of IE4, a conserved protein among all α-herpesviruses, as a potential alternative antiviral target in addition to the non-essential "axonal guidance" protein p65. Thus, our results present models for the anterograde axonal transport of VZV and lead to further investigations into the axonal trafficking patterns of VZV in order to interfere with the pathogenesis of the neuropathogenic and neuropathic functions of VZV.

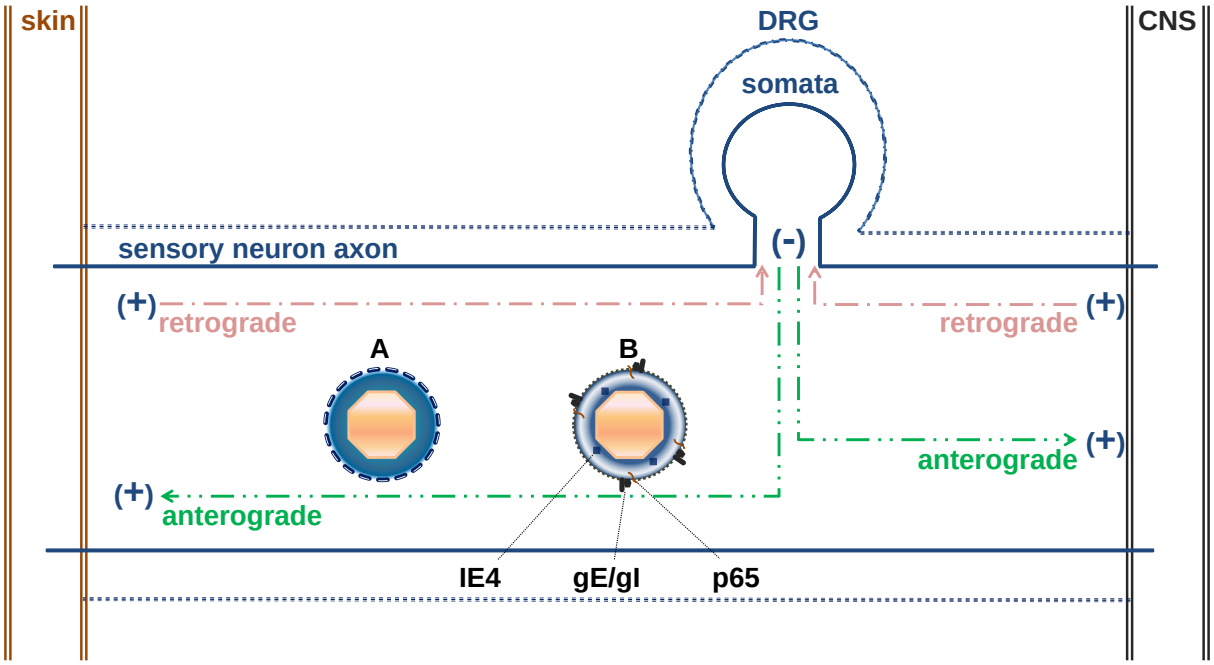

Fig. 29: Scheme of VZV anterograde transport models. In this drawing, two models of the anterograde transport of VZV particles are depicted within an axon of a sensory neuron. Somata of sensory neurons are clustered in the dorsal root ganglia (DRG) with axonal connections to the central nervous system (CNS) and to the skin. Retrograde axonal transport of cellular and viral particles occurs along the microtubules from the positive ends at the periphery to the negative ends at the somata (dashed light-red arrows); in contrast, anterograde axonal transport takes place along the microtubules in an opposite direction from the negative ends at the somata to the positive ends at the periphery (dashed green arrows). (A) The drawing represents a "married model" of the anterograde axonal transport of a VZV virion by which the virus travels as a completely assembled enveloped virion. (B) The drawing represents an "alternative model" of the anterograde axonal transport of a VZV particle by which the capsid of an incompletely assembled virion migrates together with a portion of the tegument involving IE4 and a portion of the envelope involving the "axonal guidance" p65 and the heterodimer gE/gI.

6 MATERIALS AND METHODS

6.1 Materials

6.1.1 Plasmid, BACs, and viruses

All BACs, plasmids, and reconstituted viruses that have been used or constructed during this study are listed below (Tab. 7). The generated virus strains are maintained within infected MeWo cells, since VZV is a cell-associated virus.

Tab. 7. Plasmids, bacterial artificial chromosomes, and recombinant varicella zoster viruses

Variable	Feature	Reference
Plasmids		
pEP-EGFP-in	transfer vector of the positive selection marker gene (Kan^R) with eGFP sequences and an I-SceI recognition site	Tischer et al., 2006
pEP-mRFP1-in	transfer vector of the positive selection marker gene (Kan^R) with mRFP sequences and an I-SceI recognition site	Tischer et al., 2006
Bacterial artificial chromosomes (BACs)		
pHJO	genome of the European wild-type isolate HJO of VZV including the mini-F cassette located at the genomic terminal junction	Wussow et al., 2009
pG4	pHJO with eGFP fused to the N-terminus of ORF4	Spieckermann, 2013
pG4R23	pG4 with mRFP fused to the N-terminus of ORF23	
pG23	pHJO with eGFP fused to the N-terminus of ORF23	Spieckermann, 2013
pG23R4	pG23 with mRFP fused to the N-terminus of ORF4	
pG23-4R	pG23 with mRFP fused to the C-terminus of ORF4	
pG65	pHJO with eGFP fused to the N-terminus of ORF65	Spieckermann, 2013
pG65R23	pG65 with mRFP fused to the N-terminus of ORF23	Spieckermann, 2013
Viruses		
HJO	pHJO without the mini-F cassette upon reconstitution and passaging in melanoma MeWo cells	Wussow et al., 2009
G23	pG23 without the mini-F cassette upon reconstitution and passaging in melanoma MeWo cells	Spieckermann, 2013
G23-4R	pG23-4R without the mini-F cassette upon reconstitution and passaging in melanoma MeWo cells	
G65	pG65 without the mini-F cassette upon reconstitution and passaging in melanoma MeWo cells	Spieckermann, 2013
G65R23	pG65R23 without the mini-F cassette upon reconstitution and passaging in melanoma MeWo cells	Spieckermann, 2013

6.1.2 Buffers and chemicals

Tab. 8. Buffers for the Western blot (WB) analysis

Component	Composition	
Resolving gel (10%,15 ml)	5.9 ml	water
	5.0 ml	30% acrylamide mix
	3.8 ml	1.5 M Tris (pH 8.8)
	0.15 ml	10% (w/v) sodium dodecyl sulfate (SDS)
	0.15 ml	10% (w/v) ammonium persulfate (APS)
	6 µl	Tetramethylethylenediamine (TEMED)
Stacking gel (5%, 5 ml)	3.4 ml	water
	0.83 ml	30% acrylamide mix
	0.63 ml	1.0 M Tris (pH 6.8)
	50 µl	10% SDS
	50 µl	10% APS
	5 µl	TEMED
10x SDS running buffer	250 mM	Tris
	1920 mM	glycine
	1% (w/v)	SDS
1x transfer buffer	10 ml	10x SDS running buffer
	10 ml	methanol
	80 ml	water
5x Laemmli buffer	312 nm	Tris-HCl (pH 6.8)
	10% (w/v)	SDS
	50% (v/v)	glycerol (Gerbu, Heidelberg)
	25% (v/v)	2-mercaptoethanol (freshly added)
	0.1 % (w/v)	bromophenol blue in water
Radioimmunoprecipitation assay buffer (RIPA)	50 mM	Tris-HCl (pH 7.5)
	150 mM	NaCl
	5 mM	ethylenediaminetetraacetic acid (EDTA, pH 8)
	1% (v/v)	Igepal CA-630 (Nonidet P-40)
	0.1% (v/v)	SDS
	0.5% (w/v)	Na deoxycholate
RIPA-PIC buffer	50 ml	RIPA buffer
	1 tablet	proteinase inhibitor cocktail (PIC)
TBST buffer (Tris buffered saline with 0,05% tween 20)	0.05% (v/v)	Tween 20
	5 M	Tris (pH 7.5)
	2M	NaCl
WB blocking buffer	5% (w/v)	non-fat dried milk in TBST buffer
WB stripping buffer (Yeung & Stanley, 2009)	6 M	guanidinium chloride
	0.2% (v/v)	Nonidet P-40
	0.1 M	2-mercaptoethanol
	20 mM	Tris-HCl (pH 7.5)

All chemicals presented were obtained from the following companies, Sigma-Aldrich (Taufkirchen), Roth (Karlsruhe) or Merck (Darmstadt). Exceptions are specifically mentioned. The water used is distilled, sterile water, when nothing else is mentioned.

Tab. 9. Buffers for the agarose gel electrophoresis

Component	Composition	
1x Tris-borate EDTA buffer (TBE)	89 mM 89 mM 2 mM	Tris boric acid EDTA (pH 8)
Agarose gel	0.6-1.0%	agarose (Life technologies, Darmstadt) in 1x TBE and 5:100,000 ethidium bromide
6x DNA loading buffer	50% (v/v) 10 mM 0.25% (v/w)	glycerol EDTA (pH 8) bromophenol blue in water

Tab. 10. Buffers for the DNA-analysis

Buffer	Composition	
Buffer I	10 mM 25 mM 100 µg/ml	EDTA, pH 8 Tris-HCl, pH 8 RNase A (Thermo Scientific)
Buffer II	0.2 M 1% (v/v)	Na hydroxide (NaOH) Na dodecyl sulfate (SDS)
Buffer III	3 M	K acetate, pH 5.5
Lysis buffer	1x 0.5% 0.7%	10x PCR-buffer Tween20 proteinase K (Roche); in water

6.1.3 Media and reagents

Tab. 11. Bacteria media

Medium	Composition	
LB-medium (*Luria-Bertani-Broth*)	10 g/l 10 g/l 5 g/l	tryptone yeast extract NaCl (pH 7)
LB agar with Kanamycin (Kan) Chloramphenicol (Cm) Ampicillin (Amp)	15 g/l 35 µg/ml 30 µg/ml 100 µg/ml	agarose in LB-medium kanamycin (in water) chloramphenicol (in ethanol) ampicillin (in water)

Tab. 12. Cell culture reagents and media

Variable	concentration	Manufacturer
Cell culture (virus)		
Dulbecco modified Eagle's minimal essential medium (DMEM) without L-glutamine ("*high glucose*")	4.5 g/l glucose	Biochrom (Berlin)
DMEM with L-glutamine ("*low lucose*")	1 g/l glucose	Biochrom
Fetal bovine serum (FBS)	-	PAA (Cölbe)
L-glutamine (100x)	200 mM	Biochrom
OptiMEM (improved minimal essential medium MEM)	-	Life technologies
PBS (Phosphate buffered saline) without Ca^{2+} und Mg^{2+}	-	Biochrom
Penicillin/streptomycin (P/S, 100X)	10,000 U/ml or 10 mg/ml U = units	Biochrom
10x trypsin (1:250)/EDTA	0.5% trypsin, 0.2% EDTA	Biochrom
Trypsin 2.5% in PBS	-	Biochrom
Lipofectamine 2000	-	Thermo Scientific (Darmstadt)
Trypan blue	-	Biochrom

Variable	concentration	Manufacturer
Cell culture (DRG)		
Hank's balanced sault solution (HBSS)	-	Gibco
Neurobasal medium NBM (21103-049)	-	Gibco
B-27-supplement (50x) serum free (protein-lipid complex)	-	Gibco
GlutaMAX supplement (100x)	200 mM L-alanyl-L-glutamine-dipeptide in 0.85 % NaCl solution	Gibco
Nerve growth factor (NGF 2.5S native mouse protein)	-	Invitrogen
Defined trypsin inhibitor 1x (DTI)	-	Gibco
Cytosine β-D-arabinofuranoside hydro-chloride (cytosine arabinoside, Ara-C)	-	Sigma-Aldrich
Poly-L-lysine hydrobromide (70-150 MDa)	-	Sigma-Aldrich
Laminin	-	Sigma-Aldrich
Nerve growth factor (NGF 2.5S native mouse protein)	-	Invitrogen

Tab. 13. Used cell culture media and solutions

Variable	Composition
D10	DMEM „*high glucose*", 10% (v/v) FBS, 100 U/ml or 100 µg/ml P/S, 2 mM L-glutamine
supplemented NBM	NBM, 100 U/ml P/S, B-27 0.02% (v/v), 0.5-2 mM GlutaMAX, 12.5 ng/ml NGF
Freezing medium	FBS 10% (v/v) in dimethyl sulfoxide (DMSO, Biomol, Hamburg)
10% (v/v) FBS	FBS in 1x PBS
4% paraformaldehyde	4% paraformaldehyde in 1x PBS, pH 7.2
Saponin	saponin in 1x PBS
Sucrose-glutamate-serum buffer (PSGC) buffer	5% (w/v) sucrose, 0.1% (w/v) Na-glutamate, 10% (v/v) FBS in 1x PBS (freshly added)
Zamboni's fixative buffer	2% (w/v) paraformaldehyde, 15% (v/v) saturated 1.2% picric acid in 0.1 M phosphate buffer, pH 7.3

Tab. 14. PCR reagents

Variable	Reagents	Manufacturer
	dNTPs (10 mM)	Thermo Scientific
PCR with Taq DNA-polymerase	10x Taq-buffer	Thermo Scientific
	$MgCl_2$ (25 mM)	Thermo Scientific
	10x $(NH_4)_2 SO_4$	Thermo Scientific
	Taq polymerase (1 U/µl)	Thermo Scientific
PCR with HotStar DNA-polymerase	10x PCR buffer	Qiagen
	HotStar polymerase	Qiagen
PCR with Phusion DNA-polymerase	5x GC-buffer	Finnzymes
	DMSO	Finnzymes
	Phusion polymerase	Thermo Scientific
Sequencing PCR	SB-buffer	Applied Biosystems, Darmstadt
	BigDye	

6.1.4 Oligonucleotides

Oligonucleotides were manufactured by Biomers (Ulm).

Tab. 15. Primers (for, forward orientation; rev, reverse orientation)

Code	Description	Sequence (5´→3´)
1) en-passant mutagenesis		
2232	eGFP-23 for	GTG GTG GGG TTG CTG GGA TCA AAG ACT ACA CGA GAC GAT GCG GGT TGT GTC TTG TAC AGC TCG TCC ATG C
2233	eGFP-23 rev	CGC AGA TGT ACG TGT ATG CTG TTA TCG ATT GTC CCG TAA ACT AAT AAA CGA TGG TGA GCA AGG GCG AGG A
3077	4-mRFP for	ATA CAA ATT AGT ATG TTT TGA CAA GCA TGA AAA AGG TAT TTT TTA TTT TAC AAG GCG CCG GTG GAG TGG C
3078	4-mRFP rev	CTG ACG CCC GTC CAT ACG GTA AAT ATT TTA AGT GTA GTA CCT TTA ACT GCG CCT CCT CCG AGG ACG TCA T
2409	eGFP-65 for	GGT ATT AAA CAC TTT TAA ACT AGC CTG CTG GCC TTA CAA TCT GGA TTT CTA TGG TGA GCA AGG GCG AGG A
2410	eGFP-65 rev	GCT TCC ATC AGT AAG GCC ACG GCC TCA CCC TCC ATG GTG TTT TGT CCG GCC TTG TAC AGC TCG TCC ATG C
2559	mRFP-23 for	GTG GTG GGG TTG CTG GGA TCA AAG ACT ACA CGA GAC GAT GCG GGT TGT GTC AAG GCG CCG GTG GAG TGG C
2560	mRFP-23 rev	CGC AGA TGT ACG TGT ATG CTG TTA TCG ATT GTC CCG TAA ACT AAT AAA CGA TGG CCT CCT CCG AGG ACG T
3075	mRFP-4 for	TCT TCA CAA ATA GTA GAC ACG TCT GGG TCG GTT GGA ATT GAA GCA GAG GCC AAG GCG CCG GTG GAG TGG C
3076	mRFP-4 rev	CGG AAG ATA CAG GCA ACT GCA AAC ACG CAA TTG TCA GAT ATT TTG CAG CCA TGG CCT CCT CCG AGG ACG T
2) PCR-primers		
1836	eGFP-23 for	AGC AAG GGC GAG GAG CTG TTC
1521	eGFP-23 rev	TTC TGG CAT CAG CGA TGT C
1549	ORF-23 rev	GAC ATA TGC CCT GTT CGT TG
925	ORF4 rev	ATA TAT CCC CAA CGT CGC C
2368	ORF4 for	AAT GCA AAG TCA TCC GAA GG
2369	ORF4 rev	TGA CTA AAC ACG CCC ATT GC
1158	4-mRFP for	GCG TGA GAG AGT CAT ACG TGG
3210	4-mRFP rev	TTG GTC ACC TTC AGC TTG GC
1836	eGFP-65 for	AGC AAG GGC GAG GAG CTG TTC
1527	eGFP-65 rev	CTC CCG TCA TAG CAA ATA C
1578	mRFP-23 for	CGA CAT CAA GCT GGA CAT C
1521	mRFP-23 rev	TTC TGG CAT CAG CGA TGT C
3211	GAPDH for	GCA GGG GGG AGC CAA AAG GG
3212	GAPDH rev	TGC CAG CCC CAG CGT CAA AG

6.1.5 Restriction enzymes

All used restriction enzymes were manufactured by Thermo Scientific.

Tab. 16. Restriction enzymes

Enzyme	Recognition sequence
XhoI	5′ …C▼T C G A G… 3′ 3′ …G A G C T▲C… 5′
BglII	5′ …A▼G A T C T… 3′ 3′ …T C T A G▲A… 5′
HindIII	5′ …A▼A G C T T… 3′ 3′ …T T C G A▲A… 5′

6.1.6 Antibodies

Tab. 17. Antibodies and their origin, application, dilution, and manufacturer

Antibody	Species, application, dilution	Manufacturer
primary antibody		
Anti-VZV glycoprotein I, VZV-gI, monoclonal	mouse, immunofluorescence, 1:1000	Merck Millipore (Darmstadt)
Golgin 97 (monoclonal)	mouse, immunofluorescence, 1:200	Santa Cruz (Heidelberg)
ß-III-Tubulin (monoclonal)	mouse, immunofluorescence, 1:50-1:200	Invitrogen
Anti-GFP (polyclonal)	rabbit, immunoblot, 1:1000	Invitrogen
Anti-RFP (monoclonal)	mouse, immunoblot, 1:750	Abcam (Cambridge, UK)
ß-Actin (monoclonal)	mouse, immunoblot, 1:1000	CellSignaling (Leiden, Netherlands)
secondary antibody		
Alexa Fluor-488-conjugated, goat anti-mouse, polyclonal	goat, immunofluorescence, 1:1000	Invitrogen
Alexa Fluor-568-conjugated, goat anti-mouse, polyclonal	goat, immunofluorescence, 1:1000	Invitrogen
Alexa Fluor-350-conjugated, anti-mouse, polyclonal	goat, immunofluorescence, 1:250	Invitrogen
Horseradish peroxidase, (HRP-conjugated), anti-rabbit, poly-clonal	goat, immunoblot, 1:3000	CellSignaling
Horseradish peroxidase, (HRP-conjugated), anti-mouse, poly-clonal	goat, immunoblot, 1:3000	CellSignaling

6.1.7 Cell culture materials

The materials were obtained from the mentioned manufacturers (Tab. 18).

Tab. 18. Used materials

Material	Manufacturer
Culture slides	Hartenstein (Würzburg)
Cover slips 5-8 mm	Hartenstein
Cell culture flasks	Greiner bio-one
Cell culture multi-well plates	Greiner bio-one (Frickenhausen)
Cell culture pipettes	Greiner bio-one
Cell culture pipettes 25 ml	Sarstedt (Nümbrecht)
Conical screw cap tubes 15 ml	Sarstedt
Conical screw cap tubes 50 ml	Greiner
Cryo screw cap tubes	Greiner
Cuvettes for electroporation	Bio-rad (München)
Erlenmeyer flasks	Schott
Filter-pipette tips	Sarstedt
PCR tubes	Biozym Scientific (Hessisch Oldendorf)
Pipette tips	Sarstedt
Reaction tubes	Sarstedt
Round filter	Hartenstein
Spatulas and spoons	Aesculap (Tuttlingen)
Sterile filter 0.45 µm und 0.22 µm	VWR (Darmstadt)

6.1.8 Equipment

The following equipment were obtained from the manufacturers mentioned below (Tab. 19).

Tab. 19. Equipment

Equipment	Manufacturer
32°C incubator	Binder
-80°C freezer	Heraeus
Amaxa Nucleofector	Lonza (Basel, Switzerland)
Bunsen burner	Camping Gaz
CO_2-incubator HeraCell 240	Hereaus/Thermo Scientific
Cryo freezing Container	Nalgene/Thermo Scientific
Electrophoresis PowerSupply EPS301	GE Healthcare (Freiburg)
Fluorescence microscope BZ-9000	Keyence (Osaka, Japan)
Fluorescence microscope IX81	Olympus (Tokyo, Japan)
Freezer	Liebherr
Gel chambers	PeqLab
Gel iX imager	Intas (Göttingen)
Gene Pulser XCell	BioRad (München)
Heat-magnetic stirrer COMBIMAG RET	IKA (Staufen)
Image system LAS-300 (CCD-Kamera)	Fuji (Tokyo, Japan)
inverted microscope DM IL	Leica (Wetzlar)
Laser scanning confocal microscope 510	Zeiss (Oberkochen)
Laser scanning confocal microscope FV1000	Olympus (Tokyo, Japan)
Micro scale BP 210 S	Sartorius (Göttingen)
Multifuge 4KR	Hereaus, Thermo Scientific
NanoDrop 2000/2000c	PeqLab
pH-meter SevenEasy	Mettler Toledo (Gießen)
Photometer	Eppendorf (Wesseling-Berzdorf)
Pipetteboy	Integra
Refrigerator	Liebherr
Roller/Mixer Smart SRT9	BioCote (Wolverhampton, UK)
Scale EG	Kern (Balingen)
SDS-electrophoresis-chambers dual gel caster	GE Healthcare
Semi-dry blot-device TransBlot SD	BioRad (München)
Shaker-incubator HT Multitron	Infors (Basel, Schweiz)
Shaker Rotamax 120	Heidolph
Sonifier 250	Branson (Danbury, USA)
Stage top heater (for the Keyence microscope)	TOKAI HIT (Fujinomiya-shi, Shizuoka, Japan)
Sterile hood (Laminar Flow) HeraSafe	Heraeus, Thermo Scientific
Table-top centrifuge 5804 R	Eppendorf
Table-top centrifuge Pico/Fresco	Heraeus/Thermo Scientific
Thermo cycler T3000	Biometra (Göttingen)
Thermo mixer compact	Eppendorf
Ultrasonic bath	Brandelin (Berlin)
Vacuum pump system	Vacuubrand
Vortex Genius 3	IKA
Water bath	Memmert (Schwabach)
Water bath Grant GLS 400	VWR (Darmstadt)

6.2 Molecular biology methods

6.2.1 Plasmid-DNA preparation

The isolation of plasmids and BACs from *E. coli* for analysis and cloning purposes were performed by alkaline lysis (Birnboim & Doly, 1979). Bacteria harboring the constructs were grown overnight in 7 ml LB medium with the corresponding antibiotics (30 µg/ml Cm, 35 µg/ml Kan, and/or 100 µg/ml Amp) at 32°C (GS1783) or 37°C (XL-1 Blue) and 220 rounds per minute (rpm) until the stationary phase was reached and then pelleted by centrifugation at 3,500 rpm for 10 min (75006475-rotor, Heraeus). The pellet was resuspended in 300 µl of ice-cold buffer I (Tab. 10) with RNAse A for bacterial RNA degradation. For bacterial lysis, 300 µl of buffer II at room temperature (Tab. 10) were added to the suspension and the mixture was incubated for 3-5 min at room temperature. Immediately, 300 µl of ice-cold buffer III (Tab. 10) were added to the mixture and the resulting solution was incubated on ice for 10 min. At room temperature, the genomic DNA and cell debris were sedimented by centrifugation of the mixture at 13,000 rpm for 15 min (75003424-rotor, Thermo Scientific) and the supernatant was then mixed with 600 µl isopropanol. The plasmid DNA was precipitated in isopropanol and pelleted at 13,000 rpm for at least 30 min (75003424-rotor). The plasmid DNA was washed with 800 µl 70% ethanol, pelleted again at 13,000 rpm for 10 min (75003424-rotor). Finally, the ethanol residues were allowed to evaporate and the pellet was allowed to dissolve in 50 µl water for approximately 30 min at room temperature. For further experiments, the isolated plasmid DNA was stored at -20°C, BAC-DNA at 4°C. The prepared DNA was used for PCR analysis, RFLP analysis, and cloning purposes. BAC DNA for transfection into permissive MeWo cells was prepared with the Plasmid Maxi Kit (Qiagen, Hilden, Germany) according to the manufacturer's instructions. The purified DNA was allowed to dissolve in 100 µl water and was stored at 4°C. The DNA concentration was then measured via Nano-Drop at 1 OD = 50 µg/µl.

6.2.2 Polymerase chain reaction

DNA amplification via PCR serves as analytical procedure for DNA fragments analysis, preparation for cloning, recombination, and DNA sequencing. For the DNA fragments analysis, Taq DNA-polymerase was used (Tab. 14). Usually, plasmids and BAC DNA served as matrices for PCR analysis. However, for the colony PCR, cell material was directly picked from the grown colonies and resuspended in the PCR solution (25-50 µl). In order to identify the positive colonies, all picked colonies were separately grown onto selective agar plates.

The PCR program started with an initial denaturation at 95°C for 5 min. Afterwards, 35 cycles were applied consisting of a denaturation at 95°C for 30 s, an annealing of the oligonucleotides at 55°C for 30 s, and an elongation of the DNA fragment with Taq DNA-polymerase at 72°C for 1 min/kb. The final elongation step was achieved at 72°C for 10 min followed, when

necessary, by a hold time at 4°C. The PCR products were then stored at -20°C for further experiments.

For the preparation of larger DNA fragments with homologous sequences (*e.g.,* primers used for the en-passant mutagenesis), HotStar DNA-polymerase (Tab. 14) was used to avoid self-annealing of the homologous sequences of the used primers. In this case, the PCR program started with an initial denaturation at 95°C for 15 min. Subsequently, 35 cycles were applied consisting of a denaturation at 95°C for 30 s, an annealing of the oligonucleotides at 55°C for 30 s, and an elongation of the DNA fragment with the HotStar DNA-Polymerase at 72°C for 1 min/kb. The final elongation step was achieved at 72°C for 10 min followed, when necessary, by a hold time at 4°C. The PCR products were then stored at -20°C for further experiments.

The Phusion High-Fidelity DNA-Polymerase is used for critical applications such as cloning purposes, since the very low error rate of this polymerase is determined to 4.4 x 10^{-7}. Accordingly, the PCR procedure was performed following the manufacturer's instructions.

For PCR analysis of the viral DNA, permissive melanoma MeWo cells were first infected with 300-400 PFU/ml of the virus in a 6-well dish. After 4 d of infection, the infected MeWo cells were harvested with 10 ml D10 medium and pelleted at 1200 rpm for 10 min (A-4-44-rotor, Eppendorf). The pellet was then resuspended in 200 µl lysis buffer (Tab. 10) and incubated at 56°C for 1-2 h for the degradation of all cellular and viral proteins by proteinase K. In order to prevent the proteinase K from digesting the DNA polymerase during the PCR, the proteinase K was then inactivated for 10 min at 95°C. Similarly, the PCR constructs were stored at -20°C.

The resulting PCR products were analyzed electrophoretically by a 1% agarose gel, visualized by ethidium bromide staining, and the desired PCR fragments were, as necessary, extracted from the gel and purified with the NucleoSpin Extract II kit (Macherey-Nagel, Düren). The purified DNA fragments were applicable for electroporation or for sequencing.

6.2.3 Restriction fragment length polymorphisms

The integrity of the BAC DNA was analyzed for expected restriction fragment length polymorphisms (RFLP). For every RFLP analysis of the generated BAC DNA, 1 µl of the desired restriction enzyme (0.3-0.5 U/µl) was used per 20 µl digestion solution including 2 µl 10x enzyme buffer and 15 µl of the mini-prepared BAC DNA. The digestion was performed at required temperatures according to the manufacturer's instructions (New England Biolabs or Thermo Scientific), mostly overnight (approximately 16 h) at 37°C. The digested BAC DNA was then analyzed electrophoretically by a 0.6% agarose gel resulting in different explicit DNA fragment patterns that were identified in comparison with those of reference data via the Vector NTI software (Life technologies).

6.2.4 Agarose gel electrophoresis

The agarose gel electrophoresis serves for the separation of the DNA fragments according to their sizes. The DNA fragments resuspended in the loading buffer were visualized by ethidium bromide staining under ultraviolet light. The agarose gel was used in different concentrations according to the size of the DNA fragments. The low concentration (0.6%) agarose gel is used for large DNA fragments, whereas the high concentration (1.0%) agarose gel is more appropriate for small DNA fragments. The DNA was separated at 120 V and 400 mA in 1 h. In contrast, the digested BAC DNA constructs were separated electrophoretically overnight via a 0.6% (w/v) agarose gel at 50 V and 400 mA. The visualization and detection of the DNA fragments were achieved via the gel documentation software Gel iX imager (Intas, Göttingen) and then represented as inverted images.

6.2.5 Electrocompetent bacteria preparation

In order to prepare the bacteria (*E. coli* GS1783 strain) for the transfection with the PCR product of interest, the bacteria were subjected to several treatment steps. First, an overnight culture containing the corresponding clone was incubated in 10 ml LB medium with Cm at 32°C and 220 rpm. The next day, the overnight cell culture was inoculated 1:20 in 50 ml LB medium with Cm. This main culture was then incubated at 32°C and 220 rpm until it reached an optical density (OD_{600}) of 0.5-0.7. In order to induce the expression of the Red-protein genes exo, beta, and gam needed for the recombination steps, the culture was incubated in a 42°C water bath and at 220 rpm for 15 min. Subsequently, the culture was transferred to an ice-water bath for 20 min and 220 rpm. After centrifugation of the culture at 4,500 x g and 0°C for 5 min, the bacterial sediment was washed three times with 50 ml ice-cold 10% (v/v) glycerol in distilled water und finally resuspended in 500 µl of 10% glycerol (1:100 of the original culture volume). At last, the suspension was portioned into 50 µl samples and shock-frozen in a dry ice ethanol bath then stored at -80°C.

6.2.6 En-passant mutagenesis

The Red-recombination steps were performed via the en-passant mutagenesis technique in the *E. coli* GS1783 strain which is a derivative of the DY380 strain. The expression cassette of the Red-recombination proteins exo, beta, and gam is regulated by a temperature sensitive promoter on a defective λ-prophage integrated within the bacterial genome. Furthermore, the GS1783 strain includes the endonuclease I-SceI gene (Aph AI) whose expression is inducible by L(+)-arabinose (Lee et al., 2001; Tischer et al., 2006).

First, the en-passant PCR product was amplified with the HotStar DNA polymerase using the corresponding oligonucleotides. This PCR product is needed for the first Red-recombination step and it is composed of the positive selection marker (Kan^R), eGFP or mRFP sequences, and the I-SceI recognition site. The PCR product was analyzed on a 1% (w/v) agarose gel

and purified. A portion (100 ng) of the purified PCR product were electroporated into the electrocompetent bacteria in 1 mm cuvettes at 1500 V, 25 µF, and 200 Ω. Immediately after the second pulse, the bacteria were mixed with 1 ml LB medium (without antibiotics) and then incubated at 32°C and 350 rpm for 2 h. After the recombination through the homologous 50 bp sequences of the PCR product, the positive colonies were selected on Petri dishes with selective agar containing Cm and Kan, since the positive colonies were resistant against Cm and Kan after the first Red-recombination step.

In order to generate a seamless fusion mutant, the kanamycin cassette was excluded from the BAC-cloned genome via a second Red-recombination step. First, an over-night culture of the bacteria from the first Red-recombination was inoculated in 5 ml LB medium containing Kan and Cm. The next day, 100 µl of the overnight culture were inoculated in 2 ml LB medium containing just Cm and then incubated at 32°C and 220 rpm. After 3-4 h, a mixture of 2 ml LB medium containing Cm and 1% (w/v) L(+) arabinose was added to the culture and incubated again at 32°C and 220 rpm for 60 min. This step is applied in order to induce the expression of the endonuclease I-SceI gene that cleaves the genome at the I-SceI recognition site resulting in a double strand cleavage close to the Kan cassette. Subsequently, the Red-proteins genes were induced at 42°C and 220 for 30 min for the following Red-recombination of the homologous duplications at the cleavage site. The bacteria were then incubated for another 4 h at 32°C and 220 rpm and finally plated in different dilutions (10^{-4} - 10^{-6}) onto LB-agar plates containing Cm and 1% (w/v) L(+) arabinose for 2 d. The positive colonies were then, as mentioned before, detected by colony PCR, identified by RFLP analysis, and finally verified by sequencing the flanking areas of the fusion sites.

6.2.7 Sequencing

For the DNA sequencing of BAC and plasmid DNA after cloning or recombination processes, the Sanger sequencing method using chain-terminating inhibitors was applied (Sanger et al., 1977). Accordingly, 50-100 ng of the purified DNA fragment were used. The entire sequencing solution of 10 µl was composed of 1/10 BigDye Version 1.1 (Applied Biosystems, Darmstadt), 0.5x sequencing buffer, and 0.5 µM of the corresponding oligonucleotides. The sequencing program started with an initial denaturation at 96°C for 1 min. Afterwards, 24 cycles were applied consisting of a denaturation at 96°C for 10 s, an annealing of the oligonucleotides at 50°C for 5 s, and an elongation of the DNA fragment at 60°C for 4 min. The samples were then sequenced on a capillary sequencer (DNA Analyser 3700, Applied Biosystems, Darmstadt) in the Institute for Clinical Molecular Biology of Kiel University. Finally, the sequencing data were analyzed by the Vector NTI software (Life technologies).

6.2.8 RNA isolation and reverse transcriptase PCR

RNA was extracted from infected cells according to a published protocol (Chomczynski & Sacchi, 1987). VZV-infected MeWo cells were scraped from a T75 cell culture flask at 3-4 dpi in 4 ml ice-cold PBS. Infected cell suspension was then centrifuged at 1200 rpm and 4°C for 10-15 min (A-4-44-rotor). After discarding the supernatant, the pellet were shock-frozen and stored at -80°C until needed for further experiments. For RNA isolation, the pellet was resuspended in 1 ml Trizol reagent (Invitrogen, Darmstadt, Germany) and incubated at room temperature for 5 min. Hereafter, 200 µl chloroform (Fluka, Merck, Darmstadt, Germany) were added and the suspension was shaken for 15 s before incubating again at room temperature for 2-3 min. For the phase separation, the mixture was centrifuged for 15 min at 13,000 rpm and 4°C (75003424-rotor). The RNA-containing aqueous phase was then isolated and collected in 500 µl isopropanol for RNA precipitation. After incubation for 10 min at room temperature, RNA was sedimented by centrifugation at 13,000 rpm and 4°C for 15 min (75003424-rotor). RNA-sediment was then washed in 1 ml 70% ethanol by centrifugation at 8,000 rpm and 4°C for 10 min (75003424-rotor) and ethanol was allowed to evaporate before dissolving the RNA-sediment in 30 µl ice-cold PCR-water (5 PRIME, Hilden). The RNA concentration was then measured via Nano-Drop at 1 OD = 40 µg/µl. Thereafter, 16 µg RNA were treated with 5 U DNase I (10 U/µl; Roche), 1x DNase buffer (5 µl), and 20 U RNase-inhibitor (Thermo Scientific) in a total volume of 50 µl for 20 min at 37°C to degrade residual genomic DNA. Finally, DNase I was deactivated upon incubation at 75°C for 10 min and the RNA was then stored, when needed, at -80°C.

For the complementary cDNA synthesis, 1 µg (2 µl) oligo (dT)12-18 primer (Invitrogen) and 500 µM (2 µl) dNTPs (Thermo Scientific) were added to 25 µl DNase-I-treated RNA, then incubated at 65°C for 5 min before cooling on ice. The mixture was then supplemented with 5x transcription buffer (8 µl) and 5 mM (2 µl) dithiothreitol (DTT, Thermo Scientific), then incubated at 42°C for 2 min. Subsequently, 200 U (1 µl) superscript II RT (Invitrogen) were added for the cDNA synthesis upon incubation at 42°C for 15 min before RT deactivation at 70°C for 15 min. In parallel, negative-control samples were prepared without RT supplement, in order to confirm the absence of cellular and viral DNA contaminations.

For the RT-PCR analysis, the viral fusion genes sequences were amplified from total cellular cDNA mix with phusion polymerase. As a positive cellular reference, glyceraldehyde 3-phosphate dehydrogenase (GAPDH) transcripts were detected in all samples to confirm the correct cDNA synthesis. As a negative control, fusion genes were detected in RNA isolates from wild-type HJO-infected MeWo cells. In a total volume of 20 µl, 2 µl cDNA, 1x (4 µl) HF buffer, 200 µM (0.4 µl) dNTPs, 0.5 µM (0.2 µl) of each forward and reverse oligonucleotide (Tab. 20), and 0.4 U (0.2 µl) phusion polymerase were mixed for RT-PCR analysis. All melting

temperatures of the used oligonucleotides were calculated via the TM calculator of Thermo-Fisher (www.finnzymes.com/tm_determination.html) as summarized in Tab. 20.

Tab. 20. Melting temperatures of RT-PCR oligonucleotides and annealing temperatures of the fusion genes

Code	Oligonucleotide	Melting temperature	Annealing temperature
1836	eGFP-23 for	71.2°C	68.6°C
1521	eGFP-23 rev	65.6°C	
1158	4-mRFP for	65.2°C	68.2°C
3210	4-mRFP rev	67.9°C	
1836	eGFP-65 for	71.2°C	60.7°C
1527	eGFP-65 rev	57.7°C	
1578	mRFP-23 for	62.5°C	62.5°C
1521	mRFP-23 rev	65.6°C	
3211	GAPDH for	74.7°C	74.7°C
3212	GAPDH rev	75.0°C	

The RT-PCR program started with an initial denaturation at 98°C for 30 s. Afterwards, 35 cycles were applied consisting of a denaturation at 98°C for 10 s, an annealing of the oligonucleotides at (annealing temperatures, Tab. 20) for 30 s, and an elongation of the DNA fragment at 72°C for 30 s/1 kb. The final elongation step was achieved at 72°C for 10 min followed, when necessary, by a hold time at 4°C. PCR products were stored at -20°C for further experiments.

6.2.9 Immunoblot analysis

For the detection of the fluorescent fusion proteins, infected MeWo cells of a T75 culture flask were scraped into 4 ml ice-cold PBS. The suspension was then centrifuged at 1500 rpm and 4°C for 15 min (A-4-44-rotor). Thereafter, the pellet was resuspended in 300 µl ice-cold RIPA-PIC buffer (Tab. 8) and then incubated on ice for 30 min. Cell debris was then centrifuged at 13,000 rpm and 4°C for 20 min (75003424-rotor). After that, the protein lysates were collected in 50 µl portions and stored, when needed, at -80°C. For the protein concentration measurement, the Quick Start Bradford protein-assay kit (Bio-Rad, München) was used. In brief, three samples of each protein lysate were tested in parallel by which 1 µl of each sample was added to 149 µl water and mixed with 150 µl Bradford dye reagent then incubated for 5 min at room temperature. The absorption was then spectrophotometrically measured at λ = 595 nm via Safire^2 fluorimeter (TECAN, Crailsheim).

For the Western blot analysis, approximately 50-70 µg of each protein lysate were heat-denatured in 1x Laemmli buffer with 2-mercaptoethanol at 95°C for 10 min before incubation on ice (Laemmli, 1970). As a positive control, protein lysates from MeWo cells infected with an mRFP-expressing VZV Oka strain (provided by Benedict Kaufer, Berlin) and lysates from HeLa cells transfected with an expression vector of eGFP-β-actin fusion protein (provided by Gregor Maschkowitz, Kiel) were used to control the expression of the mRFP and eGFP

moieties, respectively. As a negative control, protein lysates from uninfected MeWo and HeLa cells were tested. Proteins were separated according to their molecular masses by using 10% SDS-polyacrylamide gel electrophoresis (SDS-PAGE) at 90 V and 400 W for 30 min then at 110 V and 400 W for 90 min. Subsequently, the proteins were blotted onto nitrocellulose membranes (Merck Millipore) at 20 V and 400 W for 30 min then incubated in WB blocking buffer (Tab. 8) for 1 h at room temperature or overnight at 4°C. Under the same incubation conditions, anti-VZV-gI as a viral control, anti ß-actin as a cellular control, anti-GFP, and anti-RFP antibodies (Tab. 17) were used for the proteins detection. After three to five washings with TBST buffer (Tab. 8) within 15 min, membranes were incubated with HRP-conjugated goat anti-rabbit or anti-mouse secondary antibody (Tab. 17) for 1 h at room temperature followed by washes as described above. Detection was completed using the SuperSignal West Pico and Femto chemiluminescence substrates (Thermo Scientific) and protein signals were monitored via LAS-3000 CCD camera system (Tab. 19).

6.3 Cell biology methods

6.3.1 Cell culture

VZV-permissive human melanoma MeWo cells (ATCC-HTB-65) were cultivated in 25 ml D10 medium (Tab. 13) in 175 cm^2-flasks at 37°C, 5% CO_2, and 95% relative humidity as previously described (Grose & Brunell, 1978). As the MeWo cells formed a confluent monolayer after 5-7 d, they were harvested by trypsinization and passaged at a ratio of 1:6 in new D10 medium that was replaced by fresh D10 medium after further 3-4 d. In cultivated MeWo cells, BAC-cloned genomes were transfected for the reconstitution of the corresponding viruses. The infected MeWo cells were cocultivated with uninfected cells in different ratios and later on, as needed, were harvested by trypsinization, resuspended in PBS, and pelleted at 1200 rpm for 10 min (A-4-44-rotor). The pellet containing the virus-infected MeWo cells was resuspended either in ice-cold FBS medium and stored in portions in 9% DMSO at -80°C for further experiments, or in lysis buffer (Tab. 10) as previously described for the PCR-analysis (6.2.2). The portions were frozen gradually at approximately 1°C per min using an isopropanol-box in a -80°C freezer, in order to prevent the MeWo cells from destruction by a too fast freezing process.

6.3.2 BAC DNA transfection and virus reconstitution

VZV-permissive MeWo cells were lipofected with the corresponding BAC-cloned genomes via Lipofectamine 2000 (Life technologies). First, permissive MeWo cells in 6 ml D10 medium were seeded in three wells of a 6-well cell culture plate at a concentration of 1.5 * 10^6 MeWo cells in each well (2 ml). Next day, the 90% confluent MeWo cells in each well were transfected with 500 µl of the transfection solution after replacing the D10 medium with DMEM medium without additives (Tab. 12). The transfection solution is a mixture of two parts. The

first solution was prepared mixing 10 µl Lipofectamine 2000 and 240 µl OptiMEM for 5 min. Separately, the second solution was prepared mixing 4 µg BAC DNA in a total volume of 250 µl OptiMEM. The transfection solution was prepared by mixing the first and second solutions and incubating the mixture for 20 min at room temperature, in order to allow the formation of DNA-harboring liposomes. The following day, the DMEM medium without additives was replaced by fresh D10 medium and the cell culture was incubated for another 24 h. At that time, the infected MeWo cells from the three wells were harvested via trypsinization, resuspended all together in 6 ml D10 medium, and finally cocultivated in 25 ml D10 medium in a 175 cm^2-flask. The first plaques were detectable under the microscope after approximately 5 d of the last incubation.

For the transfection via the electroporation-based nucleofection technique, 2 * 10^6 MeWo cells or 4-5 * 10^5 HFF cells were resuspended in 100 µl OptiMEM medium at room temperature. Thereafter, 5 µg of the BAC-DNA were added to the suspension in a 2 mm electroporation-specific cuvette. The cuvette was then placed in the Amaxa-Nuleofector device using the program (T2O for MeWo cells), which allows the BAC-DNA to penetrate into the cell. Subsequently, the suspension was further cultivated in 2 ml fresh D10 medium in a well of a 6-well-plate at 37°C and 5% CO2. The well was then daily monitored for CPE formation.

6.3.3 Virus titration and replication kinetics

Titration experiments for the wild-type and recombinant viruses were performed by a modifycation of previously published methods (Grose et al., 1979). In short, 2-3 x 10^5 MeWo cells were seeded in each well of a 24-well plate one d before and were inoculated with 500 µl of serially 10-fold diluted infected MeWo cells in quadruplicates. At 3 dpi, fluorescent cytopathic effects (CPEs) were counted under the Olympus fluorescence microscope IX80 (Tab. 19) and then calculated as PFU/ml considering the dilution factors. For the titration of the non-fluorescent wild-type HJO virus, the indirect immunofluorescence method was applied by which HJO-infected MeWo cells in 24-well cell culture plates were prepared. At 3 dpi, the D10 medium was removed and the cells were rinsed once with 1x PBS and then fixed with 2% paraformaldehyde in 1x PBS for 20 min. Afterwards, the fixed cells were rinsed twice with 1x PBS and then permeabilized with 1% (w/v) saponin in 1x PBS for 5 min and then rinsed twice again with 1x PBS. The unspecific bonds were blocked with 10% (v/v) FBS in 1x PBS for 1 h. Thereafter, the cells were incubated for 1 h in a mixture of the primary anti VZV-gI antibody in 1x PBS (Tab. 17), 10% (v/v) FBS, and 0.02% sodium azide as a preservative. The cells were then rinsed three times with 1x PBS and PFU detection was achieved by the secondary antibody staining (Alexa Fluor 488, 1:1000) in 1x PBS (Tab. 17) with 10% (v/v) FBS for 1 h. Finally, the cells were rinsed thrice with 1x PBS, and the visualization and analysis of the detected PFUs were achieved by the Olympus fluorescence microscope IX81 (Tab. 19).

The replication kinetics of the generated fluorescently tagged mutants in comparison to those of the wild-type HJO strain were performed by infecting the same number of VZV-permissive MeWo cells with equal PFU quantity of each viral variant. Accordingly, 50-60% confluent MeWo cells were seeded and infected with 100 PFU per well in a 6-well plate and simultaneously in a 24-well plate (for the titration at 0 dpi) per recombinant virus. Over 5 dpi, the infected cells of the 6-well plates were washed gently with PBS, trypsinized, resuspended in D10 medium, sedimented at 1200 rpm for 10 min (A-4-44-rotor), resuspended in FBS, and stored in portions in 10% DMSO at -80°C. Later on, titration was carried out as described above in quadruplicates in 24-well plates. The replication kinetic analysis was performed independently in triplicate, in order to confirm the reliability of the results.

6.3.4 Fluorescence imaging

For confocal imaging of infected non-neuronal cells, MeWo and fibroblast cells were seeded and inoculated on coverslips. At 2 dpi, infected cells were washed with PBS and fixed with 2% paraformaldehyde in PBS for 20 min. After two washes with PBS and Hoechst 33342 nuclear staining (Thermo Scientific) for 20 min, the cells were washed again before mounted on glass slides with mounting medium without DAPI (Vectashield, Biozol, Eching, Germany). For extra TGN staining, anti golgin-97 antibody (Santa Cruz, Heidelberg, Germany) was applied using the indirect immunofluorescence method described above (6.3.3). Imaging was performed with the Olympus laser scanning confocal microscope FV1000 (Tab. 19), and images were processed with FV1000 viewer software (Version 02.0b).

For confocal imaging of infected neurons, freshly prepared embryonic rat sensory neurons (see DRG cells preparation below, 6.3.5) were seeded in channels of µ-slide $6^{0.4}$ (ibidi, Planegg, Germany) coated with (poly-L-lysine (200 µg/ml) + laminin (20 µg/ml); Tab. 12) then co-cultivated with infected fibroblasts for 2 d in supplemented NBM (Tab. 13). At 2 dpi, infected cells were fixed with Zamboni's fixative buffer (Tab. 13) for 20 min, washed with PBS, and permeabilized with 0.1% Triton-X100 in PBS for 5 min. After several washes, cells were incubated with blocking buffer (10% normal goat serum in PBS; Dianova, Hamburg, Germany) for 60 min. For the identification of neuronal cells, the mouse anti ß-III tubulin primary antibody was used and detected by Alexa Fluor 350 goat anti-mouse secondary antibody (Tab. 17). For the DNA and nuclear staining, TO-PRO-3 iodide (Thermo Scientific) was applied. The Zeiss laser scanning confocal microscope LSM 510 (Tab. 19) was used for image acquisition, and images were processed with the LSM Image Browser software and ImageJ software.

6.3.5 Cell-free VZV preparation

This experiment was modified based on several previous protocols (Bleymehl et al., 2011; Goodwin et al., 2013; Grose et al., 1979; Harper et al., 1998; Reichelt et al., 2009; Schmidt-

Chanasit et al., 2008). Cells of approximately 50%-infected confluent HFF fibroblasts from eight to ten 175 cm2 flasks were scraped and collected in ice-cold PBS, then pelleted by centrifugation at 1500 rpm and 4°C for 15 min (A-4-44-rotor). Afterwards, the cells were resuspended in 4 ml of ice-cold PSGC buffer (Tab. 13). Cells were then disrupted by a Dounce homogenizer 30 times followed by a sonication step in ice-cold water-bath 3 times for 2 min each and 30 s breaks in between. For the best yield, approximately (10^5 PFU/ml), cell-free VZV and infectious debris together were portioned and stored at -80°C.

6.3.6 Dorsal-root ganglia cells preparation and cultivation

Preparation protocols and cultivation systems were adapted from published protocols (Bauer et al., 2014). Shortly, 18-d-old rat embryos (E18) were dissected from the uterus of pregnant Wistar rats shortly after CO_2-euthanization. Immediately thereafter, E18 embryos were decapitated and rinsed with ice-cold HBSS medium (Tab. 12). DRG cells were isolated after laminectomy, then collected again in ice-cold HBSS. The sensory neurons were prepared after the dissociation of DRG cells by treatment with 2.5% trypsin in PBS (Tab. 12) for 30 min at 37°C followed by trypsin inhibitor DTI (Tab. 12) treatment for 5 min at 37°C. DRG cells and/or dissociated sensory neurons were cultivated at 37°C and 5% CO2 in supplemented NBM (Tab. 13) which was occasionally replaced.

6.3.7 Compartmentalized neuron cultivation systems

ibidi µ-slides $6^{0.4}$ were coated overnight at room temperature with a mixture of 400 µg/ml poly-L-lysine and 20 µg/ml laminin (Tab. 12) in water. After three washings and a final drying step, every channel between the pair of chambers was filled with 30 µl of 0.5% agarose (Invitrogen) in supplemented NBM without NGF, and then allowed to cool until agarose became completely solid. Subsequently, one to three freshly prepared ganglia were seeded into one chamber filled with 60 µl of supplemented NBM (Tab. 13), whereas the opposite chamber was filled with medium containing 10-fold higher NGF concentration (125 ng/ml) to accelerate axonal growth toward the distal chamber (Fig. 25A). After cultivation overnight at 37°C and 5% CO_2, DRG cells were treated with 40 µl of 10 µM Ara-C (Tab. 12) for 2-3 d to terminate the growth of ganglionic non-neuronal cells (Campenot, 1977). Hereafter, the medium was aspirated and the ganglia cells were further cultivated in a fresh supplemented NBM until axons reached the distal chamber.

Anterograde and retrograde infections were initiated by cultivating DRG cells in 60 µl of 10^4-10^5 PFU/ml of cell-free VZV at 37°C and 5% CO_2. After 2-3 h, medium was replaced with fresh virus-free medium and axons were daily monitored to trace the colocalization of the fluorescently labeled proteins using the Keyence fluorescence microscope BZ-9000 (Tab. 19).

An alternative compartmentalized cultivation system was developed using an ibidi chemotaxis µ-slide3D further improving the efficiency of the former protocol and providing an additional convenient method to study the axonal transport of VZV. In this system, 0.1% agarose in supplemented NBM without NGF was used, and axons were allowed to grow for 1-2 weeks followed by anterograde infection with 10^4-10^5 PFU/ml of cell-free VZV (Fig. 27).

7 REFERENCES

Albert B, Bray D, Lewis J, Raff M, Roberts K, Watson J (1989) The nervous system. pp. 1059-1064. Molecular biology of the cell 2nd edition, Garland publishing, New York.

Almeida JD, Howatson AF, Williams MG (1962) Morphology of varicella (chicken pox) virus. Virology 16: 353-355.

Andrei G, Topalis D, Fiten P, McGuigan C, Balzarini J, Opdenakker G, Snoeck R (2012) In vitro-selected drug-resistant varicella-zoster virus mutants in the thymidine kinase and DNA polymerase genes yield novel phenotype-genotype associations and highlight differences between antiherpesvirus drugs. J Virol 86: 2641-52.

Antinone SE, Smith GA (2010) Retrograde axon transport of herpes simplex virus and pseudorabies virus: a live-cell comparative analysis. J Virol 84:1504–1512.

Arvin AM (2001) Varicella-zoster virus: molecular virology and virus-host interactions. Curr. Opin Microbiol 4: 442-449.

Arvin A, Campadelli-Fiume G, Mocarski E, Moore PS, Roizman B, Whitley R, Yamanishi K (2007) Human herpesviruses, biology, therapy and immunoprophylaxis. Cambridge: Cambridge University Press.

Annunziato PW, Lungu O, Panagiotidis C, Zhang JH, Silvers DN, Gershon AA, Silverstein SJ (2000) Varicella-zoster virus proteins in skin lesions: implications for a novel role of ORF29p in chickenpox. J Virol 74: 2005-2010.

Asano Y, Itakura N, Kajita Y, Itakura N, Kajita Y, Suga S, Yoshikawa T, Yazaki T, Ozaki T, Yamanishi K, Takahashi M (1990) Severity of viremia and clinical findings in children with varicella. J Infect Dis 161: 1095-1098.

Baudoux L, Defechereux P, Rentier B, Piette J (2000) Gene activation by varicella-zoster virus IE4 protein requires its dimerization and involves both the arginine-rich sequence, the central part, and the carboxyl-terminal cysteine-rich region. J Biol Chem 275: 32822-32831.

Bauer A, Nolden T, Schröter J, Römer-Oberdörfer A, Gluska S, Perlson E, Finke S (2014) Anterograde glycoprotein-dependent transport of newly generated rabies virus in dorsal root ganglion neurons. J Virol 88: 14172-14183.

Birnboim HC, Doly J (1979) A rapid alkaline extraction procedure for screening recombinant plasmid DNA. Nucleic Acids Res 7: 1513-1523.

Bleymehl K, Cinatl J, Schmidt-Chanasit J (2011) Phenotypic and genetic characterization of varicella-zoster virus mutants resistant to acyclovir, brivudine and/or foscarnet. Med Microbiol Immunol 200: 193-202.

Booy FP, Trus BL, Newcomb WW, Brown JC, Conway JF, Steven AC (1994) Finding a needle in a haystack: detection of a small protein (the 12-kDa VP26) in a large complex (the 200-MDa capsid of herpes simplex virus). Proc Natl Acad Sci USA 91: 5652-5656.

Brune W, M. Messerle UH, Koszinowski U (2000) Forward with BACs: new tools for herpesvirus genomics. Trends Genet 16: 254-259.

Brunnemann AK, Bohn-Wippert K, Zell R, Henke A, Walther M, Braum O, Maschkowitz G, Fickenscher H, Sauerbrei A, Krumbholz A (2015) Drug resistance of clinical varicella-zoster virus strains confirmed by recombinant thymidine kinase expression and by targeted resistance mutagenesis of a cloned wild-type isolate. Antimicrob Agents Chemother 59: 2726-2734.

Campenot RB (1977) Local control of neurite development by nerve growth factor. Proc Natl Acad Sci USA 74: 5416-4519

Casey TA, Ruyechan WT, Flora MN, Reinhold W, Straus SE, Hay J (1985) Fine mapping and sequencing of a variable segment in the inverted repeat region of varicella-zoster virus DNA. J Virol 54: 639-642.

Chaudhuri V, Sommer M, Rajamani J, Zerboni L, Arvin AM (2008) Function of Varicella-Zoster virus ORF23 capsid protein in viral replication and the pathogenesis of skin infection. J Virol 82:10231-10246.

Chen JJ, Zhu Z, Gershon AA, Gershon MD (2004) Mannose 6-phosphate receptor dependence of varicella zoster virus infection in vitro and in the epidermis during varicella and zoster. Cell 119: 915-926.

Chlibek R, Bayas JM, Collins H, de la Pinta ML, Ledent E, Mols JF, Heineman TC (2013) Safety and immunogenicity of an AS01-adjuvanted varicella-zoster virus subunit candidate vaccine against herpes zoster in adults >=50 years of age. J Infect Dis 208: 1953-1961.

Chomczynski P, Sacchi N (1987) Single-step method of RNA isolation by acid guanidinium thiocyanate-phenol-chloroform extraction. Anal Biochem 162: 156-159.

Christensen J, Steain M, Slobedman B, Abendroth A (2013) Varicella-zoster virus glycoprotein I is essential for spread in dorsal root ganglia and facilitates axonal localization of structural virion components in neuronal cultures. J Virol 87: 13719-13728.

Cohen JI, Krogmann T, Ross JP, Pesnicak L, Prikhod'ko EA (2005) Varicella-zoster virus ORF4 latency-associated protein is important for establishment of latency. J Virol 79: 6969-6975.

Cohen JI, Sato H, Srinivas S, Lekstrom K (2001) Varicella-zoster virus (VZV) ORF65 virion protein is dispensable for replication in cell culture and is phosphorylated by casein kinase II, but not by the VZV protein kinases. Virology 280: 62-71.

Cohen JI, Straus SE, Arvin AM (2007) Varicella-Zoster virus. In: Fields B, Virology, eds. Knipe D, Howley P, Fifth Edition, pp. 2773-2818. Philadelphia: Lippincott Williams & Wilkins.

Cohrs RJ, Barbour M, Gilden DH (1996) Varicella-zoster virus (VZV) transcription during latency in human ganglia: detection of transcripts mapping to genes 21, 29, 62, and 63 in a cDNA library enriched for VZV RNA. J Virol 70: 2789-2796.

Cohrs RJ, Gilden DH, Kinchington PR, Grinfeld E, Kennedy PG (2003) Varicella-zoster virus gene 66 transcription and translation in latently infected human Ganglia. J Virol 77: 6660-6665.

Cunningham AL, Lal H, Kovac M, Chlibek R, Hwang SJ, Díez-Domingo J, Godeaux O, Levin MJ, McElhaney JE, Puig-Barberà J, Vanden Abeele C, Vesikari T, Watanabe D, Zahaf T, Ahonen A, Athan E, Barba-Gomez JF, Campora L, de Looze F, Downey HJ, Ghesquiere W, Gorfinkel I, Korhonen T, Leung E, McNeil SA, Oostvogels L, Rombo L, Smetana J, Weckx L, Yeo W, Heineman TC; ZOE-70 Study Group (2016) Efficacy of the herpes zoster subunit vaccine in adults 70 years of age or older. N Engl J Med 375: 1019-1032.

Davison AJ (1984) Structure of the genome termini of varicella-zoster virus. J Gen Virol 65: 1969-1977.

Davison AJ, Scott JE (1986) The complete DNA sequence of varicella-zoster virus. J Gen Virol 67: 1759-1816.

Defechereux P, Debrus S, Baudoux L, Rentier B, Piette J (1997) Varicella-zoster virus open reading frame 4 encodes an immediate-early protein with posttranscriptional regulatory properties. J Virol 71: 7073-7079.

Defechereux P, Melen L, Baudoux L, Merville-Louis MP, Rentier B, Piette J (1993) Characterization of the regulatory functions of varicella-zoster virus open reading frame 4 gene product. J Virol 67: 4379-4385.

Diefenbach RJ, Miranda-Saksena M, Douglas MW, Cunningham AL (2008) Transport and egress of herpes simplex virus in neurons. Rev Med Virol 18: 35-51.

DuRaine G, Wisner TW, Howard P, Williams M, Johnson DC (2017) Herpes simplex virus gE/gI and US9 promote both envelopment and sorting of virus particles in the cytoplasm of neurons, two processes that precede anterograde transport in axons. J Virol 91: e00050-17.

Fleetwood-Walker SM, Quinn JP, Wallace C, Blackburn-Munro G, Kelly BG, Fiskerstrand CE, Nash AA, Dalziel RG (1999) Behavioural changes in the rat following infection with varicella-zoster virus. J Gen Virol 80: 2433-2436.

Frame MC, McGeoch DJ, Rixon FJ, Orr AC, Marsden HS (1986) The 10K virion phospho-protein encoded by gene US9 from herpes simplex virus type 1. Virology 150: 321-332.

Furlong D, Swift H, Roizman B (1972) Arrangement of herpesvirus deoxyribonucleic acid in the core. J Virol 10: 1071-1074.

Gershon AA, Chen J, Gershon MD (2008) A model of lytic, latent, and reactivating varicella-zoster virus infections in isolates enteric neurons. J Infect Dis 197: S61-S65.

Gershon AA, Steinberg S, Silber R (1978) Varicella-zoster viremia. J Pediatr 92: 1033-1034.

Goldstein LS, Yang Z (2000) Microtubule-based transport systems in neurons: the roles of kinesins and dyneins. Annu Rev Neurosci 23: 39-71.

Gomi Y, Sunamachi H, Mori Y, Nagaike K, Takahashi M, Yamanishi K (2002) Comparison of the complete DNA sequences of the Oka varicella vaccine and its parental virus. J Virol 76: 11447-11459.

Goodwin TJ, McCarthy M, Osterrieder N, Cohrs RJ, Kaufer BB (2013) Three-dimensional normal human neural progenitor tissue-like assemblies: a model of persistent Varicella-Zoster virus infection. PLoS Pathog 9: e1003512.

Grigorian S, Kinchington PR, Yang IH, Selariu A, Zhu H, Yee M, Goldstein RS (2012) Retrograde axonal transport of VZV: kinetic studies in hESC-derived neurons. J Neurovirol 18: 462-470.

Grose C (1981) Variation on a theme by Fenner: the pathogenesis of chickenpox. Pediatrics 68: 735-737.

Grose C, Brunell PA (1978) Varicella-zoster virus: isolation and propagation in human melanoma cells at 36 and 32 degrees. C Infect Immun 19: 199-203.

Grose C, Carpenter JE, Jackson W, Duus KM (2010) Overview of varicella-zoster virus glycoproteins gC, gH and gL. Curr Top Microbiol Immunol 342: 113-128.

Grose C, Perrotta DM, Brunell PA, Smith GC (1979) Cell-free varicella-zoster virus in cultured human melanoma cells. J Gen Virol 43: 15-27.

Gross SP, Welte MA, Block SM, Wieschaus EF (2000) Dynein-mediated cargo transport in vivo. A switch controls travel distance. J Cell Biol 148: 945-956.

Hambleton S, Gershon AA (2005) Preventing varicella-zoster disease. Clin Microbiol Rev 18: 70-80.

Harper DR, Mathieu N, Mullarkey J (1998) High-titre, cryostable cell-free varicella zoster virus. Arch Virol 143: 1163-1170.

Hondo R, Yogo Y (1988) Strain variation of R5 direct repeats in the right-hand portion of the long unique segment of varicella-zoster virus DNA. J Virol 62: 2916-2921.

Hope-Simpson RE (1965) The nature of herpes zoster: A long term study and a new hypothesis. Proc Roy Soc Med 58: 9-20.

Howard PW, Wright CC, Howard T, Johnson DC (2014) Herpes simplex virus gE/gI extracellular domains promote axonal transport and spread from neurons to epithelial cells. J Virol 88:11178-11186.

Huang Y, Zhang J, Halawa MA, Yao S (2014) Nuclear localization signals of varicella zoster virus ORF4. Virus Genes 48: 243-251.

Johnson DC, Baines JD (2011) Herpesviruses remodel host membranes for virus egress. Nat Rev Microbiol 9: 382-394.

Kandel ER, Schwartz JH, Jessell TM, Siegelbaum SA, Hudspeth AJ (2013) Nerve Cells, Neural Circuitry and Behaviors. pp. 21-38. Principles of neural science 5th edition. McGrawHill Medical.

Kennedy PG, Grinfeld E, Gow JW (1999) Latent varicella-zoster virus in human dorsal root ganglia. Virology 258: 451-454.

Kinchington PR, Bookey D, Turse SE (1995a) The transcriptional regulatory proteins encoded by varicella-zoster virus open reading frames (ORFs) 4 and 63, but not ORF 61, are associated with purified virus particles. J Virol 69: 4274-4282.

Kinchington PR, Hougland JK, Arvin AM, Ruyechan WT, Hay J (1992) The varicella-zoster virus immediate-early protein IE62 is a major component of virus particles. J Virol 66: 359-366.

Kinchington PR, Vergnes JP, Turse SE (1995b) Transcriptional mapping of varicella-zoster virus regulatory proteins. Neurology 45, 12 Suppl 8: S33-35.

Koropchak CM, Diaz PS, Arvin AM (1989) Investigation of varicella-zoster virus infection of lymphocytes by in situ hybridization. J Virol 63: 2392-5.

Koropchak CM, Graham G, Palmer J, Winsberg M, Ting SF, Wallace M, Prober CG, Arvin AM (1991) Investigation of varicella-zoster virus infection by polymerase chain reaction in the immunocompetent host with acute varicella. J Infect Dis 163: 1016-1022.

Kratchmarov R, Taylor MP, Enquist LW (2012) Making the case: Married versus separate models of alphaherpes virus anterograde transport in axons. Rev Med Virol 22: 378-391.

Krause PR, Klinman DM (1995) Efficacy, immunogenicity, safety, and use of live attenuated chickenpox vaccine. J Pediatr 127: 518-525.

Krause PR, Klinman DM (2000) Varicella vaccination: evidence for frequent reactivation of the vaccine strain in healthy children. Nat Med 6: 451-454.

Kress M, Fickenscher H (2001) Infection by human varicella-zoster virus confers norepinephrine sensitivity to sensory neurons from rat dorsal root ganglia. FASEB J 15:1037-1043.

Laemmli UK (1970) Cleavage of structural proteins during the assembly of the head of bacteriophage T4. Nature 227: 680-685.

Lal H, Cunningham AL, Godeaux O, Chlibek R, Diez-Domingo J, Hwang SJ, Levin MJ, McElhaney JE, Poder A, Puig-Barberà J, Vesikari T, Watanabe D, Weckx L, Zahaf T, Heineman TC; ZOE-50 Study Group (2015) Efficacy of an adjuvanted herpes zoster subunit vaccine in older adults. N Engl J Med 372: 2087-2096.

Le P, Rothberg MB (2018) Cost-effectiveness of the adjuvanted herpes zoster subunit vaccine in older adults. JAMA Intern Med doi: 10.1001/jamainternmed.2017.7431.

Lenac Rovis TA, Bailer SM, Pothineni VR, Ouwendijk WJD, Simic H, Babić M, Miklić K, Malić S, Verweij MC, Baiker A, Gonzalez O, von Brunn A, Zimmer R, Früh K, Verjans GM, Jonjić S, Haas J (2013) Comprehensive analysis of Varicella-Zoster virus proteins using a new monoclonal antibody collection. J Virol 87: 6943-6954.

Lasek RJ, Garner JA, Brady ST (1984) Axonal transport of the cytoplasmic matrix. J Cell Biol 99: 212-221.

Lee EC, Yu D, Martinez de Velasco J, Tessarollo L, Swing DA Court DL, Jenkins NA, Copeland NG (2001) A highly efficient Escherichia coli-based chromosome engineering system adapted for recombinogenic targeting and subcloning of BAC DNA. Genomic 73: 56-65.

Longnecker R, Roizman B (1986) Generation of an inverting herpes simplex virus 1 mutant lacking the L-S junction a sequences, an origin of DNA synthesis, and several genes including those specifying glycoprotein E and the alpha 47 gene. J Virol 58: 583-591.

Lungu O, Panagiotidis CA, Annunziato PW, Gershon AA, Silverstein SJ (1998) Aberrant intracellular localization of Varicella-Zoster virus regulatory proteins during latency. Proc Natl Acad Sci USA 95: 7080-7085.

Lyman MG, Curanovic D, Brideau AD, Enquist LW (2008) Fusion of enhanced green fluorescent protein to the pseudorabies virus axonal sorting protein Us9 blocks anterograde spread of infection in mammalian neurons. J Virol 82: 10308-10311.

Lyman MG, Kemp CD, Taylor MP, Enquist LW (2009) Comparison of the pseudorabies virus Us9 protein with homologs from other veterinary and human alphaherpesviruses. J Virol 83: 6978-6986.

Markus A, Grigoryan S, Sloutskin A, Yee MB, Zhu H, Yang IH, Thakor NV, Sarid R, Kinchington PR, Goldstein RS (2011) Varicella-zoster virus (VZV) infection of neurons derived from human embryonic stem cells: direct demonstration of axonal infection, transport of VZV, and productive neuronal infection. J Virol 85: 6220-7 6233.

McGeoch DJ, Rixon FJ, Davison AJ (2006) Topics in herpesvirus genomics and evolution. Virus Res 117: 90-104.

McNabb DS, Courtney RJ (1992) Identification and characterization of the herpes simplex virus type 1 virion protein encoded by the UL35 open reading frame. J Virol 66: 2653-2663.

Meier JL, Holman RP, Croen KD, Smialek JE, Straus SE (1993) Varicella-zoster virus transcription in human trigeminal ganglia. Virology 193: 193-200.

Messerle M, Crnkovic I, Hammerschmidt W, Ziegler H, Koszinowski UH (1997) Cloning and mutagenesis of a herpesvirus genome as an infectious bacterial artificial chromosome. Proc Natl Acad Sci USA 94: 14759-14763.

Mettenleiter TC, Lomniczi B, Sugg N, Schreurs, C, Ben-Porat T (1988) Host cell-specific growth advantage of pseudorabies virus with a deletion in the genome sequences encoding a structural glycoprotein. J Virol 62: 12-19.

Miranda-Saksena M, Boadle RA, Diefenbach RJ, Cunningham AL (2016) Dual role of herpes simplex virus 1 pUS9 in virus anterograde axonal transport and final assembly in growth cones in distal axons. J Virol 90: 2653-2663.

Modrow S, Falke D, Truyen U (2003) Molekulare Virologie. 2. Auflage, pp. 540-581. Spektrum Akademischer Verlag, Heidelberg, Berlin.

Moriuchi H, Moriuchi M, Smith HA, Cohen JI (1994) Varicella-zoster virus open reading frame 4 protein is functionally distinct from and does not complement its herpes simplex virus type 1 homolog, ICP27. J Virol 68: 1987-1992.

Muyrers JP, Zhang Y, Testa G, Stewart AF (1999) Rapid modification of bacterial artificial chromosomes by ET-recombination. Nucleic Acids Res 27: 1555-1557.

Ng TI, Keenan L, Kinchington PR, Grose C (1994) Phosphorylation of Varicella-Zoster virus open reading frame (ORF) 62 regulatory product by viral ORF47-associated protein kinase. J Virol 68:1350-1359.

Niizuma T, Zerboni L, Sommer MH, Ito H, Hinchliffe S, Arvin AM (2003) Construction of varicella-zoster virus recombinants from parent Oka cosmids and demonstration that ORF65 Protein is dispensable for infection of human skin and T cells in the SCID-hu mouse model. J Virol 77: 6062-6065.

Oliver SL1, Brady JJ, Sommer MH, Reichelt M, Sung P, Blau HM, Arvin AM (2013) An immunoreceptor tyrosine-based inhibition motif in varicella-zoster virus glycoprotein B regulates cell fusion and skin pathogenesis. Proc Natl Acad Sci USA 110: 1911-1916.

Oliver SL, Sommer MH, Reichelt M, Rajamani J, Vlaycheva-Beisheim L, Stamatis S, Cheng J, Jones C, Zehnder J, Arvin AM (2011) Mutagenesis of Varicella-Zoster virus glycoprotein I (gI) identifies a cysteine residue critical for gE/gI heterodimer formation, gI structure, and virulence in skin cells. J Virol 85: 4095-4110.

Ote I, Piette J, Sadzot-Delvaux C (2010) The varicella-zoster virus IE4 protein: A conserved member of the herpesviral mRNA export factors family and a potential alternative target in antiherpetic therapies. Biochem Pharmacol 12:1973-1980.

Ouwendijk WJ, Mahalingam R, Traina-Dorge V, van Amerongen G, Wellish M, Osterhaus AD, Gilden D, Verjans GM (2012) Simian varicella virus infection of Chinese rhesus macaques produces ganglionic infection in the absence of rash. J Neurovirol 18: 91-99.

Oxman MN, Levin MJ (2008) Vaccination against herpes zoster and postherpetic neuralgia. J Infect Dis 197 Suppl 2: S228-S236.

Oxman MN, Levin MJ, Johnso GR, Schmader KE, Straus SE, Gelb LD, Arbeit RD, Simberkoff MS, Gershon AA, Davis LE, Weinberg A, Boardman KD, Williams HM, Zhang JH, Peduzzi PN, Beisel CE, Morrison VA, Guatelli JC, Brooks PA, Kauffman CA, Pachucki CT, Neuzil KM, Betts RF, Wright PF, Griffin MR, Brunell P, Soto NE, Marques AR, Keay SK, Goodman RP, Cotton DJ, Gnann JW Jr, Loutit J, Holodniy M, Keitel WA, Crawford GE, Yeh SS, Lobo Z, Toney JF, Greenberg RN, Keller PM, Harbecke R, Hayward AR, Irwin MR, Kyriakides TC, Chan CY, Chan IS, Wang WW, Annunziato PW, Silber JL (2005) A vaccine to prevent herpes zoster and postherpetic neuralgia in older adults. N Engl J Med 352: 2271-2284.

Ozaki T, Ichikawa T, Matsui Y, Kondo H, Nagai T, Asano Y, Yamanishi K, Takahashi M (1986) Lymphocyte-associated viremia in varicella. J Med Virol 19: 249-253.

Perera LP, Kaushal S, Kinchington PR, Mosca JD, Hayward GS, Straus SE (1994) Varicella-zoster virus open reading frame 4 encodes a transcriptional activator that is functionally distinct from that of herpes simplex virus homology ICP27. J Virol 68: 2468-2477.

Puvion-Dutilleul F, Pichard E, Laithier M, Leduc EH (1987) Effect of dehydrating agents on DNA organization in herpes viruses. J Histochem Cytochem 35: 635-645.

Reichelt M, Brady J, Arvin AM (2009) The replication cycle of varicella-zoster virus: analysis of the kinetics of viral protein expression, genome synthesis, and virion assembly at the single-cell level. J Virol 83: 3904-3918.

Reichelt M, Wang L, Sommer M, Perrino J, Nour AM, Sen N, Baiker A, Zerboni L, Arvin AM (2011) Entrapment of viral capsids in nuclear PML cages is an intrinsic antiviral host defense against Varicella-Zoster virus. PLoS Pathog 7: e1001266.

Ross JL, Wallace K, Shuman H, Goldman YE, Holzbaur EL (2006) Processive bidirectional motion of dynein-dynactin complexes in vitro. Nat Cell Biol 8: 562-570.

Sanger F, Nicklen S, Coulson AR (1977) DNA sequencing with chain-terminating inhibitors. Biotechnology 24: 104-108.

Sato B, Sommer M, Ito H, Arvin AM (2003) Requirement of varicella-zoster virus immediate-early 4 protein for viral replication. J Virol 77: 12369-12372.

Sawyer MH, Chamberlin CJ, Wu YN, Aintablian N, Wallace MR (1994) Detection of varicella-zoster virus DNA in air samples from hospital rooms. J Infect Dis 169: 91-94.

Schmidt M, Kress M, Heinemann S, Fickenscher H (2003) Varicella-zoster virus isolates, but not the vaccine strain OKA, induce sensitivity to alpha-1 and beta-1 adrenergic stimulation of sensory neurons in culture. J Med Virol 70 Suppl 1: S82-89.

Schmidt M (2005) Rekombinante Varianten eines Wildtyp-Isolats des Varicella-Zoster-Virus. Dissertation, Friedrich-Alexander-Universität Erlangen-Nürnberg.

Schmidt-Chanasit J, Bleymehl K, Rabenau HF, Ulrich RG, Cinatl J Jr, Doerr HW (2008) In vitro replication of varicella-zoster virus in human retinal pigment epithelial cells. J Clin Microbiol 46: 2122-2124.

Shizuya H, Birren B, Kim UJ, Mancino V, Slepak T, Tachiiri Y, Simon M (1992) Cloning and stable maintenance of 300-kilobase-pair fragments of human DNA in Escherichia coli using an F-factor based vector. Proc Natl Acad Sci USA 89: 8794-8797.

Sloutskin A, Kinchington PR, Goldstein RS (2013) Productive vs non-productive infection by cell-free varicella zoster virus of human neurons derived from embryonic stem cells is dependent upon infectious viral dose. Virology 443: 285-293.

Smith G (2012) Herpesvirus transport to the nervous system and back again. Annu Rev Microbiol 66: 153-176.

Smith GA, Gross SP, Enquist LW (2001) Herpesviruses use bidirectional fast-axonal transport to spread in sensory neurons. Proc Natl Acad Sci USA 98: 3466-3470.

Sperber SJ, Smith BV, Hayden FG (1992) Serologic response and reactogenicity to booster immunization of healthy seropositive adults with live or inactivated varicella vaccine. Antiviral Res 17: 213-222.

Spieckermann T (2013) Visualisierung phasentypisch exprimierter viraler Proteine des neurotropen Varicella-Zoster-Virus nach Mutagenese bakterieller artifizieller Chomosome. Dissertation, Christian-Albrechts-Universität zu Kiel.

Steain M, Slobedman B, Abendroth A (2010) Experimental models to study varicella-zoster virus infection of neurons. Curr Top Microbiol Immunol 342: 211-228.

Stevenson D, Colman KL, Davison AJ (1994) Characterization of the putative protein kinases specified by varicella-zoster virus genes 47 and 66. J Gen Virol 75: 317-326.

Suenaga T, Satoh T, Somboonthum P, Kawaquchi Y, Mori Y, Arase H (2010) Myelin-associated glycoprotein mediates membrane fusion and entry of neurotropic herpesviruses. Proc Natl Acad Sci USA 107: 866-871.

Tischer BK, Einem J, Kaufer B, Osterrieder N (2006) Two-step red-mediated recombination for versatile high-efficiency markerless DNA manipulation in Escherichia coli. Biotechniques 40: 191-197.

van Zijl M, Quint W, Briaire J, de Rover T, Gielkens A, Berns A (1988) Regeneration of herpesviruses from molecularly cloned subgenomic fragments. J Virol 62: 2191-2195.

Vázquez M, Russa P, Gershon A, Steinberg S, Freudigman K, Shapiro E (2001) The effectiveness of the varicella vaccine in clinical practice. N Engl J Med 344: 955-960.

Wagstaff AJ, Bryson HM (1994) Foscarnet: a reappraisal of its antiviral activity, pharmacokinetic properties and therapeutic use in immunocompromised patients with viral infections. Drugs 48: 199-226.

Wagner M, Ruzsics Z, Koszinowski UH (2002) Herpesvirus genetics has come of age. Trends Microbiol 10: 318-324.

Whitley RJ, Gnann JW (1992) Acyclovir: a decade later. N Engl J Med 327: 782-789.

Wussow F, Fickenscher H, Tischer BK (2009) Red-mediated transposition and final release of the mini-F vector of a cloned infectious herpesvirus genome. PLoS One 4: e8178.

Yeung YG, Stanley ER (2009) A solution for stripping antibodies from polyvinylidene fluoride immunoblots for multiple reprobing. Anal Biochem 389: 89-91.

Zerboni L, Berarducci B, Rajamani J, Jones CD, Zehnder JL, Arvin A (2011) Varicella-zoster virus glycoprotein E is a critical determinant of virulence in the SCID mouse-human model of neuropathogenesis. J Virol 85: 98-111.

Zerboni L, Reichelt M, Jones CD, Zehnder JL, Ito H, Arvin AM (2007) Aberrant infection and persistence of varicella-zoster virus in human dorsal root ganglia in vivo in the absence of glycoprotein I. Proc Natl Acad Sci USA 104: 14086-14091.

Zerboni L, Sen N, Oliver SL, Arvin A (2014) Molecular mechanisms of varicella zoster virus pathogenesis. Nat Rev Microbiol 12: 197–210.

Zhang Y, Buchholz F, Muyrers JP, Stewart AF (1998) A new logic for DNA engineering using recombination in Escherichia coli. Nat Genet 20: 123-128.

Zhang Z, Selariu A, Warden C, Huang G, Huang Y, Zaccheus O, Cheng T, Xia N, Zhu H (2010) Genome-wide mutagenesis reveals that ORF7 is a novel VZV skin-tropic factor. PLoS Pathog 6: e1000971.

8 ABBREVIATIONS

Amp	ampicillin
BAC	bacterial artificial chromosome
bp	base pairs
cDNA	complementary DNA
Cm	chloramphenicol
CPE	cytopathogenic effect
DAPI	4',6-diamidino-2-phenylindole
DMEM	Dulbecco's Modified Eagle Medium
DMSO	dimethyl sulfoxide
DNA	deoxyribonucleic acid
dNTPs	deoxyribonuclotide triphosphates
dpi	day post infection
dpt	day posttransfection
DRG	dorsal root ganglia
dsDNA	double-stranded deoxyribonucleic acid
DTI	defined trypsin inhibitor
E	early genes
E. coli	*Escherichia coli*
EDTA	ethylenediaminetetraacetic acid
eGFP	enhanced green fluorescent protein
FBS	fetal bovine serum
for	forward
GAPDH	glyceraldehyde 3-phosphate dehydrogenase
gI	glycoprotein I
HFF	human foreskin fibroblasts
HRP	horseradish peroxidase
HSV-1	herpes simplex virus type 1
IE	immediate early protein
IRL	internal repeat long
IRS	internal repeat short
Kan	kanamycin
Kan^R	kanamycin cassette
kb	kilo base pairs
L	late genes
LB	Luria Bertani broth

M	marker, DNA ladder
MeWo	human melanoma cell line
Mini-F	minimal components of a fertility plasmid
mRFP	monomeric red fluorescent protein
NBM	neurobasal medium
NGF	nerve growth factor
OD	optical density
Opti-MEM	improved minimal essential medium MEM
ORF	open reading frame
PAGE	polyacrylamide gel electrophoresis
PBS	phosphate buffered saline
PCR	polymerase chain reaction
PFU	plaque forming unit
pHJOpac	plasmid of the European VZV wild-type isolate HJO
PIC	protease inhibitor cocktail
PrV	pseudorabies virus
R	repetitive region
rev	reverse
RIPA	radioimmunoprecipitation assay
RFLP	restriction fragment length polymorphism
RNA	ribonucleic acid
rpm	round per minute
RT	reverse transcriptase
SDS	sodium dodecyl sulfate
TBE	tris borate EDTA buffer
TBS	tris buffered saline
TBST	tris buffered saline with tween
TGN	trans Golgi network
Tris	tris(hydroxymethyl)aminomethane
TRL	terminal repeat long
TRS	terminal repeat short
U	unit
UL	unique long region
US	unique short region
v/v	volume per volume
w/v	weight per volume
VZV	varicella-zoster virus

9 PRESENTATIONS AND PUBLICATION

ORAL PRESENTATIONS

Taher H, Petersen N, Vogt F, Moock M, Brunnemann AK, Fickenscher H (2014) Deletion mutagenesis of varicella-zoster virus for the optimization of the vaccine Oka strain by multiple homologous recombination in bacteria. Oral presentation, 9th mini-herpesvirus workshop, 19 Sep 2014, Berlin.

Taher H, Vogt F, Petersen N, Moock M, Brunnemann AK, Fickenscher H (2015) Clonal varicella zoster virus vaccine strain Oka variants with minimized genome size. Oral presentation, 25th Annual Meeting of the Society for Virology, 20 Mar 2015, Bochum.

Taher H, Petersen N, Moock M, Vogt F, Brunnemann AK, Fickenscher H (2016) Clonal Oka varicella vaccine variants with reduced viral genome size and presumed higher clinical safety. Oral presentation, 6th European Congress of Virology, 21 Oct 2016, Hamburg.

Taher H, Spieckermann T, Nemitz S, Maschkowitz G, Fickenscher H (2018) Axonal tracing of fluorescence-labeled varicella-zoster virus proteins in antero- and retrograde infection of embryonic rat dorsal root ganglia. Oral presentation, 28th Annual Meeting of the Society for Virology, 16 Mar 2018, Würzburg.

PUBLICATION

Taher H, Spieckermann T, Nemitz S, Maschkowitz G, Fickenscher H (2018) Axonal tracing and colocalization of the fluorescence-labeled varicella-zoster virus proteins IE4 and p65 together with the capsid protein p23 upon anterograde and retrograde infection of embryonic rat dorsal root ganglia neurons. Scientific Reports, in preparation.

10 ACKNOWLEDGEMENTS

First, I would like to thank Prof. Dr. Helmut Fickenscher for giving me the opportunity to work on this attractive research topic and to enhance my scientific knowledge, experimental skills and my creative thinking and for his friendly guidance and supportive ideas.

To Prof. Dr. Axel Scheidig I would like to express my profound gratitude for his constant instantaneous support by accepting to be the second reviewer.

I am grateful to Prof. Dr. Stefan Finke and Dr. Sabine Nemitz at the Friedrich-Loeffler Institute (Greifswald) for sharing their experience with embryonic rat DRG cell preparation and culture and to Benedict Kaufer at the Department of Veterinary Virology at the Free University of Berlin for providing the mRFP-expressing VZV Oka strain.

I would like also to acknowledge Sandra Kissing for help at the Olympus confocal microscope (Biochemistry, Kiel) and Jürgen Fritsch for support at the Zeiss laser-scanning microscope (Immunology, Kiel).

A special thank goes to Dr. Gregor Maschkowitz for sharing his wide knowledge with me, whenever required, which made this project easier and more accurate. Besides, I thank Neel Petersen MD., Dr. Oliver Braum, Dr. Linda Bremer, Dr. Tanja Spieckermann, Dr. Anne Brunnemann, Ines Heyn M.Sc., and Andrea Hölzgen for the delightful and constructive teamwork, who also did not hesitate to share their scientific and experimental skills whenever needed. Moreover, they provided a very friendly and joyful environment within the research department making it more enjoyable.

To my Nesrin I am grateful for being my strength in the weak moments and for your patience on encouraging me perpetually to pursue my ambition.

Last but not the least, I would like to thank my family especially my parents who supported me all the time with their warm words and lovely truthful wishes.

11 ERKLÄRUNG

Hiermit erkläre ich, dass die vorliegende Dissertation, abgesehen von der Beratung durch meinen Betreuer Prof. Dr. Helmut Fickenscher, nach Inhalt und Form die eigene Arbeit ist. Ich habe dabei die in der Arbeit angegebenen Quellen benutzt. Teile dieser Arbeit sind zur Publikation eingereicht. Des Weiteren entstand die vorliegende Arbeit unter Einhaltung der Regeln guter wissenschaftlicher Praxis der Deutschen Forschungsgemeinschaft. Zudem erkläre ich, kein anderes Promotionsverfahren ohne Erfolg beendet zu haben und dass keine Aberkennung eines bereits erworbenen Doktorgrades vorliegt.

Husam Taher, M.Sc.

Kiel, den 13.02.2018